Evaluation of the effect of colloidal systems on biodistribution of selected prostate cancer radiopharmaceuticals

V Mandiwana

orcid.org / 0000-0002-2647-9780

Thesis submitted in fulfilment of the requirements for the degree *Doctor of Philosophy in Pharmaceutics* at the North-West University

Promoter: Prof JR Zeevaart

Co-Promoter: Prof RK Hayeshi

Co-Promoter: Mr ML Kalombo

Graduation: October 2019

Student number: 24045756

PREFACE

This thesis is submitted in fulfilment of the requirements of a Doctor of Philosophy in Pharmaceutics using the article format in accordance with the General Academic Rules (A.7.5.7.4) of the North-West University. Each experimental chapter was written in accordance with specific guidelines as stipulated by the journals intended for publication.

I Vusani Mandiwana, the student did the following work:

- Planned and designed the experiments
- Carried out and participated in all the experiments with the exception of analysis done at independent laboratories
- Interpreted the results and discussed them with various co-authors and/or supervisors
- Drafted the manuscripts

Manuscript 1 has been accepted for publication in the Journal of Labelled Compounds and Radiopharmaceuticals, manuscript 2 and manuscript 3 will be submitted to the Journal of Nanomaterials and Journal of Nanoparticle Research respectively.

All the co-authors have given permission that the manuscripts may be submitted for degree purposes as stipulated in the Manual for Post Graduate Students of the North-West University.

ACKNOWLEDGEMENTS

I would love to express my sincerest gratitude to the following people and institutions, all of who played a significant role during the course of my PhD study.

Prof Jan Rijn Zeevaart, my supervisor, thank you so much for allowing me the opportunity to complete a study such as this under your supervision. Your knowledge, expert advice and suggestions made this research so much easier. Thank you for all the assistance, support and encouragement throughout my study and continuously being patient with me.

Mr Lonji Kalombo, my co-supervisor, thank you for being my father in science. Your motivation, words of wisdom and supervision/mentorship will forever be appreciated. Thank you for believing in me, for boosting my confidence when I doubted my abilities, for giving me a platform and continuously encouraging me to do better.

Prof Rose Hayeshi, your drive and efficiency is just amazing, it inspired me to work harder and it often made me feel guilty when I was slacking. Thank you most especially for your patience.

Dr Thomas Ebenhan, thank you for your valuable input in my experimental work and all your plan B's. I was never short of supervisors thanks to you coming on board to assist and advice whenever and wherever possible.

Dr Yolandy Lemmer, thank you for all your assistance, the sisterly advice, your emotional support and your scientific contribution to my study, you make science so enjoyable. Thank you for your loving and motivating energy, it always encouraged me.

Prof Anne Grobler, North West University, Preclinical Drug Development Platform (NWU/PCDDP), thank you for your helpful suggestions and input in my research. Your passion for research is inspiring.

Prof Mike Sathekge, thank you for welcoming me into your department with open arms and allowing me access to work and learn from your staff and lab facilities. Thank you for the opportunity to learn and grow as a scientist.

Dr Hester Oosthuizen, thank you for your assistance, advice and all the input you made in putting my thesis together. You made the writing up process a breeze and I appreciate all your assistance.

All my colleagues, at the Council for scientific and industrial research (CSIR), Nuclear energy corporation of South Africa (Necsa), NWU/PCDDP and the Steve Biko Academic Hospital

Department of Nuclear Medicine, thank you for all your input and assistance in my research, for challenging me and all the fun times. Your contributions made my study so much easier. Your efforts, time and various contribution made my study possible.

To my team at CSIR, I would like to extend my gratitude to Phuti Chelopo, Heena Ranchod, Patric Nkuna, Nthwaleng Mogamme, Bathabile Ramalapa, Philip Labuschagne, Andri Swanepoel.

Thank you to all my friends and colleagues at NWU/PCDDP namely Antoinette Fick, Cor Bester, Kobus Venter, Jacob Mabena, Nico Minnaar, Hyltton Bunting, Liezl-Marie Scholtz, Zaan Welgemoed, Matthew Glyn, Adelle As, Ambrose Okem, Palesa Koatale, Lerato Thindisa, Magda Lombard.

Team Necsa and Steve Biko Academic Hospital, I would like to thank the following people; Brenda Mokaleng for teaching me so much on radiochemistry and being patient with me, Janke Kleinhans, Amanda Mdlophane, Cathryn Driver, Janie Duvenhage, Mariana Miles, Collins Maledimo, Johncy Mahapane, Thato Sello, Delene van Wyk, Cindy Els, Danka Erasmus (Axim), Nadia Capelo (Axim) and Adolf Nordin (Axim).

My family has been my saving grace, thank you to my parents Emma and Jeffrey Mandiwana for your constant motivation, love and support in everything I pursued. Your faith in me drives me to do better and be better in everything I do and it helped me to reach higher without giving up, “ndo livhuwa”. My sisters Onica, Sedzani and Mpho, thank you for making me feel like a super-woman who can do anything no matter how tough it may seem. Your support and encouragement is always highly appreciated. I love you girls. To my sons, Andani and Londani, I did this for you guys. You’ve always been my inspiration, the reason, my purpose and my driving force. I love you both so much.

Nuclear technologies in medicine and the biosciences initiative (NTeMBI), thank you for hosting me and for the financial support. I would like to extend my sincerest gratitude for allowing me this opportunity to be a part of a great team of institutions and to complete my study. A special thank you to the Carl and Emily Fuchs Foundation for assisting in funding my PhD, thank you, thank you, thank you.

ABSTRACT

It has been reported that microemulsion (ME) delivery systems provide an opportunity to enhance the bioavailability and efficacy of a therapeutic agent whilst minimising side effects. The prostate-specific membrane antigen (PSMA) targeting agents PSMA-11 and PSMA-617, which accumulate in prostate tumours, allows for [^{68}Ga]Ga^{3+}-radiolabelling and PET imaging of PSMA-expression *in vivo*. Radiolabelled [^{68}Ga]Ga-PSMA-617 can be encapsulated in a ME delivery system which is hypothesized to enhance its pharmacokinetic properties. This study investigated the synthesis of [^{68}Ga]Ga-PSMA-617 and [^{68}Ga]Ga-PSMA-617 contained within a ME, the toxicity profile, and microPET/CT imaging and biodistribution in PC3 tumour xenograft male BALB/c mice. [^{68}Ga]Ga-PSMA-617 was synthesized in a combined solid phase and solution chemistry strategy. The formulation of [^{68}Ga]Ga-PSMA-617 into a ME was then evaluated for *in vitro* and *in vivo* toxicity and biodistribution. The cytotoxicity of [^{68}Ga]Ga-PSMA-617-ME was tested in HEK293 and PC3 cells. [^{68}Ga]Ga-PSMA-617-ME indicated negligible cellular toxicity at different concentrations. HEK293 cells showed a statistically higher tolerance towards the [^{68}Ga]Ga-PSMA-617-ME compared to PC3 cells. [^{68}Ga]Ga-PSMA-617 and [^{68}Ga]Ga-PSMA-617-ME was administered intravenously in BALB/c mice with or without PC3-tumours followed by microPET/CT imaging and *ex vivo* biodistribution determination. The *ex vivo* biodistribution in PC3-tumour bearing BALB/c mice showed the highest amounts of [^{68}Ga]Ga-PSMA-617 radioactivity accumulation in the kidneys and the lowest uptake was seen in the brain. Both the [^{68}Ga]Ga-PSMA-617 and [^{68}Ga]Ga-PSMA-617-ME followed an expected clearance profile for small-sized polar radiopharmaceuticals, with predominant renal clearance. The ME did alter the biodistribution pattern of [^{68}Ga]Ga-PSMA-617 but maintained distribution to the kidneys, albeit at statistically significant higher levels. Similarly, encapsulation in the ME may have resulted in delayed uptake into tumours as can be seen from the higher blood pool values.

The incorporation of [^{68}Ga]Ga-PSMA-617 into ME was successfully demonstrated and resulted in a stable non-toxic formulation as evaluated by *in vitro* and *in vivo* means. Both the [^{68}Ga]Ga-PSMA-617 and [^{68}Ga]Ga-PSMA-617-ME showed enterohepatic metabolism of [^{68}Ga]Ga-PSMA-617.

Keywords

Biodistribution, Ex vivo, ^{68}Ga-PSMA-617, In vitro, In vivo, Microemulsion, MicroPET/CT imaging, Prostate cancer, Toxicity

TABLE OF CONTENTS

Chapter 1: Problem Statement

1.1. Introduction

Prostate cancer is the second most frequent cancer and the sixth leading cause of cancer deaths in men worldwide (Afshar-Oromieh *et al.,* 2014; Akhtar *et al*., 2012; Sathekge *et al.,* 2018). It is a challenge to select appropriate treatment options for disseminated prostate cancer due to the lack of sensitive imaging agents for diagnosis and therapy monitoring (Eder *et al.,* 2013). Prostate-specific membrane antigen (PSMA) is expressed in nearly all prostate cancers with increased expression in poorly differentiated, metastatic and hormone-refractory carcinomas (Eder *et al.,* 2013). PSMA is a cell surface membrane-type zinc protease, also called glutamate carboxypeptidase II (GCPII) (Eder *et al.,* 2014) and is primarily restricted to the prostate. It is expressed in all stages of the disease, on the tumour cell surface and not shed into the circulation (Eder *et al.,* 2013). PSMA exhibits very high expression in prostate cancer cells compared to other PSMA expressing tissues such as the small intestine, kidneys or salivary glands (Afshar-Oromieh *et al.,* 2013; Baur *et al.,* 2014). PSMA is a transmembrane protein with a large extracellular domain (Afshar-Oromieh *et al.,* 2015). Its enzyme activity permits the development of specific inhibitors and their internalization after binding to a ligand (Afshar-Oromieh *et al.,* 2013). This characteristic thus makes it an ideal and a promising target for prostate cancer-specific imaging and therapy (Eder *et al.*, 2013). Linking of PSMA ligands to small molecules labelled with a positron emitting radionuclide is a potential approach for the diagnosis of prostate cancer using positron emission tomography (PET).

Methods have been developed to label PSMA ligands with gallium-68 ($[^{68}Ga]Ga^{3+}$) or ^{177}Lu, enabling their use for PET (Srirajaskanthan *et al.,* 2010) or single photon emission computed tomography (SPECT) imaging and therapy respectively (Afshar-Oromieh *et al.,* 2014). Experience with positron emission tomography/computed tomography (PET/CT) using Glu-NH-CO-NH-Lys-(Ahx)-[^{68}Ga-N,N'-bis[2-hydroxy-5-(carboxyethyl)benzyl] ethylenediamine-N,N'-diacetic acid (HBED-CC)] ($[^{68}Ga]Ga^{3+}$-PSMA-11) as a $[^{68}Ga]Ga^{3+}$-labelled PSMA ligand, suggests that this tracer can detect prostate cancer relapses and metastases with high contrast by binding to the extracellular domain of PSMA, followed by internalization (Afshar-Oromieh *et al.,* 2014). SPECT is usually performed using a rotating gamma camera system (Perkins and Frier, 2004), whereas PET is performed on a dedicated PET scanner comprising a circular array of detectors which looks more like a computed tomography scanner (Afshar-

Oromieh *et al.,* 2014). A PET scan looks at the biological activity of a tumour, whereas a CT scan gives anatomical information such as the exact location, size and shape of a tumour in relationship to other structures. PET scanners have a higher spatial resolution than SPECT systems (Afshar-Oromieh *et al.,* 2013).

There is a need to develop high-resolution PET imaging technologies using the extracellular domain of PSMA. Methods have been developed to label PSMA ligands with radionuclides such as [^{68}Ga]Ga^{3+}, technetium-99m (^{99m}Tc) and iodine-123/131 ($^{123/131}$I), to enable their use in scintigraphic imaging and radioligand therapy (Afshar-Oromieh *et al.,* 2013). Of these, [^{68}Ga]Ga^{3+} is the most widely used radionuclide. It is a positron emitter with a half-life of 68 min. Germanium-68/Gallium-68 (^{68}Ge/^{68}Ga) generators are commercially available, which enable convenient elution of cationic [^{68}Ga]Ga^{3+} with dilute acid (0.1 M HCl). An effective purification of the ^{68}Ge/^{68}Ga eluate (Asti *et al.,* 2008), a crucial step for clinical use (Zhernosekov *et al.,* 2007), was applied to the production of ^{68}Ga-1,4,7,10-tetra-azacyclododecane-1,4,7,10-tetraacetic acid–D-Phe^{1}-Tyr^{3}-octreotide (^{68}Ga-DOTATOC), the most widely used [^{68}Ga]Ga^{3+}-based PET radiopharmaceutical (Prata, 2012; Singh *et al.*, 2011). This purification technique has also been used to optimise [^{68}Ga]Ga^{3+}-labelling methods for 1,4,7,10-tetraazacyclododecane-N,N',N'',N'''-tetraacetic acid (DOTA)-derived peptides. Decristoforo *et al*. (2007) described a fully automated synthesis for [^{68}Ga]Ga^{3+}-labelled peptides with high, reproducible yields. ^{68}Ga-1,4,7,10-tetra-azacyclododecane-1,4,7,10-tetraacetic acid–D-Phe^{1}-Tyr^{3}-octreotate (^{68}Ga-DOTATATE) is used for neuroendocrine tumour diagnosis using PET/CT. ^{68}Ga-DOTATATE PET/CT has a much higher sensitivity compared to indium-111 octreotide imaging. ^{68}Ga-DOTATATE is a conjugate of an amide of the acid DOTA, which acts as a chelator for a radionuclide, and (Tyr^{3})-octreotate, a derivative of octreotide. The latter binds to somatostatin receptors, which are found on the cell surfaces of a number of neuroendocrine tumours, and thus directs the radioactivity into the tumour.

PSMA catalyses the hydrolysis of N-acetyl-L-aspartyl-L-glutamate (NAAG) into N-acetyl-L-aspartate (NAA) and L-glutamate (Baur *et al.,* 2014). Based on the chemical structure of NAAG, several glutamate-urea-glutamate-based peptides have been developed (Baur *et al.,* 2014). These molecules have a high affinity and specific binding to PSMA and differ mainly in the selection of the chelator for the complexation of the desired radionuclide (Baur *et al.,* 2014). Due to their good affinity for PSMA, it is therefore desirable to develop radionuclide based therapeutic strategies using adapted PSMA targeting.

In recent years ^{68}Ga-DOTA-PSMA (Figure 1) conjugates have been used as a diagnostic tool to detect tumour lesions. However, the application of lutetium-177 (^{177}Lu) and yttrium-90 (^{90}Y) is favoured for radiometal therapy (Kam *et al.*, 2012). This means that [^{68}Ga]Ga^{3+}-PSMA can be used to diagnose prostate cancer followed by further diagnosis and/or treatment therapy using ^{177}Lu-DOTA-PSMA (^{177}Lu-PSMA) applications. The use of ^{177}Lu ($E_{\beta max}$: 0.5 MeV, $t_{1/2}$: 6.7 d) is more suitable for the treatment of smaller lesions and metastases, accompanied by a minimization of kidney dose in comparison to the application of ^{90}Y labelled peptides (Baur *et al.*, 2014). Yttrium-90 ($E_{\beta max}$: 2.3 MeV, $t_{1/2}$: 64 h) is more appropriate for the treatment of larger tumour lesions and metastases (Baur *et al.*, 2014). ^{177}Lu is also a useful diagnostic tool for the scintigraphy of tumour uptake due to beta and gamma emission (Baur et al. 2014). For both targeting and treatment applications, DOTA (Kam *et al.*, 2012) is the most commonly used chelator for the complexation of radiometals (i.e. ^{68}Ga, ^{177}Lu, and ^{90}Y) to small molecules and peptides (Baur *et al.*, 2014).

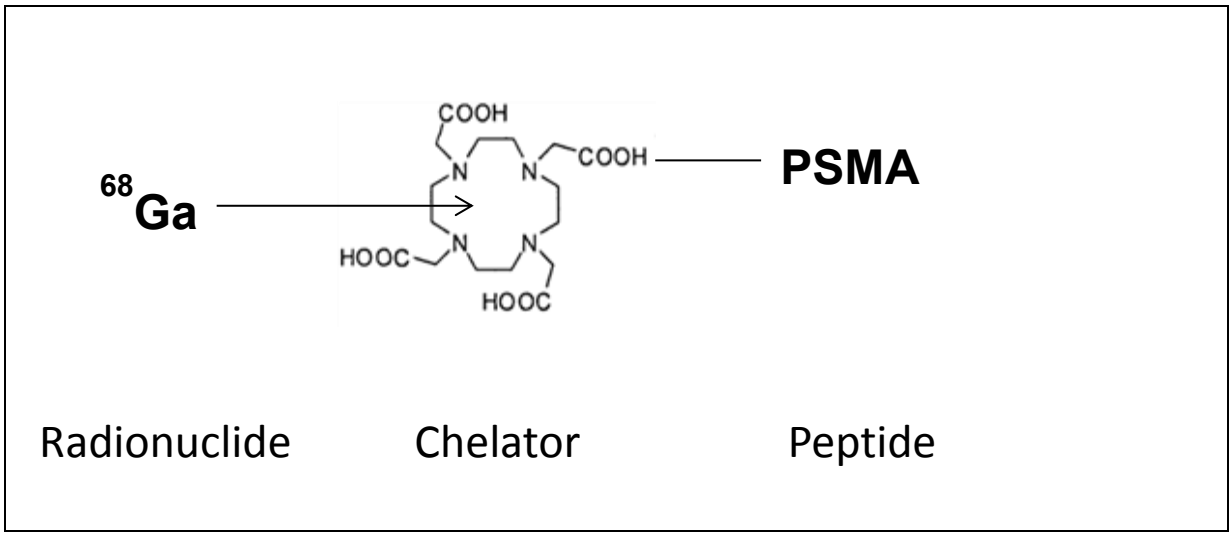

Figure 1.1: Representation of a gallium-68 labelled DOTA conjugate of a PSMA targeting molecule

Theranostics is a term which refers to the inseparability of diagnosis and therapy and takes into account the personalised management of the disease for a specific patient (Baum and Kulkarni, 2012; Werner *et al.*, 2014). Theranostic radionuclides emit radiation energy suitable for both diagnostic and treatment purposes due to the physical behaviour of the decay of the parent nuclide during the emission of gamma, beta and alpha radiation. Molecular phenotypes of

tumours can be determined by molecular imaging, using techniques such as PET, SPECT, magnetic resonance imaging (MRI) or optical methods so that the treatment is specifically targeting the tumour. To meet the demands of theranostics, the target, ligand, labelling chemistry, the most appropriate radionuclide, biodistribution modifier and the patient for the personalised treatment need to be defined (Baum and Kulkarni, 2012). Theranostics of neuroendocrine tumours using [^{68}Ga]Ga^{3+}-labelled tracers for diagnostics with PET/CT and using ^{177}Lu or other radionuclides for radionuclide therapy by applying the same peptide is proving to be useful (Baum and Kulkarni, 2012). Although treatment with ^{177}Lu has shown good response, side effects such as renal impairment with a decline in creatinine clearance has been reported (Werner *et al.,* 2014). Amino acid solutions are recommended directly prior and during peptide receptor radionuclide therapy (PRRT) to reduce the renal absorbed dose and damage to the renal parenchyma (Werner *et al.,* 2014).

The use of delivery systems (such as microemulsions) can improve the efficacy of a drug, allowing the total dose to be reduced and thus minimising side effects and toxicity of the encapsulated compound (Muzaffar *et al.*, 2013).

Microemulsions (MEs) are a macroscopic system of water, oil and amphiphile which is optically isotropic (Muzaffar *et al.,* 2013). MEs are clear or translucent and form spontaneously with an average droplet diameter of 10 to 140 nm (Muzaffar *et al.,* 2013). They are thermodynamically stable and nanostructured (Moghimipour *et al.,* 2013). This distinguishes them from ordinary milk-like emulsions which are thermodynamically unstable but kinetically stable. The advantages of MEs include enhanced bioavailability of the encapsulated compound, improved solubility of a poorly soluble drug, protection of unstable drugs against environmental conditions and a long shelf life. MEs can be classified as water-in-oil (w/o), oil-in-water (o/w) or bicontinuous phase MEs (Moghimipour *et al.,* 2013).

This study aims to formulate and characterize a ME as an intravenous delivery system of [^{68}Ga]Ga^{3+}-labelled PSMA conjugated with the chelator DOTA (this will be referred to as [^{68}Ga]Ga-PSMA-617) for the diagnosis of prostate cancer. The ME will serve to encapsulate the radiopharmaceutical ([^{68}Ga]Ga-PSMA-617) to assist in a rapid release of the radiopharmaceutical into the target organ (prostate) while altering the clearance mechanism of peptides away from rapid kidney clearance towards excretion via the liver and bile.

1.2 Research Question

Mortality from metastasising prostate cancer is still high despite the use of novel therapeutic approaches (Baur *et al.*, 2014). There is therefore an urgency to diagnose prostate cancer early to prevent tumour dissemination. Furthermore, effective strategies for disseminated prostate cancer are needed urgently. Selective targeting of prostate cancer or its metastases is a significant task in molecular imaging with PET and for targeted internal radiation therapy.

Scintigraphy techniques (gamma camera) usually show lower spatial resolution when compared to PET. Furthermore, imaging with radiolabelled compounds, for example antibodies, is relatively complex: after injection, multiple acquisitions over several days are needed to obtain the best images with high contrast between background and tumour lesions (Afshar-Oromieh *et al.*, 2013).

^{68}Ga-DOTATATE on the other hand is rapidly excreted from non-target sites, offers a good target to background ratio and has documented efficacy for imaging neuroendocrine tumours (Shastry *et al.*, 2010). However, evaluation of a lesion with low or atypical uptake of ^{68}Ga-DOTATATE is a challenge, especially if the lesion is located in an organ showing physiological uptake, such as the kidneys, adrenals, spleen or bowels.

Significant accumulation of [^{68}Ga]Ga^{3+} radioactivity levels in tumours, kidneys and the bladder after *in vivo* administration of ^{68}Ga-DOTATATE in mice has been reported (Müller, 2013). The kidneys tend to have a very high uptake of radioactive [^{68}Ga]Ga^{3+}, with a high and fatal risk of dysfunction. Whole body SPECT/computed tomography (SPECT/CT) image scans with ^{177}Lu-DOTATATE have also reportedly shown high physiological uptake in the spleen, kidneys, bladder and increased abnormal uptake in the liver (Singh *et al.*, 2011). Therefore, the design and development of drug delivery systems with the intention of enhancing drug availability while minimising accumulation in kidneys and other non-target tissues and subsequent side effects are an ongoing process in pharmaceutical research. Despite abnormal uptake and risk of nephrotoxicity, the prediction of therapeutic response would be more accurate based on ^{177}Lu-DOTATATE diagnostic or therapy scans as compared to other ^{177}Lu-labelled somatostatin analogues (Poeppel *et al.*, 2011; Singh *et al.*, 2011) and therefore ^{177}Lu-labelled PSMA.

The use of colloidal particles as delivery systems can improve the efficacy of the drug, allowing the total dose to be reduced and therefore minimizing side effects (Bhattacharya *et al.*, 2016).

This study will attempt to answer the following questions:
The advantages of MEs over other emulsions include short preparation time, thermodynamic stability, increased drug loading, increased bioavailability and enhanced penetration through the biological membranes. These are versatile delivery systems which can be used to deliver therapeutic compounds via several routes. Considering these advantages, can

i.) this delivery system lead to the rapid absorption of an encapsulated therapeutic compound,
ii.) reduce the toxic side effects of the drug while being maintained within the efficacious concentrations for a prolonged period in the blood stream?

This approach to encapsulate [^{68}Ga]Ga-PSMA-617 prostate cancer targeting compounds into a ME delivery system could lead to optimised delivery systems with decreased toxicity and reduced accumulation of the compound in the kidneys. The ME delivery system will aid to make the diagnostic and therapeutic compound which has been encapsulated, safe *in vivo* due to reduced toxicity and side effects to the kidneys and other non-target organs. These delivery systems will aid to distribute the entrapped radioactive [^{68}Ga]Ga-PSMA-617 to the prostate cancer while reducing toxic uptake or accumulation in the kidneys. In this study, the following hypothesis should be tested:

a) The use of MEs as delivery systems can improve the efficacy of a drug or encapsulated therapeutic compound, allowing the total dose to be reduced and thus minimising side effects.
b) The development of this characteristic nano-sized delivery system will minimize toxicity risks by reducing the duration of exposure to the radioactive, entrapped compound (Longmire *et al.*, 2008). Additionally, nano-sized particles with characteristic size, shape, charge, polarity and lipophilicity will show tumour uptake to a certain extent via the enhanced permeability and retention (EPR) effect (Heneweer *et al.*, 2011).

Therefore, the expected outcomes of this delivery system are:

- Enhanced bioavailability and increased absorption rates of [^{68}Ga]Ga-PSMA-617, without any toxicity and

- Improved intracellular delivery of the encapsulated [^{68}Ga]Ga-PSMA-617 into the prostate cancer.

1.3 Aim and research objectives

The aim of this study was to initially encapsulate a [^{68}Ga]Ga^{3+}-labelled PSMA ligand in a ME and to investigate the uptake of this PSMA formulation in healthy and mice with human tumour xenografts to evaluate its applicability for prostate cancer or tumour imaging vs the non-encapsulated [^{68}Ga]Ga-PSMA-617. This encapsulated radiopharmaceutical complex will serve as a diagnostic tool. Therefore, the specific objectives of this study are as follows:

i. To produce a radiolabelled ME
   - Encapsulate [^{68}Ga]Ga-PSMA-617 in a ME delivery system for diagnosis of prostate cancer.

ii. To evaluate the impact of the ME on the biodistribution of [^{68}Ga]Ga-PSMA-617 as measured by microPET after IV administration.
   - Assess the biodistribution of [^{68}Ga]Ga-PSMA-617 encapsulated in a ME delivery system (henceforth [^{68}Ga]Ga-PSMA-617-ME) in healthy male BALB/c mice.
   - Compare the biodistribution of [^{68}Ga]Ga-PSMA-617-ME vs non-encapsulated [^{68}Ga]Ga-PSMA-617 in prostate cancer PC3 tumour bearing male BALB/c mice.

iii. Evaluate the *in vitro* cellular toxicity of [^{68}Ga]Ga-PSMA-617-ME and [^{68}Ga]Ga-PSMA-617 to PSMA-positive PC3 and PSMA-negative HEK293 cell lines.

iv. Evaluate the *in vivo* toxicity of a ME delivery system and of a ME containing [^{68}Ga]Ga-PSMA-11in healthy male BALB/c mice.

References

Afshar-Oromieh A, Malcher A, Eder M, Eisenhut M, Linhart HG, Hadaschik BA, Holland-Letz T, Giesel FL, Kratochwil BA, Haufe S, Haberkorn U and Zechmann CM. 2013. PET imaging with a [^{68}Ga]gallium-labelled PSMA ligand for the diagnosis of prostate cancer: Biodistribution in humans and first evaluation of tumour lesions. *European Journal of Nuclear Medicine and Molecular Imaging* 40: 486–495

Afshar-Oromieh A, Zechmann CM, Malcher A, Eder M, Eisenhut M, Linhart HG, Holland-Letz T, Hadaschick BA, Giesel FL, Debus J and Haberkorn U. 2014. Comparison of PET imaging with a ^{68}Ga-labelled PSMA ligand and ^{18}F-Choline-based PET/CT for the diagnosis of recurrent prostate cancer. *European Journal of Nuclear Medicine and Molecular Imaging* 41: 11–20

Afshar-Oromieh A, Hetzheim H, Kratochwil C, Benesova M, Eder M, Neel OC *et al.* 2015. The novel theranostic PSMA-ligand PSMA-617 in the diagnosis of prostate cancer by PET/CT: biodistribution in humans, radiation dosimetry and first evaluation of tumor lesions. *Journal of Nuclear Medicine* 56(11)

Akhtar NH, Pail O, Saran A, Tyrell L and Tagawa ST. 2012. Prostate-specific membrane antigen-based therapeutics. *Advances in Urology* 2012: Article ID 973820

Asti M, De Pietri G, Fraternali A, Grassi E, Sghedoni R, Fioroni F, Roesch F, Versari A and Salvo D. 2008. Validation of ^{68}Ge/^{68}Ga generator processing by chemical purification for routine clinical application of ^{68}Ga-DOTATOC. *Nuclear Medicine and Biology* 35: 721–724

Baum RP and Kulkarni HR. 2012. Theranostics: From molecular imaging using Ga-68 labeled tracers and PET/CT to personalized radionuclide therapy - The Bad Berka Experience. *Theranostics* 2 (5): 437–447

Baur B, Solbach C, Andreolli E, Winter G, Machulla HJ and Reske SN. 2014. Synthesis, radiolabelling and in vitro characterization of the gallium-68-, yttrium-90- and lutetium-177-labelled PSMA ligand, CHX-A"-DTPA-DUPA-Pep. *Pharmaceuticals* 7: 517–529

Bhattacharya R, Mukhopadhyay S and Kothiyal P. 2016. Review on microemulsion- As a potential novel drug delivery system. *World Journal of Pharmacy and Pharmaceutical Sciences* 5(6): 700-729

Eder M , Neels O, Müller M, Bauder-Wüst U, Remde Y, Schäfer M, Hennrich U, Eisenhut M, Afshar-Oromieh A, Haberkorn U and Kopka K. 2014. Novel preclinical and radiopharmaceutical aspects of [^{68}Ga]Ga-PSMA-HBED-CC: A new PET tracer for imaging of prostate cancer. *Pharmaceuticals* 7: 779–796

Eder M, Eisenhut M, Babich J and Haberkorn U. 2013. PSMA as a target for radiolabelled small molecules. *European Journal of Nuclear Medicine and Molecular Imaging* 40: 819–823

Kam BLR, Teunissen JJM, Krenning EP, De Herder WW, Khan S, Van Vliet EI and Kwekkeboom DJ. 2012. Lutetium-labelled peptides for therapy of neuroendocrine tumours. *European Journal of Nuclear Medicine and Molecular Imaging* 39(1): S103-S112

Moghimipour E, Salimi A and Eftekhari S. 2013. Design and characterization of microemulsion systems for naproxen. *Advanced Pharmaceutical Bulletin* 3(1): 63–71

Müller C. 2013. Folate-based radiotracers for PET imaging-update and perspectives. *Molecules* 18: 5005–5031

Muzaffar F. Singh UK and Chauhan L. 2013. Review on microemulsion as futuristic drug delivery. *International Journal of Pharmacy and Pharmaceutical Sciences* 5(3): 39–53

Poeppel TD, Binse I, Petersenn S, Lahner H, Schott M, Antoch G, Brandau W, Bockisch A and Boy C. 2011. ^{68}Ga-DOTATOC versus ^{68}Ga-DOTATATE PET/CT in functional imaging of neuroendocrine tumors. *Journal of Nuclear Medicine* 52 (12): 1864–1870

Prata IM. 2012. Gallium-68: A new trend in PET radiopharmacy. *Current Radiopharmaceuticals* 5: 142–149

Sathekge M, Lengana T, Maes A, Vorster M, Zeevaart JR, Lawal I *et al.* 2018. ^{68}Ga-PSMA-11 PET / CT in primary staging of prostate carcinoma : preliminary results on differences between black and white South-Africans. *European Journal of Nuclear Medicine and Molecular Imaging* 45: 226–234

Shastry M, Kayani I, Wild D, Caplin ME, Visvikis D, Gacinovic S, Reubi JC and Bomanji JB. 2010. Distribution pattern of ^{68}Ga-DOTATATE in disease-free patients. *Nuclear Medicine Communications* 31: 1025–1032

Srirajaskanthan R, Kayani I, Quigley AM, Soh J, Caplin ME and Bomanji JB. 2010. The Role of ^{68}Ga-DOTATATE PET in patients with neuroendocrine tumors and negative or equivocal findings on ^{111}In-DTPA-octreotide scintigraphy. *Journal of Nuclear Medicine* 51: 875–882

Werner RA, Bluemel C, Allen-Auerbach MS, Higuchi T and Herrmann K. 2014. ^{68}Gallium- and ^{90}yttrium-/^{177}lutetium: 'Theranostic twins' for diagnosis and treatment of NETs. *Annals of Nuclear Medicine* 29: 1–7

Zhernosekov KP, Filosofov DV, Baum RP, Aschoff P, Bihl H, Razbash AA, Jahn M, Jennewein M and Rösch F. 2007. Processing of generator-produced ^{68}Ga for medical application. *Journal of Nuclear Medicine* 48: 1741–1748

Chapter 2: Literature Review

2.1 Prostate cancer

The prostate gland (Figure 2.1) is a small, round pea or walnut-sized (in adult life) gland that lies in the pelvic cavity in front of the rectum and slightly below the bladder (Kgatle *et al.*, 2016). The prostate gland is a gland found only in men and serves to produce seminal fluid that assists in transporting sperm during ejaculation (Kgatle *et al.*, 2016).

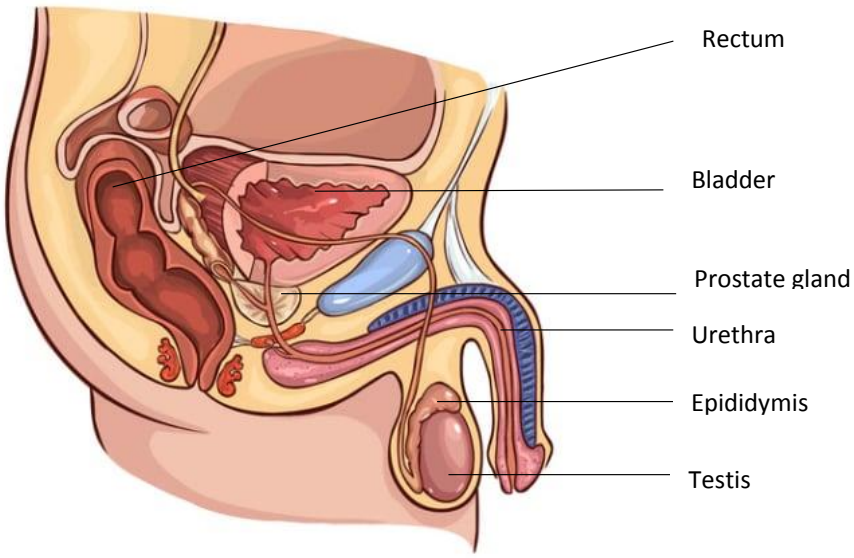

Figure 2.1: Diagram showing the position of the prostate gland in the male reproductive system

Prostate cancer is a type of cancer which begins when cells in the prostate gland start to grow uncontrollably (Kgatle *et al.*, 2016; Sathekge *et al.*, 2018(a)). It is caused by changes in the deoxyribonucleic acid (DNA) of normal prostate cells (Kgatle *et al.*, 2016). In normal cells, the fate of damaged DNA would normally result in cell death or its repair (Kgatle *et al.*, 2016). However, in cancer cells, the cells do not die or get repaired as they should be. These cells then continue replicating into cells that the body does not need (Kgatle *et al.*, 2016) and no longer function as healthy cells. Cancerous prostate cells exhibit the following; abnormal structure, uncontrolled growth and the ability to move to other parts of the body (invasive) (Kgatle *et al.*, 2016).

Prostate cancer is one of the most prevalent cancers in males worldwide and also one of the leading causes of morbidity and mortality globally (Emmett *et al.,* 2017; Zhu *et al.,* 2016) and also in South Africa (Sathekge *et al.,* 2018(a)). Epidemiological studies demonstrate vital differences in incidence and clinical behaviour of prostate cancer among patients in South Africa (Vorster *et al*., 2015; Sathekge *et al.,* 2018(a)). Race is a risk factor and the incidence and mortality rate in black men is almost twice that of white men (Sathekge *et al.,* 2018) and five times higher than that of Asian men (Hsing *et al.,* 2015; Tindall *et al.,* 2014;Vorster *et al*., 2015). Therefore black men are at higher risk of developing prostate cancer (Table 2.1) and often develop an aggressive type of prostate cancer (CANSA, 2016; Kgatle *et al.,* 2016; Sathekge *et al.,* 2018(a); Vorster *et al.,* 2015).

Table 2.1: The incidence of prostate cancer in South Africa according to the National Cancer Registry (CANSA, 2016).

Group - Males 2010	No of Cases	Lifetime Risk	Percentage of All Cancers
All males	4 652	1:27	17,15%
Asian males	144	1:32	19,65%
Black males	2 050	1:39	19,34%
Coloured males	518	1:21	16,22%
White males	1 940	1:15	15,39%

At a molecular level, the development of prostate cancer may be a result of a complex interaction between important genetic and cellular factors (Afaq *et al.,* 2018; Kgatle *et al.,* 2016; Vorster *et al.,* 2015).

2.2 Risk factors of prostate cancer

The risk factors of prostate cancer would be anything that affects the chances of a male getting the disease. Risk factors do not necessitate acquiring the disease. Some men may exhibit more than one risk factor and never get the disease whereas other men may have few or no known risk factors and still get cancer. Some of the known risk factors of prostate cancer are discussed in the following paragraphs.

2.2.1 Age

The chances of developing the disease increases as men become older. The risk rises after the age of 50 (Sathekge *et al.,* 2018(a)) with most cases of prostate cancer diagnosed in men over the age of 65 years (Kgatle *et al.,* 2016).

2.2.2 Race

Prostate cancer is reported to be more common in black or African men as compared to Asian and Caucasian males (Sathekge *et al.,* 2018(a)). It is likely that hormonal, dietary and molecular factors may contribute significantly to the racial disparity of prostate cancer in black African men (Sathekge *et al.,* 2018(a)). It is also suggested that the racial differences in the cancer profile may be the cause for faster prostate cancer growth and earlier transformation from indolent to aggressive prostate cancer in black men as compared to Caucasians (Sathekge *et al.,* 2018(a)). When looking at nationality, prostate cancer is less common in Asia, Central America and South America (Kgatle *et al.,* 2016). It is however, most common in North America, North-western Europe, Australia and the Caribbean Islands (American Cancer Society).

2.2.3 Family history

The risk of developing prostate cancer is most probably higher for men with several affected relatives, particularly a father or brother who was diagnosed at a young age (Kgatle *et al.,* 2016). The observation that prostate cancer seems to run in some families suggests that in some cases it may be inherited or genetically acquired (Kgatle *et al.*, 2016; Sathekge *et al.,* 2018(a)).

2.2.4 Nutrition and lifestyle

There are a few lifestyle choices that could either increase or decrease a person's chances of developing prostate cancer, such as smoking, high alcohol intake, exercise and a good diet (Kgatle *et al.*, 2016; Vorster *et al.*, 2015). With regards to smoking, most studies have not yet found the link between smoking and the risk of developing prostate cancer. Some studies have found that obese men have a higher risk of developing an aggressive form of prostate cancer

and dying from it, but have a lower risk of developing a less dangerous form of the cancer (Kgatle *et al.,* 2016). Men with a high consumption of red meat and /or high-fat dairy products have an increased chance of developing prostate cancer (Kgatle *et al.,* 2016). Processed food, whole-milk dairy products and fatty meat contain a lot of saturated fat which increases the production of testosterone, which may subsequently assist the growth of prostate cancer cells (Kgatle *et al.,* 2016).

2.3 Detection of prostate cancer

2.3.1 Signs and symptoms of prostate cancer

Prostate cancer does not always show any symptoms in its early stages, thus necessitating annual screening for early diagnosis. Advanced prostate cancer can cause some of the following symptoms (Kgatle *et al.,* 2016):

- Blood in the urine (haematuria)
- Impotence or difficulty getting an erection
- Difficulty urinating, increased urinating frequency especially at night and a slow or weak urinary stream
- Loss of bladder or bowel control
- Numbness or weakness in the legs and/or feet
- Pain in the chest (ribs), back (spine) and hips especially if the cancer has spread to bones

These symptoms may be caused by prostate cancer but can more often than not also be caused by other conditions that are not cancer, most commonly benign prostatic hyperplasia (BPH) (Kgatle *et al.,* 2016). Some of the symptoms are experienced as a result of the prostate gland becoming enlarged and pressing on and blocking the urethra and bladder (UCSF Medical Center; Kgatle *et al.,* 2016). This enlargement of the prostate happens as men age (Kgatle *et al.,* 2016).

2.3.2 Prostate-specific antigen test

The prostate-specific antigen test is usually used to detect prostate cancer early in men who may not have symptoms. It is however also one of the first tests which are done in patients who have symptoms that may be caused by prostate cancer (Sathekge *et al.,* 2018(a)). Prostate-

Specific Antigen (PSA) is a protein which is produced by prostate cells and is found in the blood (Sathekge *et al.,* 2018(a)). It represents both the volume of the normal and cancerous prostate cells (Kgatle *et al.,* 2016; Sathekge *et al.,* 2018(a)). The higher the level of PSA, the more likely it is that the person may have prostate cancer (Sathekge *et al.,* 2018(a); Vorster *et al.,* 2015). PSA test results are reported as nanograms per millilitre (ng/ml) (Kgatle *et al.,* 2016). In previous years, PSA results of 4.0 ng/ml or below were considered normal, and above 4.0 ng/ml were considered high (UCSF Medical Center). Recent research has shown that prostate cancer can be detected at all PSA levels, however, the chances of detecting prostate cancer increases as PSA increases (Kgatle *et al.,* 2016; Vorster *et al.,* 2015; Sathekge *et al.,* 2018(a)). PSA levels may also increase with age and prostate size (Sathekge *et al.,* 2018(a)). There are a few conditions or activities which can cause the production of high PSA, such as (Kgatle *et al.,* 2016):

- An acute urinary tract infection
- Benign prostatic hyperplasia
- Ejaculation up to three days prior to testing
- A recent prostate biopsy (the patient should wait at least six weeks after a prostate biopsy before testing for PSA levels)
- Prostatitis (an inflammation of the prostate that was treated successfully with antibiotics)
- Bicycle riding (very rare cases)

Similarly, low or normal PSA levels do not imply that prostate cancer is not present (Sathekge *et al.,* 2018(a)). Results from other tests such as a digital rectal examination (DRE), a colour Doppler transrectal ultrasound (TRUS), the percentage free-PSA and the PSA velocity should also be considered to make an assessment (Ebenhan *et al.,* 2015). Prostate cancer in some men produces very little PSA. There are certain herbal preparations and medication which may lower PSA levels and thus possibly mask the presence of prostate cancer, especially in its early stages of development (Kgatle *et al.,* 2016; UCSF Medical Center). These may include Estrogens, Finasteride (Proscar or Prospecia), Dutasteride (Avodart or Avocar), Saw palmetto (herb used to treat benign prostatic hyperplasia) and herbal mixtures such as Prostasol (UCSF Medical Center).

PSA tests are most commonly used for the early detection of prostate cancer but it also plays an important role in other situations (Vorster *et al.,* 2015). PSA tests are used to monitor the

effectiveness of prostate cancer treatment (during and after treatment) and should be done regularly after treatment (Kgatle *et al.*, 2016; Vorster *et al.*, 2015). The rise in PSA levels after surgery, radiation or during hormonal treatment could be an indication that the cancer is recurring or continuing to grow (Afaq *et al.*, 2018; Bouchelouche *et al.*, 2010; Vorster *et al.*, 2015). If the recurrence of the cancer happens early with a rapid rise in PSA after localised treatment, the more likely that the cancer cells were already distant from the site of the prostate (Afaq *et al.*, 2018; Vorster *et al.*, 2015; UCSF Medical Center).

2.3.3 Digital rectal examination

Digital rectal examination (DRE) is a physical examination of the prostate wherein a doctor inserts a gloved, lubricated finger into the male patient's rectum to feel for any irregular or abnormally hard areas in the prostate that might be cancer.

2.4 Diagnosis of prostate cancer

PSA and DRE are screening tests which cannot diagnose prostate cancer, but can indicate whether further tests to diagnose or confirm prostate cancer need to be done (Kgatle *et al.*, 2016). There are a few diagnostic tests which can be done (Table 2.2).

Table 2.2: Screening and diagnostic tests which are done to determine the presence of prostate cancer (derived from the American Cancer Society)

PC Test	What is it?	Additional Info
DRE	Insert finger into rectum	Not accurate detection
PSA test	Blood test	PC can be diagnosed even if PSA is in the normal range
TRUS	Insert probe into rectum to visualize prostate gland	Used to measure size of gland and detect tissue abnormalities
Prostate biopsy	Remove prostate tissue sample and examine under microscope	Urologist usually take 10-12 biopsies covering the entire gland
Bone scan	Tc-99m radioisotope is injected	Increased uptake of Tc-99m suggests presence of cancer
CAT scan	X-ray that shows both bones and soft tissue	Used to look at enlarged lymph nodes which may indicate the spread of PC
MRI scan	X-ray scan gives detailed images of the prostate and surrounding tissue	Useful in detecting/ determining disseminated cancer
PET scan	Similar to a bone scan, using radioactive F-18	More sensitive and shorter scan times

* PC: Prostrate Cancer, DRE: digital rectal exam, PSA: prostate specific antigen, TRUS: transrectal ultrasound, CAT: computerized axial tomography, MRI: magnetic resonance imaging, PET: positron emission tomography

2.4.1 Transrectal ultrasound

Transrectal ultrasound (TRUS) is a diagnostic technique which uses sound waves to create an image of the prostate. A probe which gives off sound waves is inserted into the rectum of the patient (Bouchelouche *et al.,* 2010). The probe picks up echoes which are created by the prostate when it receives the sound waves from the probe (Bouchelouche *et al.,* 2010). A computer then creates the pattern of echoes into an image of the prostate, which is viewed on a video screen.

The procedure takes less than 10 min. This test is done when high PSA levels are detected, when the DRE results are abnormal, as a guide during some treatment methods such as brachytherapy (internal radiation therapy) or cryosurgery and it can be used to measure the size of the prostate gland (Bouchelouche *et al.,* 2010). TRUS is also used during a prostate biopsy to guide the needles into the correct area of the prostate (American Cancer Society; Bouchelouche *et al.,* 2010).

2.4.2 Prostate biopsy

A prostate biopsy is usually done when the results of a PSA or DRE test suggest the presence of prostate cancer and confirmation or a diagnosis needs to be made (Kgatle *et al.,* 2016). The procedure involves removing a sample of body tissue and viewing it under a microscope. During a TRUS examination test, a thin, hollow needle is inserted through the wall of the rectum into the prostate gland (Bouchelouche *et al.,* 2010). As the needle is removed, it contains a small cylinder of prostate tissue sample. This process is repeated about 6 to 18 times (Bouchelouche *et al.,* 2010). A biopsy usually takes 10 min and can be done in a doctor's rooms during consultation.

2.4.3 Bone scan

A bone scan is usually done where there are signs of increased PSA levels (>15 ng/ml) and aggressive cancer (Vorster *et al.,* 2015; UCSF Medical Center). It can also be done in cases of

bone pain, a large tumour and a high Gleason grade (a prostate cancer grading system) (Vorster *et al.,* 2015). Bone scans involve injecting radioactive material (radiotracers) into the body which will subsequently be taken up by diseased bone cells (Bouchelouche *et al.,* 2010). A special camera detects the radioactivity and creates an image of the skeleton. Disease bone scan images may suggest that metastatic cancer is present (Kgatle *et al.,* 2016; Vorster *et al.,* 2015). A bone scan may not detect very small metastases (Bouchelouche *et al.,* 2010).

2.4.4 Computerized axial tomography scan

A computerized axial tomography (CAT) scan can often help determine if prostate cancer has spread to nearby lymph nodes (Kgatle *et al.,* 2016). This procedure allows the use of a rotating x-ray beam to make a series of images of the body used to create a detailed cross-sectional image. These images display abnormally enlarged pelvic lymph nodes and/or the spread of the cancer to other organs (Bouchelouche *et al.,* 2010). Before a scan, a patient drinks or is injected with a contrast agent before the first set of images is taken, to help contrast the intestines from the tumours and other organs in the body. This test is usually done if PSA levels are elevated above 20 ng/ml, including evidence of a large tumour and/or a high Gleason grade (Sathekge *et al.,* 2018(a)). A CAT scan creates detailed images of soft tissue in the body. CAT scans, although like x-rays, take longer than regular x-ray acquisition (American Cancer Society).

2.4.5 Magnetic resonance imaging scan

Magnetic resonance imaging (MRI) scans produce clear images of the prostate and can tell whether the cancer has spread to the seminal vesicles or other nearby structures (Bouchelouche *et al.,* 2010). These scans give information which can be used in planning the treatment of the patient. MRI scans use the same principle as CAT scans except that they use magnetic fields rather than x-rays to create images of selected areas of the body. MRI is not really effective in diagnosing microscopic or very small cancers. Like CAT scans, MRI does not give useful information on newly diagnosed prostate cancer that may be confined to the prostate (Bouchelouche *et al.,* 2010). MRI scans often take up to an hour which is longer than a CAT scan (UCSF Medical Center).

2.5 Treatment for prostate cancer

The selection of treatment options for prostate cancer is dependent on a few factors, such as a patient's age, their general health status, the type of cancer, whether the cancer has spread or not and whether they have a previous history of prostate cancer treatment (Kgatle *et al.*, 2016). Current treatment options include radiation therapy, surgery, and chemotherapy, among others (Afaq *et al.*, 2018). Surgery and radiation treatment is reported to be quite effective in the early stages of prostate cancer (Afaq *et al.*, 2018; Xu *et al.*, 2014). However, and unfortunately, there is no effective treatment for prostate cancer which has metastasised (Emmett *et al.*, 2017; Sathekge *et al.*, 2018(a)). A brief discussion of the three standard treatment options for men with organ-confined prostate cancer follows. Other treatment options which are available will also be discussed later in this chapter.

2.5.1 Active surveillance

Active surveillance, also known as "watchful waiting" is the monitoring of the disease in selected patients (Bouchelouche *et al.*, 2010. Here, the prostate cancer is monitored regularly with PSA tests, clinic evaluation and prostate biopsies to ensure that the cancer does not become aggressive (Kgatle *et al.*, 2016). This is often recommended if the cancer does not cause any symptoms and is expected to grow very slowly. This form of treatment is often selected for men who have other health problems and are older. Older men who have the disease may never require treatment because prostate cancer generally spreads very slowly.

2.5.2 Surgery

Treatment through surgery involves removing the whole prostate, including the seminal vesicles through a procedure known as radical prostatectomy (Emmet *et al.*, 2017; Kgatle *et al.*, 2016). A surgeon makes skin incisions in the lower abdomen in order to remove the prostate (Afaq *et al.*, 2018).

2.5.3 Radiation therapy

Radiation treatment uses x-rays or gamma rays to kill cancer cells through either non-invasive or minimally invasive exposure to radiation. Table 2.3 shows the three main types of radiation

therapies that may be recommended. Each patient receives a treatment plan depending on their symptoms, their overall health and the nature of the cancer. Radiation therapy is usually opted for under the following conditions (Kgatle *et al.*, 2016; Sathekge *et al.*, 2018(a)):

- As treatment for low-grade cancer that is still confined to the prostate gland
- If the cancer was not completely removed or has recurred in the prostate area after surgery
- As part of treatment in conjunction with hormone therapy for cancer that has metastasised into nearby tissue
- If the cancer is advanced
- To reduce the size of the tumour and to give relief from possible future symptoms

External beam radiation and brachytherapy (internal radiation) are the main and most common types of radiation therapies used (Afaq *et al.*, 2018; Xu *et al.*, 2014). External beam radiation therapy allows the use of medication containing radiation to be injected into the body (Kgatle *et al.*, 2016).

Table 2.3: The three types of radiation therapy (UCSF Medical Center)

Prostate seed brachytherapy	• Implant small radioactive pellets or "seeds" into the prostate • Seeds deliver high doses of radiation to tumour cells • Used in conjunction with ultrasound to position seeds
High dose rate Radiation	• Catheters are attached to empty needles and placed in prostate • Highly radioactive source is temporarily placed into needles to deliver radiation to the prostate
External beam radiation	• Uses x-ray type machines called linear accelerator (PET, SPECT) • Allows the use of radioactive isotopes which emit protons and/gamma rays • Uses proton or gamma radiation to destroy tumour cells

*PET: positron emission tomography, SPECT: single photon emission computed tomography

2.6 Radiation theranostics

2.6.1 External beam radiation

External beam radiation also known as external radiation therapy (XRT) is radiation therapy which uses beams of high energy x-rays or electrons which are delivered by a linear accelerator to the region of the patient's tumour to treat or kill cancerous cells. This technique can be used as a diagnostic and treatment tool to cure early stage prostate cancer or to help relieve

symptoms of bone pain (if the cancer has already disseminated to bones) (Benešová *et al.*, 2015). To reduce side effects in patients, an accurate dose of the radiation needed is calculated and then the radiation beams are aimed at the outlined target in order to acquire images of the areas which are affected (Velikyan, 2014) by the prostate cancer. In most cases, doctors would rather give higher doses of radiation to the prostate gland while reducing the exposure of radiation to nearby healthy tissue.

2.6.1.1 Positron emission tomography

PET is an imaging technique in nuclear medicine which applies the use of radiotracers (or radiopharmaceuticals), a special camera and a computer to evaluate organ and tissue function (Boschi *et al*., 2013). PET detects early onset of a disease because it can identify body changes at a cellular level (Sathekge *et al.*, 2018(a); Velikyan, 2014). Nuclear medicine techniques, namely PET and/or positron emission tomography/computed tomography (PET/CT) imaging procedures, are non-invasive and painless (with the exception of intravenous (IV) injections) and are used to diagnose and evaluate medical conditions (Kgatle *et al.*, 2016; Velikyan, 2014). Positron emission is based on the theory that positrons undergo instant annihilation when they collide with an electron (*matter-antimatter annihilation*). This results in the production of two high-energy gamma rays that exit the scene of the annihilation in exactly opposite directions. For neutron deficient radionuclides, there are two possibilities of decay which are positron emission or electron capture. Positron decay is only possible if an energy of 1022 keV or more is available, otherwise electron capture will occur. In practice a surplus in energy is required before a large amount of the decay occurs by positron decay channel instead of electron capture. The neutrino is a particle with zero rest mass which shares its kinetic energy with the positron or the neutron. The positron is slowed down in the tissue by collisions: at the end of track a hydrogen like atom known as a positronium, is formed by the positron and an electron. The positron and electron are antiparticles and so they will annihilate. In the annihilation process, two gamma-quanta of 511 keV are generated in a back-to-back or co-linear manner. In this way both conservation laws are obeyed. A three-quanta annihilation is also possible within the two conservation laws. The three-quanta annihilation only happens if the formed positronium is in its triplet state, which is rare, with a half-life of 7 μs. In the single state the positronium decays with a lifetime of 8 ns. To image the annihilation radiation one should profit from its unique properties at 511 keV co-linear (180°).

Depending on the type of test and radiotracer being employed, the radiotracer is either inhaled as a gas, orally ingested or intravenously injected. This radiotracer then accumulates in organs or in the body and emits high energy radiation (Weineisen *et al.,* 2015). The radiation is subsequently detected by an imaging device (or camera) that produces images which provide molecular information (Weineisen *et al.,* 2015). In recent times PET images have been superimposed with computed tomography (CT) (Ebenhan *et al.,* 2017; Sathekge *et al.,* 2018(b)) or magnetic resonance imaging (MRI) through what is known as image fusion, to allow information from two different tests to be correlated and interpreted on a single image (Velikyan, 2014). Fused images supposedly give better information leading to a more accurate diagnosis (Ebenhan *et al.,* 2018). Additionally, bimodal systems such as PET/CT and PET/MRI are more effective due to the combination of the functional image of PET with the morphological image of CT or MRI.

PET scans would thus provide information on organ or body functions (i.e. blood flow, oxygen consumption and glucose metabolism) (Sathekge *et al.,* 2018(a)). This would, for example provide information on the activity of an organ. CT scans produce multiple images of the inside of the body. This technique provides anatomic or morphological information (i.e. the location, size and shape of an organ).

Before a new drug is administered in patients, a lot of data has to be collected from animal studies to obtain information such as dose, route of administration, biodistribution of the drug, point of excretion and toxicity. Animal model-based research therefore pose a demand for a small animal PET for collection of data for medical research (Yao *et al.,* 2012). Small animal PET, well known as microPET, is a technique used for the imaging of small animals such as mice and rats using a small, high resolution PET scanner to identify critical or target organs. Mice and rats can host a number of human diseases, which make them ideal subjects for animal studies (Yao *et al.,* 2012). In recent times, detection of prostate cancer lesions using PET imaging of the prostate specific membrane antigen (PSMA) has been extensively studied with respect to its clinical impact (Eder *et al.,* 2014; Sathekge *et al.,* 2018(a)). PSMA serves as or is a cell surface target which is suitable for imaging metastatic lesions because it is expressed in almost all prostate cancer cells (Afaq *et al.,* 2018; Schäfer *et al.,* 2012). This will be discussed in more detail later in this chapter.

There are a few common uses for PET and PET/CT procedures (Afaq *et al.*, 2018; Sathekge *et al.*, 2018(a); UCSF Medical Center), namely to:

- Detect cancer
- Determine whether a cancer has disseminated
- Determine if a cancer has recurred
- Determine blood flow to and from the heart
- Assess the efficiency of a cancer treatment plan
- Map out heart function and the brain
- Evaluate brain abnormalities and other nervous system disorders

2.6.2 Radiotracers used for PET

In cases of metastatic, poorly differentiated and hormone-refractory carcinoma, there is a demand for more effective treatment options (Benešová *et al.*, 2015). Prostate cancer targeting based on low molecular weight radio-ligands could possibly offer much more accurate and rapid visualisation, improved staging and effective radiotherapy (Benešová *et al.*, 2015). Based on small molecules, a few PET radiotracers have been investigated for prostate cancer imaging, namely fluorine-18 (^{18}F) (Vorster *et al.*, 2015), carbon-11 (^{11}C) and peptidyl radiotracers based on the gastrin-releasing peptide receptor and PSMA (Benešová *et al.*, 2015). Gallium (III) (Ga(III)) complexes are becoming a favourable alternative to iron (III) (Fe(III)) complexes as PET based anticancer agents because of their similarities (Banerjee *et al.*, 2010). Positron-emitting versions of Ga(III) can be employed in tumour imaging for cancer diagnostic purposes (Sathekge *et al.*, 2018(a)). Gallium-68 (^{68}Ga)-labelled peptides have attracted interest in cancer imaging as a result of the physical characteristics of the isotope (Table 2.4) (Banerjee *et al.*, 2010; Sathekge *et al.*, 2018(a); Velikyan, 2014).

Table 2.4: Some commonly used radionuclides used in radiotherapy, PET and SPECT, including their decay properties and mode of production (Velikyan, 2014)

Radionuclide	Half-life	E_{max} (keV)	Radiation	Production
Positron emitters				
^{11}C	20.3 min	961	β^+ (100 %)	Cyclotron
^{64}Cu	12.8 h	656	β^+ (19 %)	Cyclotron
^{18}F	110 min	634	β^+ (97 %)	Cyclotron
^{66}Ga	9.5 h	4153	β^+ (56 %)	Cyclotron
^{68}Ga	67.6 min	1899, 770	β^+ (89 %)	Generator
^{124}I	4.17 d	2100	β^+ (23 %)	Cyclotron
Gamma emitters				
^{67}Ga	78.26 h	91, 93, 185, 296, 388	γ	Cyclotron
^{111}In	67.9 h	245, 172	γ	Cyclotron
^{99m}Tc	6.0 h	141	γ	Generator
Therapeutic radionuclides				
^{125}I	60 d	350	Auger electrons	Reactor
^{131}I	8.0 d	1810	β^-	Fission
^{177}Lu	6.71 d	500	β^-	Reactor
^{90}Y	64.0 h	2270	β^-	Generator

2.6.2.1 Gallium-68

^{68}Ga is easily available from a portable in-house $^{68}Ge/^{68}Ga$ generator (Ebenhan *et al.*, 2017). ^{68}Ga is a convenient alternative to cyclotron-based isotopes such as ^{18}F and ^{124}I, especially because it is readily available (Umbricht *et al.*, 2017). Germanium-68 (^{68}Ge) has a half-life of 270.8 days (Banerjee *et al.*, 2010; Velikyan, 2014). ^{68}Ga emits positron decay (89 % of its total decay by β^+ emission) (Banerjee *et al.*, 2010; Müller, 2013). The maximum positron energy of ^{68}Ga is 1.92 MeV (mean = 0.89 MeV), which is higher than that of ^{18}F ($E_{\beta max}$ = 0.63 MeV; mean = 0.25 MeV) (Banerjee *et al.*, 2010). The low energy of ^{68}Ga positron emission ($E_{\beta max}$ = 635 keV; 2.2 mm mean range in matter) serves as an advantage for better resolution of PET images and quantification of biochemical processes *in vivo* (Malik *et al.*, 2015). ^{68}Ga has a half-life of 68 min (Malik *et al.*, 2015). There is, however drawbacks to

using ^{68}Ga eluate for the radiolabelling of peptides which include breakthrough of the long-lived parent radionuclide ^{68}Ge, the high HCl concentration (0.1-1 M used for ^{68}Ga elution) and the high eluate volume (Boschi *et al.*, 2013). Subsequently, there are metallic impurities such as Fe^{3+} (from the column material) and Zn^{2+} (by-product of the decay of ^{68}Ga, Ti^{4+}) which could be present in the eluate (Boschi *et al*., 2013) and ultimately result in lowered specific activity and yield of ^{68}Ga. Impurities affect the yield of ^{68}Ga and the specific activity of the labelled product. One of the ways to reduce impurities would be to fractionate the eluate since about two-thirds of the total ^{68}Ga activity elutes within a 1-2 ml activity peak (Boschi *et al*., 2013; Mokaleng *et al.*, 2015). The Ga(III) ion forms a stable complex (formation constant $\log K_{ML} = 21.33$) with DOTA, which is commercially available (Mokaleng *et al.*, 2015).

2.7 Alternative treatment

Table 2.5 shows a summary of other treatment options which are used for prostate cancer therapy. Like most treatment methods, these aim to kill or slow down the growth of prostate cancer cells and may probably offer benefits with less side effects. Some of these treatments are only available through clinical trials that are designed to test their effectiveness as compared to currently available treatment options.

Table 2.5: Alternative prostate cancer treatment options (UCSF Medical Center)

Chemotherapy	• Drugs are injected intravenously to stop growth of cancer cells • Used in cases where cancer has metastasized • Treatment is given in cycles over a few days or weeks
Cryotherapy	• Treat localized prostate cancer by freezing the cancerous cells • Procedure performed under general/ spinal anaesthesia • Probes are inserted through anus
ADT/ Hormone therapy	• Reduce androgen (testosterone) levels using oral or injected medications (chemical castration) • This does not cure PC, it stops or slows growth of PC cells

*ADT: androgen deprivation therapy

2.8 Prostate specific membrane antigen

Prostate specific membrane antigen (PSMA) is a type of protein (Table 2.6) which is expressed in all forms of prostate cells and carcinoma (Sathekge *et al.*, 2018(a)). It is a transmembrane glycoprotein glutamate carboxypeptidase II (GCPII) (Malik *et al.*, 2015; Wiehr *et al.*, 2014),

characterised by the murine monoclonal antibody (mAb) 7E11-C5.3 (Chang 2004; Wiehr *et al.*, 2014). It is considered an ideal protein for LNCaP and PC-3 prostate cancer cell line targeting drug delivery studies because of its overexpression in prostate cancer cells (Malik *et al.*, 2015).

Table 2.6: A comparison between prostate specific antigen and prostate specific membrane antigen (Chang, 2004)

PSA	**PSMA**
• Secretory protein • Known function: liquefaction of semen • Measured in blood as a cancer marker • Decreased with androgen deprivation	• Integral membrane protein • Several enzymatic functions • Upregulated with androgen deprivation • RT-PCR is used to detect it in blood: not verified as screening tool or marker • Expression correlates with cancer aggressiveness and represents an independent indicator of poor prognosis

*RT-PCR: reverse transcriptase polymerase chain reaction

PSMA has a three-part structure (Figure 2.2) composed of a 707-amino acid external portion, a 24-amino acid transmembrane and a 19-amino acid internal portion (Chang, 2004). PSMA is found on the short arm of chromosome 11 (Chang, 2004). One of the functions of PSMA is it catalyses the hydrolysis of N-acetyl-L-aspartyl-L-glutamate (NAAG) into N-acetyl-L-aspartate (NAA) and L-glutamine (Baur *et al.*, 2014; Sathekge *et al.*, 2018(a)).

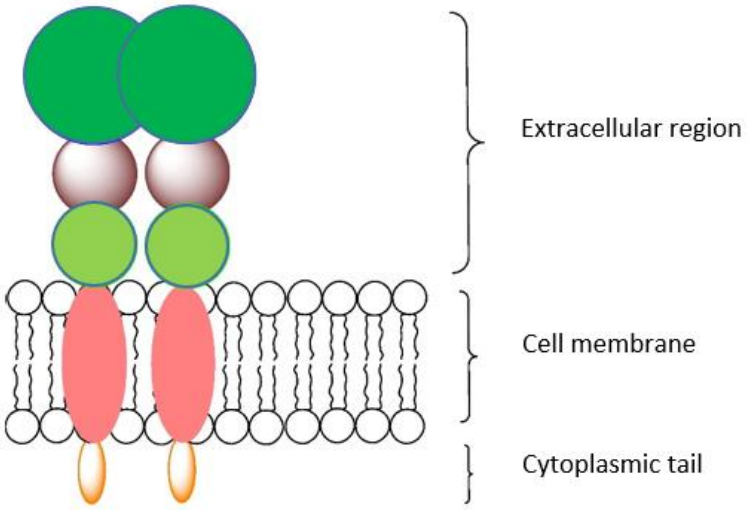

Figure 2.2: A schematic representation of prostate membrane antigen

Similar to PSMA, PSA is a glycoprotein enzyme encoded in humans by the KLK3 gene (Chang, 2004; Kgatle *et al.,* 2016). It is also known as gamma-seminoprotein or kallikrein-3 (KLK3) (Chang, 2004; Kgatle *et al.,* 2016). This protein is a member of the kallikrein-related peptidase family and secreted by the epithelial cells of the prostate gland (Chang, 2004; Kgatle *et al.,* 2016). PSA is not a reliable or effective biomarker for prostate cancer, especially in recurrent prostate cancer (Sathekge *et al.,* 2018(a); Wiehr *et al*., 2014). In most cases, the recurrence of prostate cancer is detected by a rise in PSA levels in the blood. However, PSA as a biomarker cannot distinguish between recurrent and metastatic prostate cancer (Sachpekidis *et al.,* 2016). PSMA however, has been demonstrated to be a great target for prostate cancer imaging and therapy (Sachpekidis *et al.,* 2016; Wiehr *et al.,* 2014).

2.8.1 PSMA applications

PSMA is overexpressed in prostate cancer cells compared to other PSMA-expressing organs (example kidneys, small intestines, salivary glands) (Afshar-Oromieh *et al.,* 2015; Sathekge *et al.*, 2018(a)). It is overexpressed in metastatic, poorly differentiated and hormone-refractory prostate cancer (Benešová *et al.,* 2015). This activity therefore makes PSMA a promising target for prostate cancer-specific imaging and treatment (Afshar-Oromieh *et al*., 2015; Kgatle *et al.,* 2016; Schäfer *et al.,* 2012). This type of approach requires selectively targeting PSMA with small molecules with a positron emitting radionuclide for the diagnosis of prostate cancer

with PET (Baur *et al.*, 2014). PSMA has great potential for high dose radiotherapy with minimal radioactivity related side effects because of PSMA's low expression in healthy cells (Afaq *et al.*, 2018; Benešová *et al*., 2015).

2.8.2 PSMA-targeted radiotherapy

PSMA-expressing tumours can be imaged with the use of ^{68}Ga-labelled PSMA-targeted radioligands such as Glu-NH-CO-NH-Lys-(Ahx)-[^{68}Ga(HBED-CC)] (^{68}Ga-DKFZ-PSMA-11) (Benešová *et al.*, 2015; Zhu *et al.*, 2016). ^{68}Ga-DKFZ-PSMA-11, most commonly referred to as ^{68}Ga-HBED-CC-PSMA has shown high diagnostic lesion detection efficacy (Sterzing *et al.*, 2016) as compared to other PET tracers such as ^{18}F-FDG and ^{11}C or ^{18}F-choline tracers (Zhu *et al.*, 2016). ^{68}Ga-HBED-CC-PSMA can also be used to detect lymph node metastases (Eder *et al.*, 2012; Zhu *et al.*, 2016). ^{68}Ga-DKFZ-PSMA-617 (also referred to as [^{68}Ga]Ga-PSMA-617) is also a theranostic precursor of prostate cancer containing the DOTA chelator (Eder *et al.*, 2014; Zhu *et al.*, 2016) which has a high binding affinity to PSMA. It is also demonstrated to highly contrast prostate cancer lesions (Zhu *et al.*, 2016). DOTA forms unique, thermodynamically and kinetically stable complexes when labelled with radionuclides such as ^{68}Ga (Eder *et al.*, 2014; Zhu *et al.*, 2016).

Theranostic approaches allow diagnosis and therapy to be done by the same targeting molecule by labelling it with a radionuclide that would allow both diagnostic and therapeutic outcomes. The most common examples of radionuclides used for theranostic applications are β-emitters such as ^{131}I, ^{177}Lu and ^{90}Y (Benešová *et al*., 2015), which are appropriate radiotracers for systemic radionuclide therapy. A theranostic compound should consist of three components, namely, glutamate-urea-lysine (PSMA), a radiotracer/radionuclide (^{68}Ga, ^{177}Lu, ^{131}I), and a chelator DOTA (or HBED-CC) (Figure 2.3) which is able to chelate both ^{68}Ga and ^{177}Lu (Benešová *et al*., 2015).

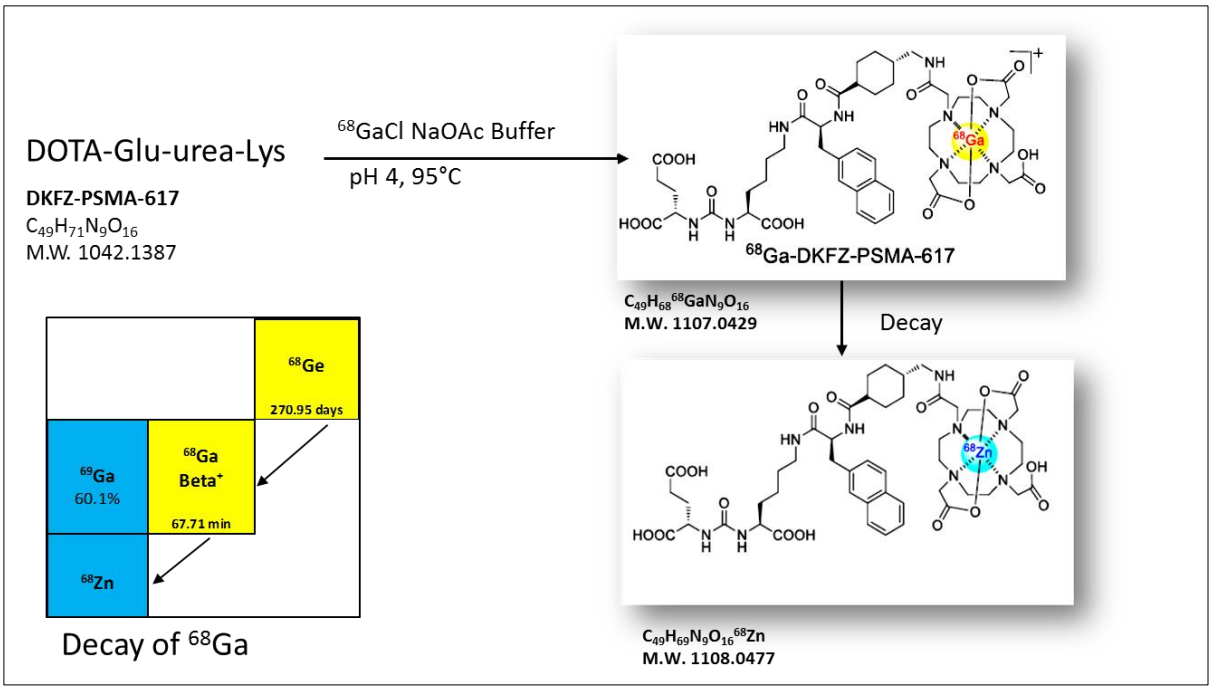

Figure 2.3: An illustration of the radiolabelling and decay of [^{68}Ga]Ga-PSMA-617. The line box shows the decay properties of the relative radionuclide

The application of ^{177}Lu and ^{90}Y is favoured in radionuclide based therapeutic approaches (Baur *et al.*, 2014). ^{90}Y ($E_{\beta max}$ = 2.3 MeV; $t_{1/2}$ = 64 h) is much more suitable for the treatment of large tumours, whereas^{177}Lu is appropriate for treatment of small tumour lesions and metastases (Baur *et al.*, 2014). For both diagnostic and treatment applications, DOTA is the most commonly used chelator for chelation of radionuclides such as ^{68}Ga, ^{177}Lu and ^{90}Y to small molecules (Baur *et al.*, 2014). DOTA, however has some disadvantages when it comes to therapy. Labelling of DOTA to radiometals is usually done at high temperatures, under acidic conditions, and prolonged time periods (Baur *et al.*, 2014). An ideal labelling procedure should be simple, fast and at room temperature with a neutral pH. The chelator should also provide stability *in vivo*. Unfavourable kinetics in the chelation of radiometals and immunogenicity in humans has also been reported (Baur *et al*., 2014).

The effective dose and duration of administration of diagnostic or therapeutic radiopharmaceuticals for prostate cancer is a challenge due to the systemic toxicity and lack of sufficient targeting to tumour cells. There is therefore a medical need to develop effective drug delivery systems that selectively carry anti-tumour radiopharmaceuticals into tumour tissues. Delivery systems (i.e. micelles, liposomes and polymeric nanoparticles) have been reported to demonstrate an improved therapeutic index with reduced side effects (Mehta *et al*., 2016; Xu

et al., 2014). In this study, the purpose is to develop PSMA-targeted nano-sized microemulsion (ME) delivery systems for prostate cancer diagnosis and therapy.

2.9 Colloidal systems: Microemulsions

2.9.1 Introduction

Like most delivery systems, MEs were designed and developed for the purpose of potential drug targeting and improving the efficacy of new and already existing drugs (Melariri *et al.*, 2015). MEs have become widely investigated in pharmaceutical research due to their high capacity for drugs (Mehta *et al.*, 2016). MEs are homogenous dispersions of water and oil, which are transparent and stabilised by the addition of large amounts of surfactant and co-surfactant (Figure 2.4) (Mehta *et al.*, 2016). They appear transparent and are thermodynamically stable isotropic mixtures (Lopes, 2014; Nirmala and Nagarajan, 2016) of oil-in-water (o/w) or water-in-oil (w/o) (Moghimipour *et al.*, 2013). These MEs are formed spontaneously by mixing the oil and water phases with selected surfactants. MEs are often referred to as swollen micelles, solubilised oil, transparent emulsions and micellar solutions (Mehta *et al.*, 2016). MEs are also defined by a particle size of less than 150 nm in diameter (Gundogdu *et al.*, 2013; Lopes, 2014).

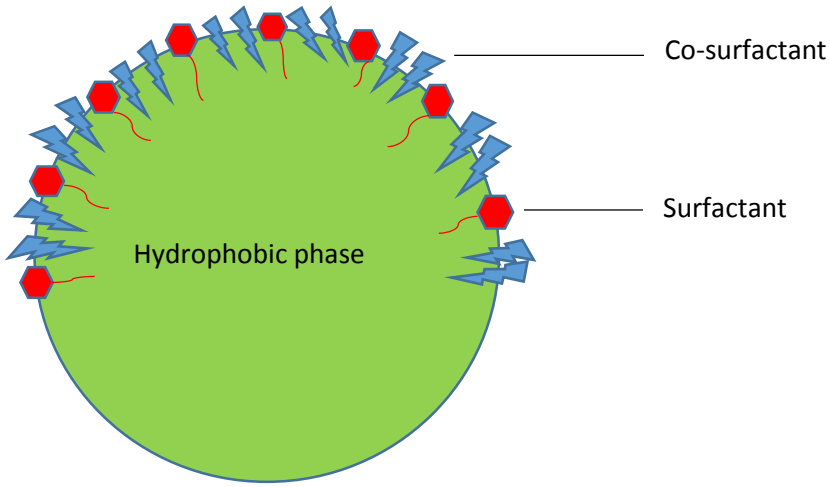

Figure 2.4: The structure of a microemulsion

MEs are different from emulsions and nanoemulsions. Emulsions are coarse and milky (turbid) dispersions with a droplet size larger than that of MEs (Lopes, 2014). Emulsions are not

thermodynamically stable and will therefore experience phase separation (Tadros, 2013). They are however kinetically stable (Lopes, 2014). MEs form spontaneously with low energy input under the right conditions (Mehta *et al.*, 2016). Nanoemulsions and MEs appear to be similar, thus the need to define them and their differences. Both these systems have low viscosity with an internal droplet size in the nano-range, smaller than 250 nm (Lopes, 2014). Nanoemulsions, however, are not thermodynamically stable but rather kinetically stable (Mehta *et al.*, 2016). They also require smaller amounts of surfactants and/or co-surfactants to form but with a higher energy input compared to MEs (Lopes, 2014). These differences are summarised in Table 2.7.

Table 2.7: A comparison of microemulsions, nanoemulsions and emulsions

Parameter	**Microemulsion**	**Emulsion**	**Nanoemulsion**
Dispersion type	Colloidal	Coarse	Colloidal
Internal droplet size (nm)	Up to 150	Above 500	Up to 250
Thermodynamic stability	Stable	Not stable	Not stable
Formation	Spontaneous	Require energy	Require energy
Composition	Requires large amounts of surfactants	Require less surfactants	Require less surfactant
Visual characteristics			
Consistency	Fluid	Fluid/Semi solid	Fluid
Turbidity	Transparent	Turbid	May vary

2.9.2 Types of microemulsions

There are four types of ME phases (referred to as Winsor phases), which are formed under defined conditions (Mehta *et al*., 2016). Different types of MEs are formed depending on the composition, ratio among compounds, and arrangements of the molecules.

2.9.2.1 O/W microemulsion or Winsor I

In o/w MEs (Winsor I), droplets of oil are surrounded by a surfactant and/or co-surfactant film that forms the internal phase dispersed in water (continuous phase), resulting in an oil-in-water ME. O/W MEs have a bigger interactive volume as compared to w/o MEs (Mehta *et al.,* 2016).

2.9.2.2 W/O microemulsion or Winsor II

W/O microemulsions (Winsor II) are also known as reverse micelles. The polar heads of the surfactant are directed into the water droplets, with the fatty acid tails directed into the oil phase (Mehta *et al.,* 2016). The continuous phase here is formed by the oil which surrounds the aqueous droplets. A water-in-oil ME which is administered parenterally or orally, may become destabilised by the aqueous biological system (Mehta *et al.,* 2016).

2.9.2.3 Bicontinuous microemulsion or Winsor III

In bi-continuous MEs (Winsor III) the amount of water and oil present in the system are the same. Therefore both the water and oil exist as a continuous phase (Ishikawa *et al.,* 2016). Transitions from o/w to w/o MEs may pass through the bicontinuous phase. This type of ME may exhibit non-Newtonian flow and plasticity (Mehta *et al.,* 2016).

2.9.2.4 Single phase homogenous mixture or Winsor IV

In single phase homogeneous mixtures (Winsor IV), the water, oil and surfactants are homogeneously dispersed. On addition of a sufficient amount of surfactant plus alcohol (amphiphile), a micellar, single-phase solution is formed (Bhattacharya *et al.,* 2016)

2.9.3 Advantages of microemulsions

MEs offer numerous advantages over other dosage systems as drug delivery systems. The following are some of the advantages (Bhattacharya *et al*., 2016; Gundogdu, 2013; Lopes, 2014; Mehta *et al.,* 2016; Moghimipour *et al.,* 2013):

- They are thermodynamically stable and therefore need minimal energy to formulate

- MEs can encapsulate both hydrophilic and lipophilic drugs
- They can act as super solvent for poorly soluble drugs
- They increase the bioavailability of the encapsulated drug
- They are easy to formulate and scale-up
- MEs allow for various drug administration routes, for instance oral, IV and topical
- Liquid dosage forms increase patient compliance
- MEs have a low viscosity compared to primary and multiple emulsions
- The formation of MEs is reversible
- They provide protection against hydrolysis and oxidation of the drug in the biological environment
- MEs as drug delivery systems allow controlled drug release and targeting
- MEs have a penetration enhancing ability
- Formulation of MEs is of low cost because no specialised equipment is used
- MEs eliminate variability in absorption
- They increase the rate of absorption
- They have a long shelf-life
- They improve the efficacy of the drug, therefore allowing the total dose to be reduced and thus reducing side effects of the drug

2.9.4 Disadvantages of microemulsions

- MEs require sufficient amounts of surfactants to stabilise the droplets
- MEs have limited capacity to solubilise high melting substances
- The stability is also influenced by pH and temperature
- They cannot be encapsulated in soft or hard gelatine because of their water content
- The surfactants and co-surfactants should be non-toxic, and the concentration kept as low as possible to avoid *in vivo* toxicity
- MEs have the potential of phase-separation as a result of pH and temperature (Bhattacharya *et al*., 2016; Mehta *et al.,* 2016):

2.9.5 Preparation of microemulsions

2.9.5.1 Phase titration method

The phase titration method of ME formulation is also known as the spontaneous emulsification method, which can be depicted with the help of phase diagrams (Bhattacharya *et al.*, 2016). MEs are formed depending on the concentration and chemical composition of each constituent, namely water, oil and surfactants. A pseudoternary phase diagram (Figure 2.5) is used to find the different zones forming MEs, in which each corner of the diagram represents 100 % either oil, water and surfactant or co-surfactant as constituents (Mehta *et al.*, 2016). The region may be defined into w/o or o/w ME depending on the composition (whether it is rich in oil or water) (Mehta *et al.*, 2016).

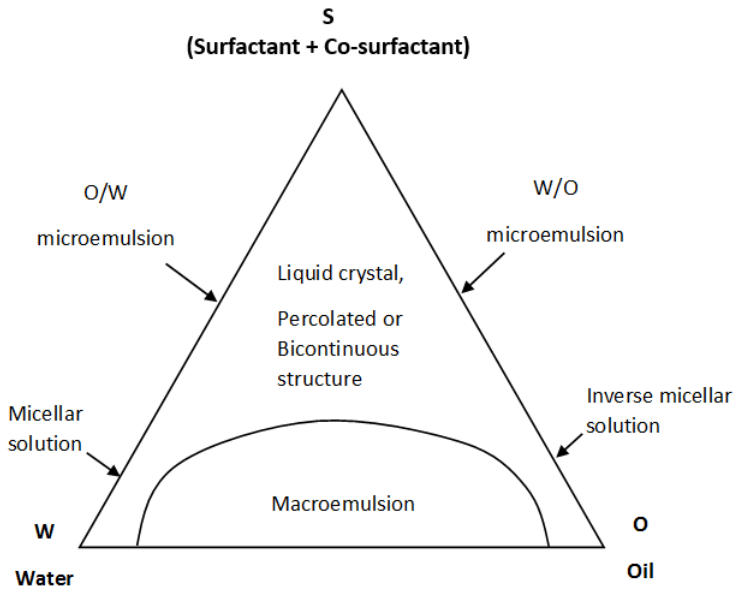

Figure 2.5: Pseudoternary phase diagram

2.9.5.2 Phase inversion method

A ME which is formed as a result of phase inversion exhibits physical changes such as particle size, which can further affect the *in vitro* and *in vivo* drug release (Bhattacharya *et al.*, 2016). Phase inversion may occur due to a change in temperature or the addition of excess water or oil to the dispersed phase. Changing the temperature of a system of non-ionic surfactants can influence the transition of the system from an o/w ME at low temperatures to a w/o ME at

higher temperatures. This transition of the system is also known as the phase inversion temperature method (Bhattacharya *et al.,* 2016). When the system is cooled, it crosses a point of zero spontaneous curvature and minimal surface tension, which promotes the formation of finely dispersed oil particles (Bhattacharya *et al.,* 2016; Mehta *et al*., 2016). Other parameters, however, may also influence phase inversion of the ME, such as pH, concentration of surfactants and changing the aqueous volume fraction. For instance, if water is successfully added into oil, water droplets are initially formed in a continuous oil phase. Increasing the water volume fraction could change the spontaneous curvature of the surfactant from stabilising a w/o ME to an o/w ME at the inversion locus (Bhattacharya *et al.,* 2017). The surfactants form flexible monolayers at the o/w interface resulting in a bicontinuous ME at the inversion point (Bhattacharya *et al.,* 2016). From Figure 2.5 it becomes clear that when the oil concentration is very high, the surfactant forms reverse micelles capable of solubilising more water in their hydrophilic interior.

2.9.6 Characterisation of microemulsions

MEs are very complex systems with various components involved in their makeup, therefore rendering limitations in their methods of characterisation. MEs are difficult to characterise, however sufficient knowledge of their characteristics is important for their commercialisation. Hence, a combination of various techniques is required to obtain a view of the structure and the physicochemical properties of the ME.

For the characterisation of physicochemical properties of MEs, the basic components are (Bhattacharya *et al.,* 2016):

- Morphology
- Phase stability and behaviour
- Interaction and dynamics
- Particle size, charge and the specific area

The particle size and the interactions and dynamics are important parameters to consider when characterising. Drug release from MEs depend greatly on these parameters, including oil/water phase ratio, distribution of the drug in the phases of the ME system and the rate of diffusion or absorption in both phases (Mehta *et al.,* 2016).

2.9.7 Factors affecting phase formation

There are a few parameters which may affect the formation of o/w or w/o MEs. Namely the properties of the surfactant, the type and nature of co-surfactant, the oil phase, temperature, the chain length, and the packing ratio (Bhattacharya *et al.*, 2016).

2.9.7.1 Surfactant

The nature of the surfactant determines the type of ME that is ultimately formed. They contain a hydrophilic head and lipophilic tail (Muzaffar *et al.*, 2013). When a high concentration of a surfactant is used, the degree of dissociation of polar groups decreases, resulting in a w/o type of ME system. Addition of water into the system may increase the degree of dissociation resulting in an o/w system.

Alcohols such as ethanol are commonly used as co-surfactants. Short chain co-surfactants give a positive curvature effect. This happens due to the presence of alcohol causing the head region to swell up. The ME system, hence becomes more hydrophilic therefore becoming an o/w system (Bhattacharya *et al.*, 2016). Long chain surfactants form w/o systems because of the alcohol which causes more swelling in the tail region than in the head region (Muzaffar *et al.*, 2013).

2.9.7.2 Oil phase

The oil composition can influence curvature by penetrating the lipophilic region of the surfactant monolayer (Mehta *et al.*, 2016). This results in increased negative curvature (Muzaffar *et al.*, 2013).

2.9.7.3 Temperature

Temperature influences ionic surfactants, therefore causing increased surfactant counter-ion dissociation (Bhattacharya *et al.*, 2016). Temperature helps determine the effective head group size of non-ionic surfactants. At high temperatures, surfactants are lipophilic and form w/o

MEs. At low temperatures, they form hydrophilic o/w ME systems. At an intermediate temperature, a ME forms a bicontinuous system.

2.9.7.4 Packing ratio

The type of ME that is formed is defined by the hydrophilic-lipophilic balance (HLB) of the surfactant by its effect on film curvature and packing (Mehta *et al.,* 2017).

2.9.8 Factors affecting behaviour of microemulsions

There are factors which may cause particle size changes and transition of the ME system. These factors are pH, alcohol concentration, nature of oil, ionic strength, salinity and surfactant hydrophobic chain strength (Bhattacharya *et al.,* 2016).

A change in the pH of a system can influence pH sensitive surfactants. Phase behaviour can change from w/o to o/w in the presence of amines and carboxylic acids when the pH is increased (Muzaffar *et al.,* 2013).

Phase titration from w/o to bicontinuous to o/w type ME may occur when low molecular weight alcohols are used (Bhattacharya *et al.,* 2016).

When ionic strength in the system increases, the ME changes from an o/w to w/o ME in equilibrium with excess water (Muzaffar *et al.,* 2013).

Salinity affects the droplet size and may also cause the oil to solubilise more in the case of o/w MEs (Bhattacharya *et al.,* 2016). In the case of o/w MEs, the droplet size increases when the salinity is low. If the salinity is increased, complete phase transition occurs resulting in a decreased droplet size (Bhattacharya *et al.,* 2016).

Increasing the hydrophobic chain length of the surfactant would transition the system from an o/w to a w/o ME via a bicontinuous phase (Muzaffar *et al.,* 2013).

2.9.9 Applications of microemulsions as drug delivery systems

MEs allow controlled and sustained drug release through various routes of administration, namely oral (Nirmala and Nagarajan, 2016), parenteral, transdermal (Lopes, 2014), topical (Lopes, 2014), percutaneous, nasal and ocular (Mehta *et al.*, 2016; Muzaffar *et al.*, 2013). Muzaffar *et al*. (2013) concluded that irrespective of the various routes of administration, there is a lack of toxicological evaluation of ME formulations (Muzaffar *et al.*, 2013). The various routes of drug delivery of MEs are briefly discussed below.

2.9.9.1 Oral delivery

Formulation of effective orally delivered MEs is a challenge because drug efficacy can be restricted by poor solubility and instability of the ME in the gastrointestinal fluid. MEs have the potential to improve the bioavailability of poorly water soluble drugs (Muzaffar *et al.*, 2013). Hydrophilic drugs can be encapsulated with varying solubility due to the presence of polar, non-polar and interfacial domains (Muzaffar *et al.*, 2013). MEs protect the incorporated drug from enzymatic degradation and oxidation and enhance membrane permeability. Currently, some commercially available ME formulations include, Fortovase® (Saquinavir), Norvir® (Ritonavir) and Sandimmune Neoral® (Cyclosporine A) (Muzaffar *et al.*, 2013).

2.9.9.2 Parenteral delivery

The development of parenteral dosage forms of hydrophilic and lipophilic drugs is a challenge (Mehta *et al.*, 2016). O/W MEs for parenteral administration have a higher physical stability in plasma than liposomes and other drug delivery systems (Muzaffar *et al.*, 2013).
The internal oil phase is also more resistant to the incorporated drug leaching out. Some partially soluble drugs have been formulated into o/w MEs for parenteral delivery using the parenterally acceptable co-surfactants polyethylene glycol 400, polyethylene glycol 660, 12-hydroxystearate, or ethanol (Muzaffar *et al.*, 2013). Maintaining a flexible surfactant film and spontaneous curvature near zero with the application of the latter, co-surfactants was able to obtain a balanced middle phase ME (Muzaffar *et al.*, 2013).

2.9.9.3 Topical delivery

Topical administration of a drug allows for direct delivery and targeting to the affected areas of the skin or eyes. This mode of drug administration bypasses hepatic first-pass metabolism and drug degradation in the stomach and related toxicity effects (Mehta *et al.,* 2016). Topical MEs are able to encapsulate both hydrophilic and lipophilic drugs and improve their permeation. Examples of hydrophilic drugs are apomorphine hydrochloride, diphenhydramine hydrochloride, tetracaine hydrochloride, 5-flurouracil and methotrexate (Muzaffar *et al.*, 2013). Lipophilic drugs which can be incorporated in topical MEs are estradiol, felodipine, finasteride, ketoprofen, meloxicam and triptolide (Muzaffar *et al.,* 2013).

2.9.9.4 Ophthalmic delivery

In conventional ophthalmic dosage forms, hydrophilic drugs are formulated in an aqueous solution whereas lipophilic drugs are delivered as suspensions or ointments (Muzaffar *et al.*, 2013). The challenge with these MEs is the low corneal bioavailability and lack of efficacy in the posterior segment of the ocular tissue (Muzaffar *et al.,* 2013). A study on dexamethasone based ME eye drops showed that the ME had better eye penetration and bioavailability which allow for the possibility of reducing the dose frequency and thereby improving patient compliance (Muzaffar *et al.,* 2013).

2.9.10 Limitations of microemulsions

There are a few factors which may limit the use of MEs, especially in pharmaceutical applications. To reduce the toxicity of MEs, surfactants and co-surfactants which are used should be of the Generally Regarded as Safe (GRAS) category. The concentrations of the surfactants and co-surfactants should be kept low to avoid toxicity. MEs are not very suitable for IV use due to the possible toxicity of the formulations (Bhattacharya *et al.,* 2016). There is also a limitation of phase separation observed in MEs.

References

Afaq A, Alahmed S, Chen S, Lengana T, Haroon A, Payne H *et al.* 2018. Impact of ^{68}Ga-prostate-specific membrane antigen PET/CT on Prostate Cancer Management. *Journal of Nuclear Medicine* 59: 89–93

Afshar-Oromieh A, Hetzheim H, Kratochwil C, Benesova M, Eder M, Neel OC *et al.* 2015. The novel theranostic PSMA-ligand PSMA-617 in the diagnosis of prostate cancer by PET/CT: biodistribution in humans, radiation dosimetry and first evaluation of tumor lesions. *Journal of Nuclear Medicine* 56(11)

American Cancer Society. 2013. Prostate cancer. www.cancer.org. Accessed April 2016

Banerjee SR, Pullambhata M, Byun Y, Nimmagadda S, Green G, Fox JJ *et al.* 2010. ^{68}Ga-Labeled inhibitors of prostate-specific membrane antigen (PSMA) for imaging prostate cancer. *Journal of Medical Chemistry* 53(14): 5333–5341

Banerjee SR, Chen Z, Pullambhatla M, Lisok A, Chen J, Mease RC *et al*. 2016. Preclinical comparative study of ^{68}Ga-labeled DOTA, NOTA, and HBED-CC chelated radiotracers for targeting PSMA. *Bioconjugation Chemistry* 27(6): 1447–1455

Baur B, Solbach C, Andreolli E, Winter G, Machulla HJ and Reske SN. 2014. Synthesis, radiolabelling and *in vitro* characterization of the gallium-68-, yttrium-90- and lutetium-177-labelled PSMA ligand, CHX-A"-DTPA-DUPA-Pep. *Pharmaceuticals* 7: 517–529

Benešová M, Schäfer M, Bauder-Wüst U, Afshar-Oromieh A, Kratochwil C, Mier W *et al*. 2015. Preclinical evaluation of a tailor-made DOTA-conjugated PSMA inhibitor with optimized linker moiety for imaging and endoradiotherapy of prostate cancer. *Journal of Nuclear Medicine* 56(6): 914–920

Bhattacharya R and Mukhopadhyay S. 2016. Review on microemulsion- as a potential novel drug delivery system. *World Journal of Pharmacy and Pharmaceutical Sciences* 5(6): 700–729

Boschi S, Malizia C and Lodi F. 2013. Overview and perspectives on automation strategies in ^{68}Ga radiopharmaceutical preparations. *Cancer Research* 194: DOI: 10.1007/978-3-642-27994-2_2

Bouchelouche K. 2010. Prostate specific membrane antigen- A target for imaging and therapy with radionuclides. *Discovery Medicine* 9(44): 55-61

CANSA Researched and Authored by Prof Michael C Herbst 2016. Fact sheet on the role of Prostate Specific Antigen (PSA) screening on prostate cancer diagnosis and treatment. CANSA. Accessed April 2016

Chang SS. 2004. Overview of prostate-specific membrane antigen. *MedReviews* 6: 13–18

Ebenhan T, Vorster M, Marjanovic-Painter B, Wagener J, Suthiram J, Modiselle M *et al*. 2015. Development of a single vial kit solution for radiolabeling of ^{68}Ga-DKFZ-PSMA-11 and its performance in prostate cancer patients. *Molecules* 20(8): 14860–14878

Ebenhan, T. Mokaleng BB, Venter JD, Kruger HG, Zeevaart JR and Sathekge M. 2017. Preclinical assessment of a ^{68}Ga-DOTA functionalized depsipeptide as a radiodiagnostic infection imaging agent. *Molecules* 22(14): 1-14

Ebenhan T, Sathekge MM, Lengana T, Koole M, Gheysens O, Govender T and Zeevaart JR. 2018. ^{68}Ga-NOTA-functionalized ubiquicidin: Cytotoxicity, biodistribution, radiation dosimetry, and first-in-human PET/CT imaging of infections. *Journal of Nuclear Medicine* 59: 1-6

Eder M, Schafer M, Bauder-Wust U, Hull WE, Wangler C, Mier W *et al*. 2012. Ga-complex lipophilicity and the targeting property of a urea- based PSMA inhibitor for PET imaging. *Bioconjugate Chemistry* 23: 688-697

Eder M , Neels O, Müller M, Bauder-Wüst U, Remde Y, Schäfer M, Hennrich U *et al*. 2014. Novel preclinical and radiopharmaceutical aspects of [^{68}Ga]Ga-PSMA-HBED-CC: A new PET tracer for imaging of prostate cancer. *Pharmaceuticals* 7: 779–796

Emmett L, Willowson K, Violet J, Shin J, Blanksby A and Lee J. 2017. Lutetium-177 PSMA radionuclide therapy for men with prostate cancer : a review of the current literature and discussion of practical aspects of therapy. *Journal of Medical Radiation Sciences* 64: 52-60

Gundogdu E. 2013. A microemulsion for the oral drug delivery of Pitavastatin. *Pharmaceutica Analytica Acta* 4(1): 1–5

Hsing AW, Yeboah E, Biritwum R, Tettey Y, De Marzo AM, Adjei A, Netto GJ *et al*. 2015. High prevalence of screen detected prostate cancer in West Africans : Implications for racial disparity of prostate cancer. *Journal of Urology* 192(3): 730–735

Ishikawa K, Behrens M, Eriksson S, Topgaard D, Olsson U and Wennerstrom H. 2016. Microemulsions of record low amphiphile concentrations are aff ected by the Ambient Gravitational Field. *The Journal of Physical Chemistry* 120: 6074-6079

Kgatle MM, Kalla AA, Islam MM, Sathekge M and Moorad R. 2016. Prostate cancer : Epigenetic alterations , risk factors , and therapy. *Prostate Cancer* 2016: 5653862

Liu S. 2008. Bifunctional coupling agents for radiolabeling of biomolecules and target-specific delivery of metallic radionuclides. *Advanced Drug Delivery Reviews* 60: 1347-1370

Lopes LB. 2014. Overcoming the cutaneous barrier with microemulsions. *Pharmaceutics* 6: 52-77

Malik N, Baur B, Winter G, Reske SN, Beer AJ and Solbach C. 2015. Radiofluorination of PSMA-HBED via $Al^{18}F^{2+}$ chelation and biological evaluations *In Vitro*. *Molecular Imaging and Biology* 17(6): 777–785

Mehta DP, Rathod HJ and Shah DP. 2016. Microemulsions: A potential novel drug delivery system. *International Journal of Pharma and Drug Development* 1(1): 37-47

Moghimipour E, Salimi A and Eftekhari S. 2013. Design and characterization of

microemulsion systems for naproxen. *Advanced Pharmaceutical Bulletin* 3(1): 63–71

Mokaleng BB, Ebenhan T, Ramesh S, Govender T, Kruger HG, Parboosing R *et al*. 2015. Assessment of a depsipeptide-derived compound as a potential PET / CT infection imaging agent. *BioMed Research International* 2015: 284354.

Müller C. 2013. Folate-based radiotracers for PET imaging-update and perspectives. *Molecules* 18: 5005–5031

Muzaffar F. Singh UK and Chauhan L. 2013. Review on microemulsion as futuristic drug delivery. *International Journal of Pharmacy and Pharmaceutical Sciences* 5(3): 39–53

Nirmala and Nagarajan. 2016. Microemulsions as potent drug delivery systems. *Nanomedicine & Nanotechnology* 7(3): 7439

Sachpekidis C, EderM, Kopka K, Mier W, Hadaschik BA, Haberkorn U and Dimitrakopoulou-Strauss A. 2016. Ga-PSMA-11 dynamic PET / CT imaging in biochemical relapse of prostate cancer. *EJNMMI* DOI 10.1007/s00259-015-3302-4

Sathekge M, Lengana T, Maes A, Vorster M, Zeevaart JR, Lawal I *et al*. 2018(a). ^{68}Ga-PSMA-11 PET / CT in primary staging of prostate carcinoma : preliminary results on differences between black and white South-Africans. *European Journal of Nuclear Medicine and Molecular Imaging* 45: 226–234

Sathekge M, Garcia-Perez O, Paez D, El-Haj N, Kain-Godoy, Lawal I and Estrada-Lobato E. 2018(b). Molecular imaging in musculoskeletal infections with ^{99m}Tc-UBI 29-41 SPECT / CT. *Annals of Nuclear Medicine* 32(1): 54–59

Schäfer M, Bauder-Wüst U, Leotta K, Zoller F, Mier W, Haberkorn U, Eisenhut M and Eder M. 2012. A dimerized urea-based inhibitor of the prostate-specific membrane antigen for 68 Ga-PET imaging of prostate cancer. *EJNMMI Research* 2(23): 1–11

Sterzing F, Kratochwil C, Fiedler H, Katayama S, Habl G, Kopka K *et al*. 2016. ^{68}Ga-PSMA-11 PET/CT: a new technique with high potential for the radiotherapeutic management of

prostate cancer patients. *European Journal of Nuclear Medicine and Molecular Imaging* 43(1): 34–41

Tadros TF. 2013. Emulsion formation, stability, and rheology. *Wiley-VCH Verlag GmbH & Co. KGaA* 1-75

Tindall EA, Monare LR, Petersen DC, van Zyl S, Hardie RA, Segone AM *et al*. 2014. Clinical presentation of prostate cancer in Black South Africans. *The Prostate* 74: 880–891

UCSF Medical Center. Prostate cancer and its treatment. PatientEducationLibrary:www.ucsfhealth.org/education. Accessed April 2017

Umbricht CA, Bene M, Schmid RM, Türler A, Schibli R, Meulen NP Van Der *et al*. 2017. Sc-PSMA-617 for radiotheragnostics in tandem with ^{177}Lu-PSMA-617- preclinical investigations in comparison with ^{68}Ga-PSMA-11 and ^{68}Ga-PSMA-617. *EJNMMI* 7(9): 1-10

Velikyan I. 2014. Prospective of ^{68}Ga-radiopharmaceutical development. *Theranostics* 4(1): 47-80

Vorster M, Modiselle M, Ebenhan T, Wagener C, Sello T, Zeevaart JR *et al*. 2015. Fluorine-18-fluoroethylcholine PET/CT in the detection of prostate cancer: A South African experience. *Hellenic Journal of Nuclear Medicine* 18(1): 53–59

Weineisen M, Schottelius M, Simecek J, Baum RP, Yildiz A, Beykan S *et al.* 2015. ^{68}Ga- and ^{177}Lu-labeled PSMA I&T: Optimization of a PSMA-targeted theranostic concept and first proof-of-concept human studies. *Journal of Nuclear Medicine* 56(8): 1169–76

Wiehr S, Buhler P, Gierschner D, Wolf P, Rolle AM, Kesenheimer C *et al*. 2014. Pharmacokinetics and PET imaging properties of two recombinant anti-PSMA antibody fragments in comparison to their parental antibody. *Prostate* 74(7): 743–755

Xu J, Yu J, Xu X, Wang L, Liu Y, Li L *et al*. 2014. Evaluation of PSMA-targeted glycol chitosan micelles for prostate cancer therapy. *Journal of Nanomaterial* 2014: 462356

Yao R, Lecomte R and Crawford ES. 2012. Small-animal PET: What is it, and why do we need it? *Journal of Nuclear Medicine Technology* 40(3): 157–165

Zhu H, Xie Q, Li N, Tian H, Liu F, Yang Z. 2016. Radio-synthesis and mass spectrometry analysis of ^{68}Ga-DKFZ- PSMA-617 for non-invasive prostate cancer PET imaging. *Journal of Radioanalytical and Nuclear Chemistry* 309(2): 575–81

Chapter 3: Preclinical assessment of ^{68}Ga-PSMA-617 entrapped in a microemulsion delivery system for applications in prostate cancer PET/CT imaging

Journal of Labelled Compounds and Radiopharmaceuticals

Vusani Mandiwana[1,5], Lonji Kalombo[1], Yolandy Lemmer[1], Philip Labuschagne[1], Boitumelo Semete-Makokotlela[1], Mike Sathekge[2], Thomas Ebenhan[2, 3], Jan Rijn Zeevaart[4, 5]

1 Centre for Polymers and Composites, Council for Scientific and Industrial Research, Pretoria, 0001, South Africa

2 Department of Nuclear Medicine, University of Pretoria, Pretoria, South Africa

3 Preclinical Imaging Facility, NuMeRI, Pelindaba, South Africa

4 Radiochemistry, South African Nuclear Energy Corporation, Pelindaba, Pretoria, 0001, South Africa

5 DST/NWU, Preclinical Drug Development Platform, North West University, Potchefstroom, South Africa

Correspondence:

* Vusani Mandiwana

Centre of Polymers and Composites, Council for Scientific and Industrial Research, P.O. Box 395, Pretoria, 0001, South Africa E-mail: +27 12 841 2985, VMandiwana@csir.co.za

Abstract

It has in recent years been reported that microemulsion (ME) delivery systems provide an opportunity to improve the efficacy of a therapeutic agent whilst minimising side effects and also offer the advantage of favourable treatment regimens. The prostate-specific membrane antigen (PSMA) targeting agents PSMA-11 and PSMA-617, which accumulate in prostate tumours, allows for [^{68}Ga]Ga^{3+}-radiolabelling and PET imaging of PSMA-expression *in vivo*. We herein report the formulation of [^{68}Ga]Ga-PSMA-617 into a ME ≤40 nm including its evaluation for improved cellular toxicity and *in vivo* biodistribution.

The [^{68}Ga]Ga-PSMA-617-ME was tested *in vitro* for its cytotoxicity to HEK293 and PC3 cells. [^{68}Ga]Ga-PSMA-617-ME was administered intravenously in BALB/c mice followed by microPET/CT imaging and *ex vivo* biodistribution determination.

[^{68}Ga]Ga-PSMA-617-ME indicated negligible cellular toxicity at different concentrations. A statistically higher tolerance towards the [^{68}Ga]Ga-PSMA-617-ME occurred at 0.125mg/ml by HEK293 cells compared to PC3 cells. The biodistribution in wild-type BALB/C mice showed the highest amounts of radioactivity (%ID/g) presented in the kidneys (31%) followed by the small intestine (10%) and stomach (9%); the lowest uptake was seen in the brain (0.5%).

The incorporation of [^{68}Ga]Ga-PSMA-617 into ME was successfully demonstrated and resulted in a stable non-toxic formulation as evaluated by *in vitro* and *in vivo* means.

Keywords

Biodistribution, In vitro, ^{68}Ga-PSMA-617, Microemulsion, PET/CT, Prostate cancer

3.1 Introduction

Prostate cancer is the most common cancer in elderly men and the second most frequent cause of cancer-related deaths (14%) [1] in western societies [2]. The highest incidence of prostate cancer was reported in North America and Oceania, and the lowest in Asia and Africa in 2012 [3]. In the United States of America, approximately 233 000 new cases and an estimated 29 480 deaths are reported annually [4]. One of the issues of prostate cancer is early detection of recurrent disease. If the tumour is accessible for external radiation therapy or surgery, the cancer could be cured and the resulting side effects could be delayed [5].

Choline-based positron emission tomography/ computed tomography (PET/CT) is widely used as a diagnostic imaging modality. However, numerous studies have reported low sensitivity and specificity, especially at low prostate-specific membrane antigen (PSMA) levels and high Gleason score [6,7,8]. Therefore, there is a requirement for the development of new and improved imaging methods.

In this regard, an ideal biomarker, PSMA, has received significant attention as a target for imaging [6, 9] and treatment of prostate cancer [10]. PSMA is a transmembrane glycoprotein hydrocellulose enzyme whose catalytic centre comprises two zinc (II) ions with a bridging hydroxide ligand [10] and is also known as N-acetyl-L-aspartyl-L-glutamate peptidase [11]. It serves as a cell surface antigen which is overexpressed in prostate cancer cells compared to other PSMA-expressing tissues i.e. kidney, small intestines and salivary glands [6]. The PSMA ligand 2-[3-(1-Carboxy-5-{3-naphthalen-2-yl-2-[(4-{[2-(4,7,10-tris-carboxymethyl-1,4,7,10-tetraaza-cyclododec-1-yl)-acetylamino]-methyl}-cyclohexanecarbonyl)-amino]-propionylamino}-pentyl)-ureido]-pentanedioic acid (PSMA-617) can be radiolabelled with the PET radioisotope Gallium-68 (^{68}Ga) [1] to image PSMA-expressing tumours. This PSMA ligand utilizes 1,4,7,10-tetraazacyclododecane-1,4,7,10-tetraacetic acid (DOTA) as a chelating moiety which can form stable complexes with a broad range of radioisotopes such as ^{68}Ga, Lutetium-177 (^{177}Lu) and Yttrrium-90 (^{90}Y) for diagnosis and therapy [10]. A diagnostic or theranostic agent, consisting of three compounds: the pharmacophore PSMA, the chelator DOTA and a radionuclide isotope i.e. ^{68}Ga and ^{177}Lu is often employed.

Specific cancer targeting based on low-molecular-weight radioligands may offer improved accuracy and rapid visualisation, highly effective diagnosis, and radiotherapy and improved staging. However, the dose and duration of administration of the radiopharmaceuticals are limited due to systemic toxicity and the lack of sufficient selectivity to tumour cells [4]. There is therefore a medical need to develop drug delivery systems that selectively transport anti-

tumour drugs or radiopharmaceuticals into the tumour cells. Delivery systems, which have demonstrated improved therapeutic index with minimal side effects, are micelles [4], liposomes [12], lipid-based emulsions [13] and polymeric nanoparticles [4]. The use of delivery systems such as swollen micelles or microemulsions (MEs) can improve the efficacy of a drug, allowing the total dose to be reduced and therefore minimise side effects and toxicity of the formulated compound [14].

A ME is a colloidal system made out of various components including water, oil and an amphiphile, which is optically isotropic and a dispersion of homogenous oil and water [14]. MEs are translucent and form spontaneously with an average droplet diameter of 10 to 140 nm [14]. They are thermodynamically stable and nanostructured [15]. The advantages of MEs include improved solubility of a poorly soluble drug resulting in enhanced bioavailability of the formulated compound, protection of unstable drugs against environmental conditions and a prolonged shelf-life. The current ME was designed to formulate the drugs so that off-target delivery could be reduced by prolonging its systemic circulation time; thus, improving delivery to target. In the case of the formulated radiolabelled-PSMA-617 the prolonged circulation time aims to deliver a greater percentage of the compound to the target by slow release from the ME into the bloodstream and subsequent uptake into tissue creating a greater concentration gradient. Furthermore the prolonged circulation and protection of the ME will reduce uptake and clearance of radiolabelled-PSMA-617 from the kidneys. Additionally PSMA is also expressed at reduced amounts in healthy cells such as the small intestines, proximal renal tubules, kidneys, liver and salivary glands. This means that radiation dose is delivered to these organs when [^{68}Ga]Ga-PSMA-617 or [^{177}Lu]Lu-PSMA-617 are used for radionuclide targeting or therapy. This has an effect on the side effect profile and safe dose that can be delivered without causing damage to non-target tissue[16]. In this study therefore [^{68}Ga]Ga-PSMA-617 was used as an imaging tool to evaluate the effect of ME on PSMA biodistribution with eventual future application for [^{177}Lu]Lu-PSMA-617. The formulation of radiopharmaceuticals into MEs offers potential prospects in the approach of diagnosing and/or treating patients with slow-release radiotherapeutics, improving their overall targeting and reducing radiation burden to vulnerable organs such as the kidneys or salivary glands.

Here we report on the development of [^{68}Ga]Ga-PSMA-617-ME as a delivery system, its stability over time, its cellular toxicity to PSMA-positive PC3 and PSMA-negative HEK293

cells as well as [^{68}Ga]Ga-PSMA-617-ME-PET/CT imaging and biodistribution in wild-type BALB/c mice.

3.2 Materials and methods

3.2.1 Materials

Sodium oleate, Tween 80, polyvinyl alcohol (PVA) (97-98% hydrolysed and Mw: 13-23kDa), lauric acid, polyethylene glycol (PEG) 4000 and d-α-tocopherol were purchased from Sigma Aldrich (St Louis, MO, USA). HPLC-grade ethanol was purchased from Radchem Products Inc. (Orlando Park, Il, USA). All chemicals, reagents and solvents for the radiosynthesis (i.e. ultrapure, metal-free water) and analysis of the compounds were at least of analytical grade or were purchased from Sigma Aldrich (St Louis, MO, USA). PSMA-617 ($C_{49}H_{71}N_9O_{16}$; MW=1042.1 g/mol) was purchased from Advanced Biochemical Compounds (Radeberg, Germany). Figure 1 shows the chemical structure of this compound including the [^{68}Ga]Ga^{3+}-complex with DOTA.

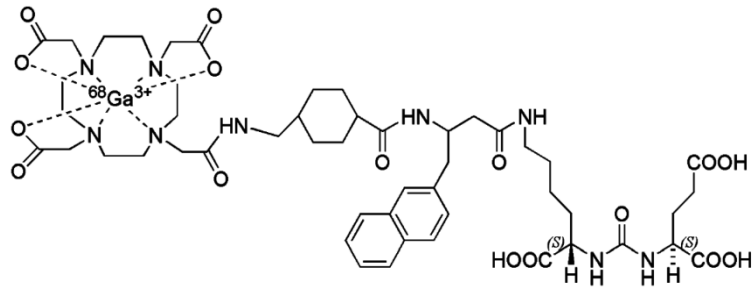

Figure 1: A schematic representation of radiolabelled ^{68}Ga-PSMA-617

3.2.1.1 Formulation of microemulsion

The basic ME loaded with PSMA-617 was formulated by mixing an aqueous solution of non-ionic surfactant and a salt of fatty acid. Briefly, an aqueous solution of sodium oleate 0.1% w/v combined with PVA 2% w/v was prepared in volume ratio of 1:1 and mixed by stirring at room temperature. A complex of Lauric acid-PEG 4000, obtained via Particles from Gas Saturated Solution supercritical fluid process, was dissolved in ethanol while stirring at 75°C for 2 min. Tween 80, d-α-tocopherol and PSMA-617 were added drop-wise to the organic phase and stirring was maintained at the same heating temperature for a further 2 min. The

resulting organic solution containing the PSMA-617 was then mixed into the PVA/sodium oleate aqueous solution at room temperature while maintaining stirring for 10 min. The resulting emulsion thereby formed spontaneously producing a translucent microemulsion whilst cooling. Saline solution and blank ME were used as controls.

3.2.1.2 Characterisation of microemulsion

Particle size and size distribution indicated as the polydispersity index (PDI) were measured by dynamic laser scattering or photon correlation spectroscopy using a Malvern Zetasizer Nano ZS (Malvern Instruments, Worcestershire, United Kingdom). Each sample was measured undiluted in triplicate. The intensity-weighted mean value was measured as the average of three independent measurements. The Zeta potential was determined using a Malvern Zetasizer Nano ZS (Malvern Instruments, Worcestershire, United Kingdom) at pH 6.8 at 25 °C. The instrument calculates the ME net-surface charge by determining the electrophoretic mobility using the Laser Doppler Velocimetry. Each sample was measured undiluted in triplicate to determine the Zeta potential. The pH values of the MEs were determined at ambient temperature after a calibration process. The conductivity of the ME was measured by using a pH and conductivity meter (PC 8, Accsen, Lasec, South Africa) at 25 °C by inserting the probe into the ME. Characterisation of [^{68}Ga]Ga-PSMA-617 formulated into ME was performed after full decay of the radioactivity to below clearance levels.

3.2.1.3 ^{68}Ge/^{68}Ga generator elution

[^{68}Ga]Ga^{3+} was obtained from a SnO_2-based generator that was loaded with 1580 MBq Germamium-68 (iThemba LABS, Somerset West, South Africa). The [^{68}Ga]Ga^{3+} activity was manually eluted by way of an eluate-fractionation method as previously described [17], measured in a dose calibrator (CRC15, Capintec Inc, Pittsburgh, PA, USA). All radioactive measurements were corrected for decay to the time of injection. [^{68}Ga]Ga^{3+} (half-life 68 min, maximum energy of positrons [β^+]: 1.9 MeV (88%)) was obtained as [^{68}Ga]$GaCl_3$ in 2-3 ml of 0.6 M HCl.

3.2.2.1 ^{68}Ga-radiolabelling of PSMA-617

[^{68}Ga]Ga^{3+}-radiolabelling of PSMA-617 was adopted from a previously described method [18] making minor adaptations to manage the more acidic [^{68}Ga]Ga^{3+} eluate. A 2.5 M sodium acetate solution was mixed with 2 ml of [^{68}Ga]Ga^{3+} eluate to adjust the pH to values ranging from 3.5- 4.5. These reaction mixtures were incubated at >95°C for 10-15 min. A Sep-Pak C18 (100 mg light) cartridge (Waters, Ireland) was used to purify the mixture from uncomplexed [^{68}Ga]Ga^{3+} and traces of ^{68}Ge which were rinsed off with saline solution. The resulting [^{68}Ga]Ga-PSMA-617 product was extracted from the cartridge with a 50% ethanol saline solution (v:v) and aseptically filtered using a 0.22 µm low protein-binding membrane filter. A product sample was used to determine the radionuclidic/radiochemical identity and purity, the percentage radiochemical yield (%RCY) and percentage labelling efficiency (%LE; decay-corrected).

3.2.2.2 HPLC and ITLC

Quality control of [^{68}Ga]Ga-PSMA-617 followed previously published described methods for High performance liquid chromatography (HPLC) [19] and instant-thin layer chromatography (ITLC) [20]. A reverse-phase HPLC column (Zorbax StableBond C18, 0.46 × 2 cm × 5 µm; Agilent Technologies, CA, USA) performing gradient elution (5-95% A-B over 15 min) at a flow rate of 1 mL/min, was employed (Solvent A = 0.1 % aqueous trifluoroacetic acid (TFA); solvent B= 0.1 % TFA in acetonitrile). The HPLC apparatus (Agilent 1200 series HPLC instrument, Agilent Technologies Inc., Wilmington DE, USA) combined radio-detection (GinaStar, Raytest, Straubenhardt, Germany) (counts per second) with a diode array detector following UV absorbance at 214, 220 and 240 nm. A radio-ITLC method employing a silica-gel based solid phase and 0.1 M sodium citrate as mobile phase (free [^{68}Ga]Ga^{3+} [R*f*=0.85] and [^{68}Ga]Ga-PSMA-617 [R*f*=0.2]) supported the HPLC analysis for the determination of %LE.

3.2.2.3 Formulation of [^{68}Ga]Ga-PSMA-617 into microemulsion

Similar to production and as described above, Tween 80, d-α-tocopherol and the radiolabelled [^{68}Ga]Ga-PSMA-617 were added dropwise respectively to a lauric acid/PEG and ethanol solution and maintained stirring at a 75°C temperature for 2 minutes. The resulting organic solution containing the [^{68}Ga]Ga-PSMA-617 was introduced dropwise, to a PVA/sodium

oleate (1:1) aqueous solution at room temperature and maintained stirring for 10 min. The resulting emulsion was then quenched at ambient temperature, thereby spontaneously producing a radioactive translucent ME. The specific activity for [^{68}Ga]Ga-PSMA-617 was in the range of 220- 450 MBq/µmol. The time it took to prepare a ME containing [^{68}Ga]Ga-PSMA-617 ranged between 40 to 60 min. The radiolabelling procedure employed here was adopted from Umbricht *et al.,* 2017[18] which would conventionally take the same amount of time. Keeping the [^{68}Ga]Ga-PSMA-617 radiolabelling procedure and time factor in mind, the ME formulation was designed and developed around these parameters so not to deviate from the clinical setup. It takes an additional 12 minutes to obtain the resulting ME containing [^{68}Ga]Ga-PSMA-617 as compared to the conventional radiolabelling of ^{68}Ga-PSMA-617 alone.

3.2.3 Cellular cytotoxicity

A WST-1 (Roche, Mannheim, Germany) colorimetric proliferation assay was used to determine the cellular toxicity of a) the blank ME, b) PSMA-617, c) PSMA-617-ME, d) [^{68}Ga]Ga^{3+}, e) [^{68}Ga]Ga-PSMA-617, and f) [^{68}Ga]Ga-PSMA-617-ME. Hereby, a tetrazolium salt (WST-1 reagent) is reduced to the water-soluble orange formazan dye by cellular mitochondrial dehydrogenase in viable cells. Human prostate cancer cells (PC3, ATCC-CRL-1435, kindly provided by the Department of Biosciences, Council for Scientific and Industrial Research, South Africa) were grown in Roswell Park Memorial Institute-1640 (RPMI-1640) media (Gibco, Life Technologies, NY, USA) containing L-glutamine and supplemented with 10% foetal bovine serum. Human embryonic kidney 293 cells (HEK-293; ATCC-CRL1573, kindly provided by the ARC, Onderstepoort, South Africa) were cultured in Dulbecco Modified Eagle Medium (DMEM) (Gibco, Life Technologies, NY, USA) containing L-glutamine, sodium pyruvate and supplemented with 10% FBS. Both cell lines were cultured at 37°C with 5% CO_2 (g) atmosphere. A density of 1x 10^5 cells/ml was seeded into 96-well culture plates and allowed to adhere for 48 hours without antibiotics. Once 80-90% confluent, the cells were washed twice with fresh media. Serial dilutions of test compounds (a-f) in complete media were added to each well and further incubated for 24 h. Thereafter, the cells were rinsed twice with fresh media. 100 µl of complete fresh media and 10 µl of WST-1 reagent was added per well and incubated for another 2 h at 37°C, 5% CO_2 (g) and processed as per manufacturer's instructions. Formazan absorbance was measured at a wavelength of

450 nm (against a reference wavelength of 650 nm) in a microplate reader (Tecan Infinite 500, LifeScience, PA, USA). Samples were measured in triplicates from 3 independent experiments.

3.2.4 MicroPET/CT imaging and biodistribution of [^{68}Ga]Ga-PSMA-617-ME

Four wild-type BALB/c mice (male, 30-40g, 8-12 weeks-old) were bred under specific pathogen free conditions at the North West University. All experiments were approved by the North-West University Animal Care, Health and Safety Research Ethics Committee (NWU-AnimCareREC); ethics number: NWU-00333-15-A5). MicroPET/CT imaging was performed utilizing small animal imaging camera (NanoScan PET/CT, Mediso Medical Systems, Hungary). Mice were immobilized on the scanner bed (orientation: prone, nose first) using a 1.5-2.5% isoflurane/ anaesthetic air mixture for the duration of the scans and were monitored for body temperature and breathing rate. CT X-ray images were acquired for anatomical reference and to allow for scatter and attenuation correction during PET data reconstruction, using the following parameters: 50KeV, 200 ms, 1:5 binning and a matrix size of 125 x 125 x 125 µm. The *ex vivo* biodistribution study employed administration of [^{68}Ga]Ga-PSMA-617-ME in mice (n=4) with the lowest injected dose of 0.76 ± 0.24 MBq and the highest injected dose of 13.96 ± 0.22 MBq. The microPET/CT imaging study employed the administration of doses ranging between 5 and 7 MBq in several mice (n=4) with an average dose of 5.89 ± 0.64 MBq. MicroPET/CT image data was acquired at 40 and 60 min scans. Mediso Nucline software was used for PET data reconstruction from list-mode: reconstruction algorithm 3D OSEM (6 iterations), energy window 400–600 keV, coincidence mode 1–5, corrections for random events, detector normalization, decay and dead time and voxel size 0.6 mm. Mediso Inter View Fusion software (version 2.02.055.2010) was used for data visualization, yielding co-registered PET/CT images in axial, coronal and sagittal orientation. Time-activity curves yielded by semi-quantification of tissue/organ tracer concentrations were analysed by way of area-under-the-curve analysis determining the normalised uptake value (SUV), which is the regional tissue radioactivity concentration normalised for the injected dose and body weight of the subject. Following microPET/CT, mice were sacrificed by cervical dislocation and tissue/organs (blood, heart, lungs, liver, spleen, kidneys, intestines, stomach, urine, tissue, bone and brain) were isolated, weighed and counted in an automated gamma counter (Hidex Gamma Counter AMG, Turku, Finland). The *ex vivo* results were expressed as percent injected dose per gram of tissue or organ (% ID/g).

For *in vivo* administration of MEs a physiological pH was desired, hence; the pH was adjusted with the addition of ~20 µl 2.5 M sodium acetate (alternatively phosphate buffered saline) successfully increasing it to pH 7.5.

3.2.5 Statistical analysis

All experiments were performed in triplicates or more. Quantitative data was expressed as mean ± standard deviation of mean. If applicable, values were compared using Student's *t* test. *P* values <0.05 were considered statistically significant. A Grubb's test, also called the extreme studentized deviate method was performed to determine whether a value was a significant outlier from the rest.

3.3 Results and Discussion

3.3.1 Size and Zeta potential

The physical and chemical properties of the ME were analysed, including particle size, surface charge, pH and conductivity. These parameters have a direct impact on the stability and release kinetics of the radiopharmaceutical that was entrapped. The bigger the Zeta potential of the suspension, the more likely it is to be stable because the charged particles repel each other and therefore overcome the natural tendency to aggregate and wherein it is accepted that Zeta potentials more than +/- 30 mV are sufficient for good electrostatic stabilization [21]. Table 1 summarises the data comparing blank ME to [^{68}Ga]Ga-PSMA-617-ME (*n*=3).

Table 1: Characterisation of ME, [^{68}Ga]Ga-PSMA-617-ME and PSMA-ME formulations

	F	Size (nm)	PDI	ZP (mV)	pH	Conductivity (µS/cm)
ME(blank) (Not buffered)	1	21.05 ± 0.06	0.23 ± 0.01	-26.06 ± 0.15	6.30	12.53
	2	21.54 ± 0.13	0.21 ± 0.02	-28.10 ± 3.55	6.22	13.20
	3	21.01 ± 0.01	0.15 ± 0.18	-28.34 ± 0.85	6.17	13.19
[^{68}Ga]Ga-PSMA-ME	4	18.30 ± 0.08	0.21 ± 0.00	-30.10 ± 0.51	7.89	13.82
	5	21.15 ± 0.26	0.30 ± 0.00	-28.70 ± 0.15	7.93	13.50
	6	35.77 ± 1.38	0.64 ± 0.04	-27.10 ± 0.66	7.88	14.35
PSMA-ME	7	22.04 ± 0.15	0.25 ± 0.01	-29.43 ± 0.40		
	8	21.84 ± 0.08	0.24 ± 0.00	-28.00 ± 0.89		
	9	22.13 ± 0.26	0.26 ± 0.00	-28.91 ± 0.70		

F= formulation; PDI=poly dispersity index; ZP=Zeta potential

Various parameters were optimised to obtain an average ME particle size ranging between 20 and 40 nm, with an average polydispersity index ≤0.3. Both types of ME formulations had a Zeta potential ranging between -22 mV and -31 mV. The stability of the ME formulations was acceptable and close to a range which is considered high (-31 mV).

For *in vivo* administration of MEs a physiological pH is desired, hence the pH was adjusted with 2.5 M sodium acetate to pH 7.5. Conductance of MEs increases as droplets tend to fuse as a result of the percolation effect, thereby allowing enhanced transportation of ions [17]. Conductivity values above 0.1 mS/cm suggest that the formed MEs were of an oil-in-water (o/w) type [17, 22]. F6 may have its high conductance as a result of the percolation effect relating to the droplet size (>21 nm) and the concentration of sodium oleate salt, which may dissociate, resulting in enhanced movement of ions. The resulting pH of blank ME was 6.23±0.13. The pH values obtained from all the formulated MEs were all ≤ 6 before buffering and approaching a neutral pH.

The conductivity increased slightly but was not significantly affected by incorporation of [^{68}Ga]Ga-PSMA-617. F1 had the lowest conductivity and F6 had the highest readings. Galium-68 was fully decayed before these analysis hence no difference between [^{68}Ga]Ga-PSMA-ME and PSMA-ME is expected.

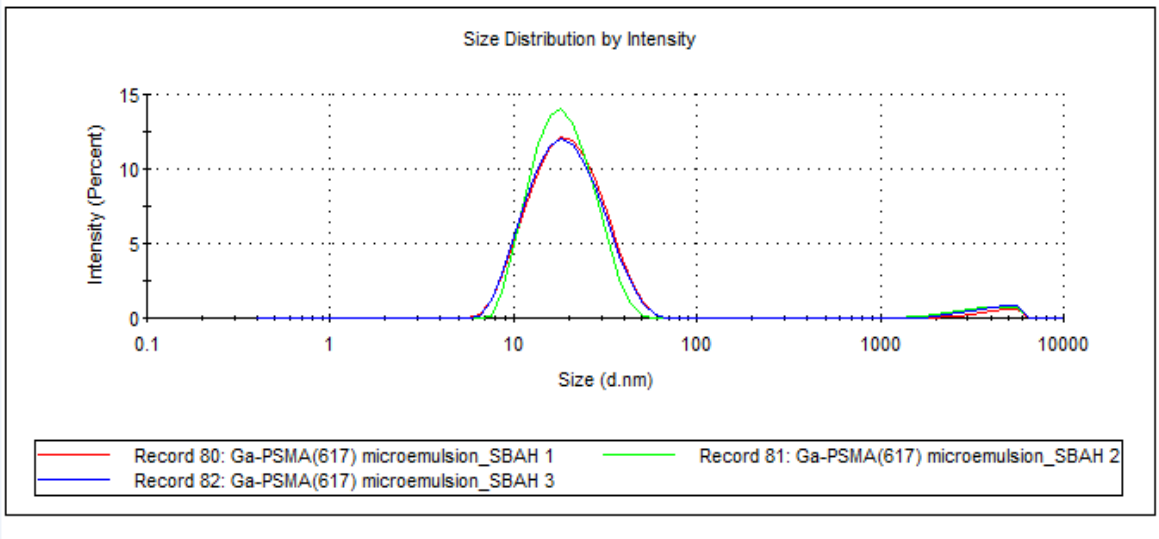

Figure 2: Graph showing the size distribution intensity of a [^{68}Ga]Ga-PSMA-617-ME (*n*=3).

For the *in vivo* applications, F4 was selected due to the high conductivity value, a small droplet size (depicted in Figure 2), small PDI and high integrity (see low ZP). As there was no significant difference between this formulation and the one without the [^{68}Ga]Ga-PSMA-617 and furthermore such formulation is radioactive it was not tested prior to the *in vivo* study.

3.3.2 Generator elution and ^{68}Ga-radiolabelling of PSMA-617

Eluate fractionation yielded 500-850 MBq (88-92% of elutable [^{68}Ga]Ga^{3+}-activity) in 2 ml, sufficient for straightforward radiolabelling (>99% radionuclide purity).
The optimal radiolabelling yield of [^{68}Ga]Ga-PSMA-617 was achieved as a function of pH (3.5-4.5) and temperature (10 -15 min at >95°C). Further optimisations have shown that as low as 20 µg PSMA-617 was sufficient to produce a high [^{68}Ga]Ga-PSMA-617 yield (%LE = 98 ± 2% at pH 4 using 110- 195 MBq/ml eluate; (*n*=5)). The % RCY of [^{68}Ga]Ga-PSMA-617 was ≥97 % (*n*=3) based on ITLC analysis. The radioactivity for the produced [^{68}Ga]Ga-PSMA-617 was in the range of 220- 450 MBq.

3.3.2.1 HPLC and ITLC

ME-free samples were analysed immediately after [^{68}Ga]Ga-PSMA-617 radiolabelling and subsequently after further 2 min and 10 min incubation at 75°C. The [^{68}Ga]Ga-PSMA-617 conjugate was heated to investigate the integrity of the radiolabelled product at 75°C. This was done in order to indirectly determine the fate and integrity of the conjugation of [^{68}Ga]Ga^{3+} to PSMA-617 at temperatures at which the ME was formulated.

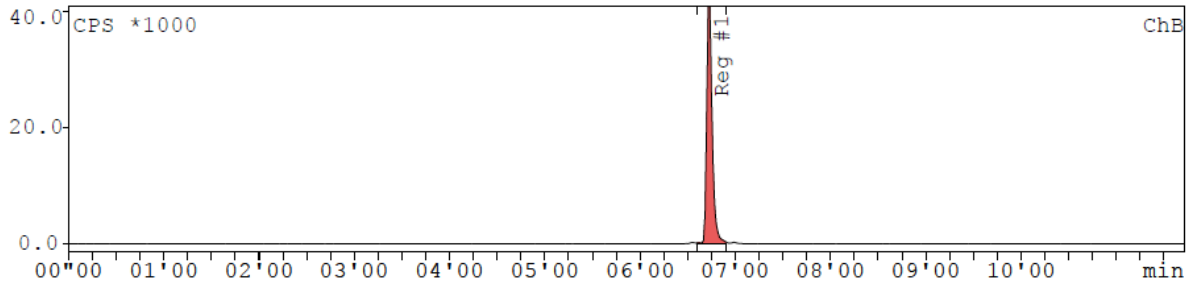

Figure 3: Radio-HPLC chromatograms of radiolabelled [^{68}Ga]Ga-PSMA-617

The retention time of [^{68}Ga]Ga-PSMA-617 was 6.44 min and no free [^{68}Ga]Ga^{3+} was detected. This was after purification of the labelled product. The radiochemical purity of the final product was 100% and the labelling yield was 98%, shown in Figure 3.

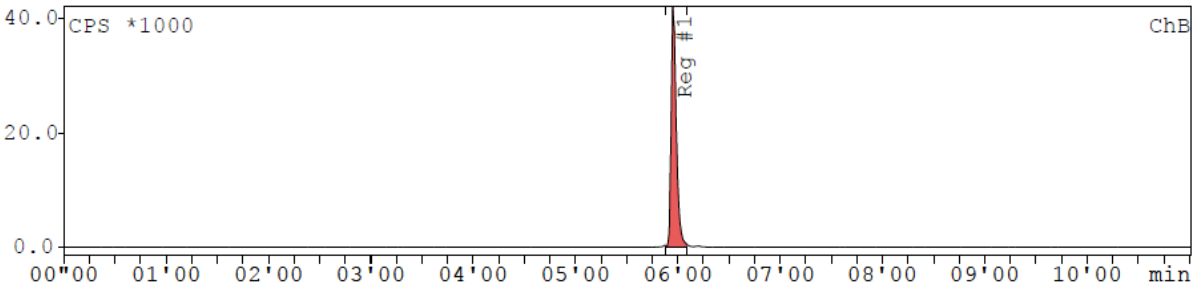

Figure 4: Radio-HPLC of [^{68}Ga]Ga-PSMA-617 which was heated at 75°C for 2 min post radiolabelling.

The radiochemical purity of [^{68}Ga]Ga-PSMA-617 remained 100% after a 2 min incubation at 75°C. After purification, the retention time was 5.58 min, shown in Figure 4.

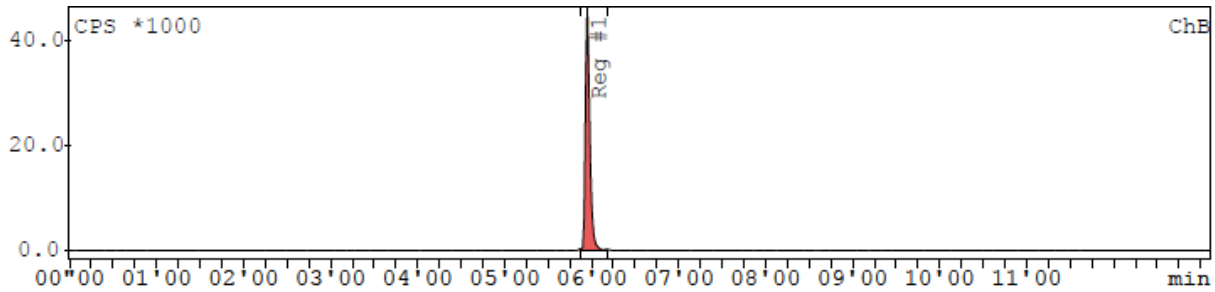

Figure 5: Radio-HPLC of [^{68}Ga]Ga-PSMA-617 which was heated at 75°C for 10 minutes post radiolabelling

The retention time after purification of the radiolabelled product was 5.58 min for the sample which was incubated for 10 min at 75°C, similar to the sample which was incubated for 2 min. The radiochemical purity was still 100% and therefore was not compromised at that particular temperature. No free [^{68}Ga]Ga^{3+} was detected in either of the HPLC chromatograms, therefore confirming the radio-synthesis of [^{68}Ga]Ga-PSMA-617, as seen in Figure 5. This confirms that the [^{68}Ga]Ga-PSMA-617 is still intact after the ME production. Inclusion of ME does not allow for HPLC analysis due to the content and particle size. The radiochemical purity of [^{68}Ga]Ga-PSMA-617 was not compromised at conventional radiolabelling temperatures and at 75°C. No free [^{68}Ga]Ga^{3+} was detected in either of the HPLC chromatograms. This observation therefore confirmed the radio-synthesis integrity of [^{68}Ga]Ga-PSMA-617. The retention time of

[^{68}Ga]Ga-PSMA-617 was detected at slightly earlier times (5.58- 6.44 min). This may be due to the consecutive alignment of the radio-HPLC detectors. Temperature may not have had any direct influence nor compromised the radiolabelling parameters.

3.3.2.2 Formulation of [^{68}Ga] Ga-PSMA-617 into microemulsion

Formulation was achieved as described above. The radioactivity for produced [^{68}Ga]Ga-PSMA-617-ME was in the range of 220- 450 MBq. The [^{68}Ga]Ga-PSMA-617-MEs which were used for IV administration into four mice were in the size range of 21.15 ± 0.26 nm to 35.77 ± 1.38 nm, a size distribution (polydispersity index) of 0.21 ± 0.00 to 0.64 ± 0.04 and a Zeta potential of -28.70 ± 0.15 mV to -30.10 ± 0.51 mV, respectively. This was determined after decay of the formulation to below exclusion levels.

3.3.3 Cellular cytotoxicity

The *in vitro* cytotoxicity of the ME, PSMA-617 peptide and the combination thereof with and without the [^{68}Ga]Ga^{3+} were tested in PC3 and HEK293 cell lines. A concentration range from 1 mg/ml up to 0.0001 mg/ml were used in a WST assay over a period of 24 hours.

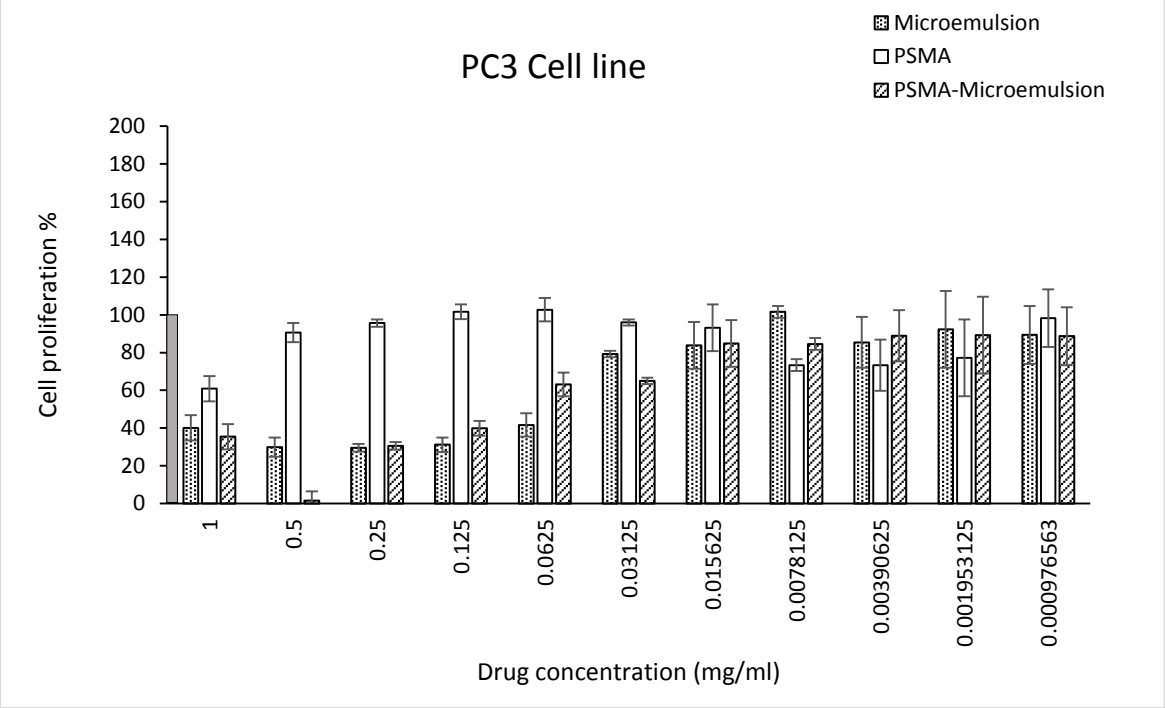

Figure 6: The *in vitro* cytotoxicity of a blank ME, PSMA-617 and PSMA-617 loaded ME against PC3 cells after 24 h (*n*=9). Grey bar represents the untreated control cells

Free PSMA-617 in PC3 cells was considered non-toxic at concentrations lower than 0.5 mg/ml with some variations at the lower concentrations used, as similarly observed in literature [18]. The ME alone showed a decrease in cell proliferation in itself and could contribute towards the cytotoxic effect of the PSMA-617 as can be seen in Figure 6. The cytotoxicity of ME indicate that there are components within the ME which affects the cell viability but it has not been further investigated yet. The final formulation may have a synergistic effect when containing for example ^{68}Ga-PSMA-617. Li *et al.*, 2009 [23] have demonstrated that Tween 80 may affect cell assays when screening for the cytotoxicity of drugs by detecting biochemical changes on the cell membrane. The combination of the PSMA-617 and ME were more cytotoxic compared to the PSMA-617 alone at higher concentrations tested above 0.03 mg/ml but would be suitable for use at concentrations below that. Interestingly the ME combination with PSMA-617 and [^{68}Ga]Ga^{3+} (Figure 7) showed more tolerance by the cells and were less toxic at higher concentrations compared to the ME with or without PSMA-617 only (Figure 6).

The [^{68}Ga]Ga-PSMA-617-MEs which were used for seeding into 96 well plates were in the size range of 21.15 ± 0.26 nm to 35.77 ± 1.38 nm, a PDI of 0.30 ± 0.00 to 0.64 ± 0.04 and a Zeta potential of -28.70 ± 0.15 mV to -30.10 ± 0.51 mV, respectively. The seeded radioactivity across all the wells (1 mg/ml) was in the range of 20.00- 30.15 MBq which was the total

cumulative radioactivity across all the wells on the plate. Mean activity of 0.70 ± 0.28 MBq was seeded in 100 µl composed of complete media containing 10% FBS per well.

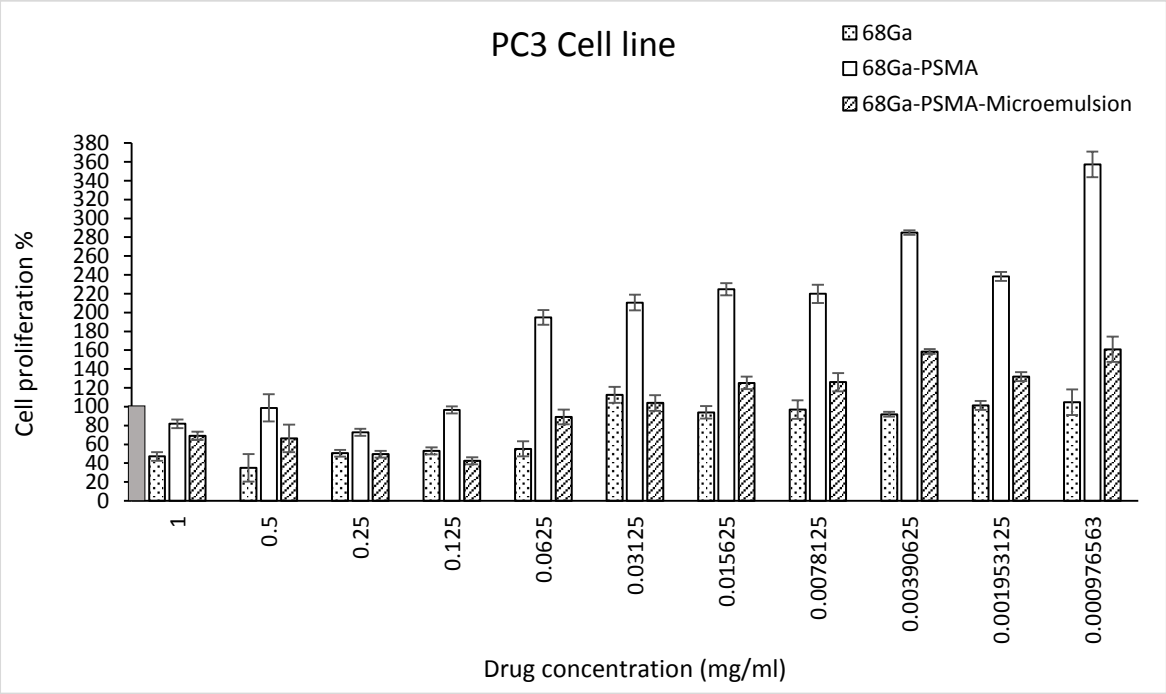

Figure 7: The *in vitro* cytotoxicity of [^{68}Ga]Ga^{3+}, [^{68}Ga]Ga-PSMA-617 and [^{68}Ga]Ga-PSMA-617- loaded ME against PC3 cell lines after 24 h (*n*=9). Grey bar represents the untreated control cells

[^{68}Ga]Ga-PSMA-617 is a radiopharmaceutical peptide conjugate which is used to diagnose prostate cancer which should ideally be non-toxic *in vivo*. Figure 7 showed that both the [^{68}Ga]Ga-PSMA-617 on its own and its ME formulated form were non-toxic to PC3 cell lines at concentrations lower than 0.0625 mg/ml. The PSMA-617 in the ME formulation serves as the ligand to the PSMA-617 receptor on the cell wall. The ME serves to alter the pharmacokinetics and delivery of the formulated PSMA-617. The *in vitro* cytotoxicity profile of the ME in the PC3 cell line showed that it had a similar effect as the [^{68}Ga]Ga^{3+} alone, where the cell viability in the PC3 cell line was affected at concentrations of 0.0625 mg/ml and higher, the main aspect could be the composition of the ME resulted in acute toxicity to the cells. The ME therefore had a seemingly protective function towards the PC3 cell line, increasing the cells tolerance towards the [^{68}Ga]^{68}Ga^{3+} at 0.0625 mg/ml or lower which could help it in serving the purpose of a diagnostic tool. The toxicity of [^{68}Ga]^{68}Ga^{3+} cannot be entirely validated if we consider the negligible ion concentration of the radioactive ^{68}Ga^{3+} ions.

Only concentrations of [^{68}Ga]Ga^{3+} (buffered with 2.5 M sodium acetate to pH 3.5) at 0.0625 mg/ml and higher inhibited cell growth of the PC3 prostate cancer cell line, comparable to what is seen in literature [24]. However, in combination with PSMA-617, the cell viability improved dramatically to more than 80% at all the concentrations except at 0.25 mg/ml which showed a significant measure of toxicity compared to the other concentrations used.

The [^{68}Ga]Ga^{3+} was eluted as [^{68}Ga]GaCl$_3$ with 0.6 M HCl and buffered to pH 3.5- 4 with NaOAc. The presence of the chloride ions and its acidic property may have rendered ≥ 0.0625 mg/ml of the [^{68}Ga]^{68}Ga^{3+} concentrations toxic to the PC3 prostate cancer cell line. [^{68}Ga]Ga^{3+} is a decay product of [^{68}Ge]^{68}Ge^{4-} which in turn decays to zinc-68 (^{68}Zn) which is a non-radioactive isotope. Given the short half-life of [^{68}Ga]Ga^{3+}, the graph data is more a representation of decayed [^{68}Ga]Ga^{3+}, i.e. ^{68}Zn which may be toxic to cells at high concentrations or doses. Zinc at low concentrations on the other hand, plays a vital role in cell division and cell growth. This could be a possible explanation for the proliferated cell growth in all the test compounds containing [^{68}Ga]Ga^{3+} at the lower concentration ranges [24, 25]. Zinc also assists in the release of testosterone and insulin-like growth factor-1 (IGF-1), which build muscle mass and a healthy metabolism [26]. The addition of [^{68}Ga]Ga^{3+} to either ME and/or in combination with PSMA-617 appeared to proliferate PC3 cell growth when compared to that in Figure 6. The [^{68}Ga]Ga-PSMA-617 loaded ME was non-toxic to PSMA-positive PC3 cell lines at very low concentrations.

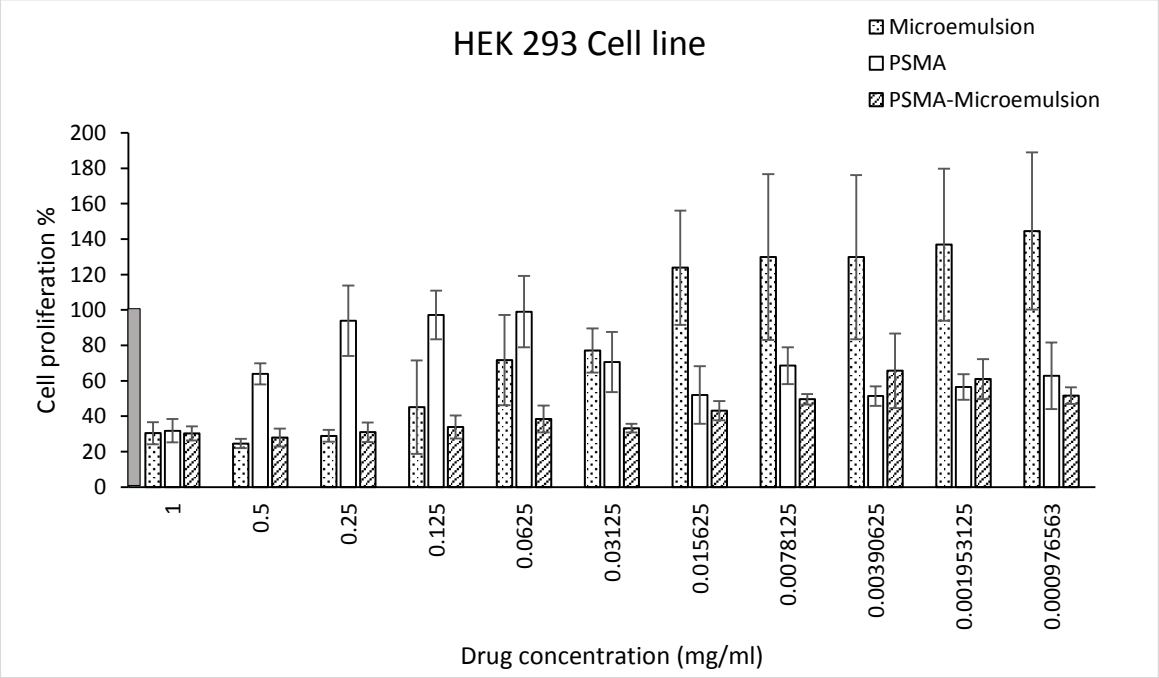

Figure 8: The *in vitro* cytotoxicity of a blank ME, PSMA-617 and PSMA-617-ME against HEK 293 cells after 24 h (*n*=9). Grey bar represents the untreated control cells

When the PSMA-617 and the ME were tested against the HEK 293 cells several observations were made. The results in Figure 8 showed that the PSMA-617-ME formulations inhibited the growth of HEK 293 cells substantially and showed to be mildly toxic even at lower concentrations. A blank ME however presented low toxicity towards the cells at concentrations < 0.0625 mg/ml. Free PSMA-617 did not show concentration dependent toxicities toward the cells. Concentrations of PSMA-617 below 0.015 mg/ml and above 0.5 mg/ml showed toxicity towards the cells. A similar trend albeit less prominent was also observed in PC3 cells [27]. The viability of all three test compounds; ME, PSMA and PSMA-617-ME in Figure 8 against HEK 293 cells was <40% at a high concentration of 1 mg/ml. The toxicity profile of PSMA to HEK293 cells did not show a classical sigmoidal response in the concentration range tested. The ME on its own however proliferated cell growth (<0.125 mg/ml) in both cell lines. Concentrations of [^{68}Ga]Ga-PSMA-617-ME ≥ 0.0078 mg/ml may have induced cell death as a result of early or late stage apoptosis and cell nuclear morphology [28]. Toxicity of the ME may be influenced by particle properties (particle chemistry, mass, surface area, size, state of aggregation and structure [28]. The low cell viability may be a result of dose and time-dependant cytotoxicity associated with cellular necrosis and apoptosis [28]. The combination of [^{68}Ga]Ga^{3+} and PSMA-617 had a synergistic effect on cell proliferation which in part may be due to the cell growth properties of ^{68}Zn, the decay product of [^{68}Ga]Ga^{3+} which probably acted as a nutritional supplement to the cell line [24].

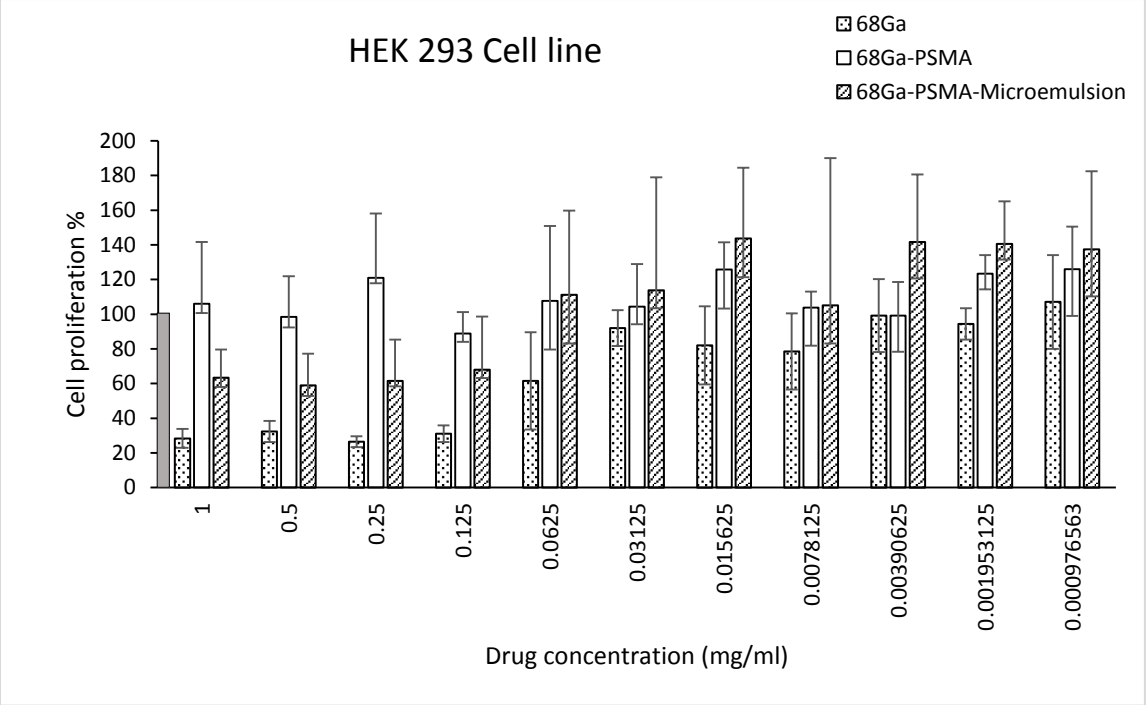

Figure 9: The cytotoxicity of [^{68}Ga]Ga^{3+}, [^{68}Ga]Ga-PSMA-617 and [^{68}Ga]Ga-PSMA-617-ME against HEK 293 cell lines after a 24 h incubation (*n*=9). Grey bar represents the untreated control cells

Figure 9 depicts enhanced cell growth of HEK 293 cells treated with [^{68}Ga]Ga^{3+} in combination with PSMA-617 and ME formulation. [^{68}Ga]Ga-PSMA-617 did not appear to be toxic at all to the concentrations of the test compound, showing cell proliferation beyond 90%. [^{68}Ga]Ga-PSMA-617-ME did not indicate cell toxicity at concentrations lower than 0.125 mg/ml and only showed moderate toxicity at higher concentrations. [^{68}Ga]Ga^{3+} on its own, however inhibited cell growth at concentrations $\geq$ 0.125 mg/ml. Figure 9 showed that both the [^{68}Ga]Ga-PSMA-617 on its own and its formulated form in a ME showed little toxicity towards the HEK293 cells. This information could be advantageous, when considering the safety or toxicity of the diagnostic [^{68}Ga]Ga-PSMA-617 radiopharmaceutical in PSMA-receptor-negative cells.

3.3.4 MicroPET/CT imaging and biodistribution of [^{68}Ga]Ga-PSMA-617-ME

To investigate the biodistribution pathway of [^{68}Ga]Ga-PSMA-617 (0.5-5 nmol) formulated ME, the test compound [^{68}Ga]Ga-PSMA-617-ME was injected into the tail vein of healthy BALB/c mice. The injected radioactivity across all the mice was in the range of 0.76- 13.96

MBq. Several mice (*n*=4) were employed in the *ex vivo* biodistribution study only where low doses were sufficient for data acquisition and quantification. The 0.76 ± 0.24 MBq and 13.96 ± 0.22 MBq were the lowest and highest injected radioactivity, whereas an average dose of 5.89 ± 0.64 MBq was administered into mice for the microPET/CT imaging study.

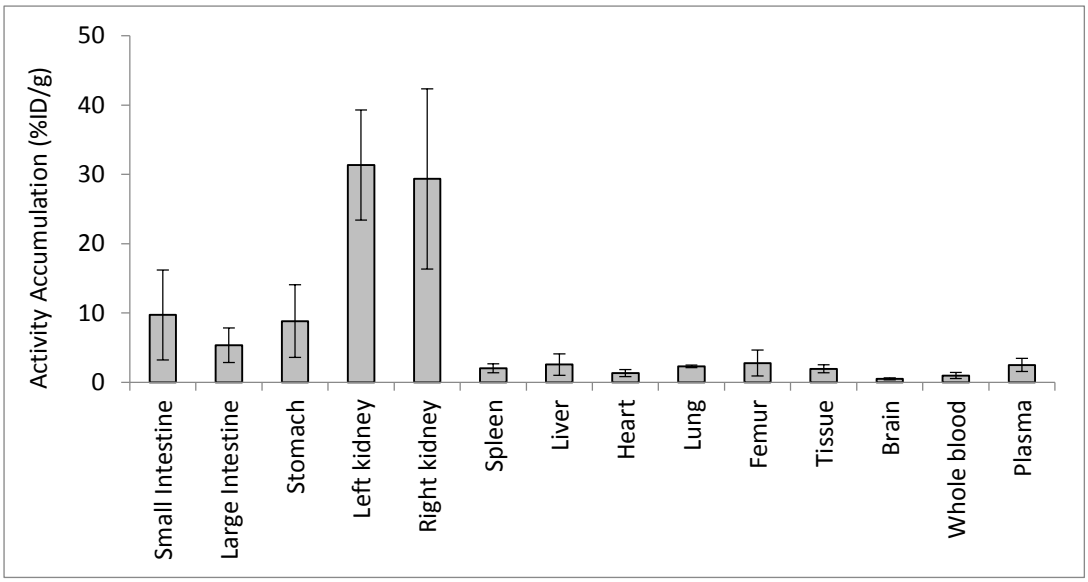

Figure 10: Relative organ biodistribution (%ID/g) analysed *ex vivo* 60 min after intravenous injection of [^{68}Ga]Ga-PSMA-617-ME. Results are expressed as mean ±SD (*n*=4)

Post administration of the [^{68}Ga]Ga-PSMA-617-ME, biodistribution analysis resulted in mainly the excretory organs, viz. the kidneys shown in Figure 10. The kidneys had an average radioactivity of 31.33 %ID/g followed by the small intestine (9.71 %ID/g) and stomach (8.83 %ID/g). Clearance into the small and large intestine will be via the biliary excretion route. This is expected from a formulation consisting of fatty acids. The highest trace amount of [^{68}Ga]Ga-PSMA-617-ME was reported in the left kidney and the lowest in the brain (0.49 %ID/g). Time activity clearance curves indicated that as early as 5 min after IV injection (as shown in Figure 11) there is clearance from the blood pool into the kidney and out via the urine in the bladder. The results in this study show a SUV (%ID/ml) for the bladder of 10 already by 30 min. Benešová *et al* [2] reported for [^{68}Ga]Ga-PSMA-617 a SUV of 6 by 30 min only reaching 10 by 60 min. The SUV for kidneys are also higher, a peak of 5 at 15 min before tailoring off. In this study the kidneys peak at 5 min with a SUV of 3. This may indicate that the kidney retention is lowered by the ME. From the biodistribution data in Figure 10, clearance into the small and large intestine were via the biliary excretion route. This is expected from a formulation consisting of fatty acids. The found %ID/g for these two organs is elevated

if compared to the [^{68}Ga]Ga-PSMA-617 alone[2]. This would also indicate that the ME does indeed alter the biodistribution of the [^{68}Ga]Ga-PSMA-617 providing some evidence that it may assist in reducing the side effects associated with [^{68}Ga]Ga-PSMA-617's solely urinary excretion pathway. This needs to be proven in a head to head study [^{68}Ga]Ga-PSMA-617-ME vs [^{68}Ga]Ga-PSMA-617 in tumour bearing mice.

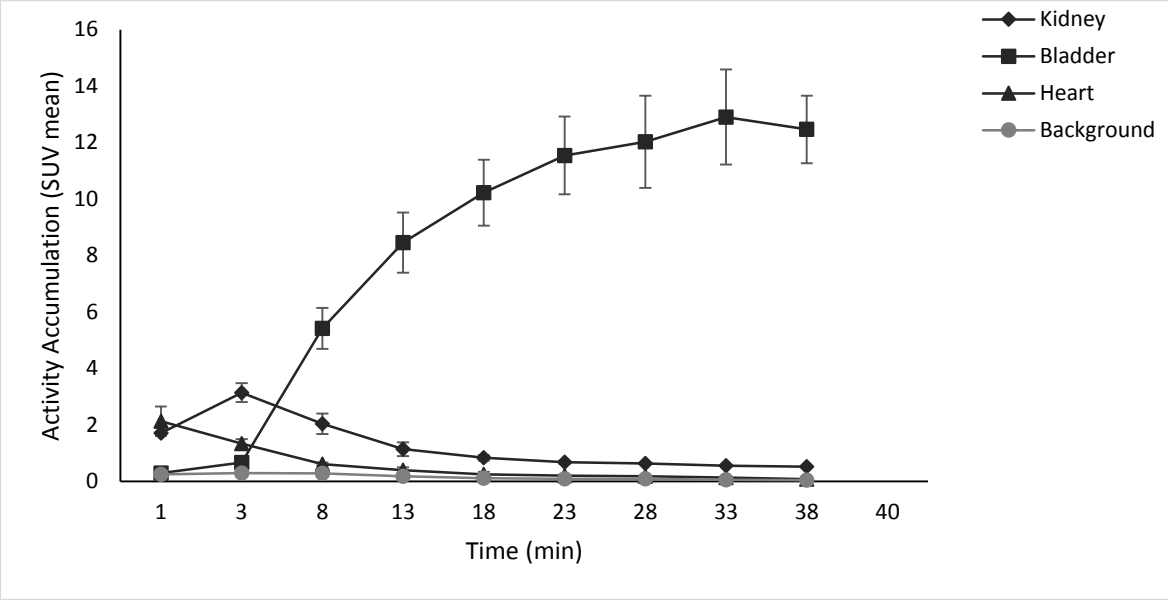

Figure 11: Time activity curve plot for blood pool (heart), kidney and bladder derived from 40 min flow dynamic small animal microPET data of [^{68}Ga]Ga-PSMA-617-ME. Results are expressed as mean standardised uptake value (SUV mean) ± SD (*n*=4)

The highest radioactivity uptake was observed in the kidneys at 2.85 %ID/ml at 3 min post IV injection and decreased to 1.01 %ID/ml after 10 min. The radioactivity subsequently accumulated in the bladder, peaking to a maximum of 12.45 %ID/ml after 38 min as depicted in Figure 11. In literature PSMA-617 was found in other organs, such as the proximal renal tubules and salivary glands [13]. This means that when [^{68}Ga]Ga-PSMA-617 is used as a target for radionuclide therapy, there will be a radiation dose delivered to these organs although at reduced doses as compared to prostate cancer cells [4, 13]. This impacts the safe dose and side effect profile of PSMA-targeted therapy because ultimately significant radiation damage to non-target organs needs to be avoided. Renal uptake of [^{68}Ga]Ga-PSMA-617 is partially due to the route of excretion of the agent and due to specific uptake from the expression of PSMA-617 in mouse proximal renal tubules [12]. The observation of high kidney radioactivity and uptake depicted in Figure 11 indicated rapid renal clearance of the [^{68}Ga]Ga-PSMA-617-ME

from the system and shows a classic clearance curve for radiopharmaceuticals with a much faster clearance through the kidney into the bladder than reported for [^{68}Ga]Ga-PSMA-617 alone [2].

3.4 Conclusion

The physical and chemical characteristics of the optimised ME formulation validated the safety and toxicity aspects of the ME for both *in vitro* and *in vivo* experiments. The physical stability of the formulation remained constant even with the incorporation of [^{68}Ga]Ga-PSMA-617 radiopharmaceutical. In this article, [^{68}Ga]Ga-PSMA-617 was successfully synthesised at a high radiochemical yield under determined conditions. The radiopharmaceutical [^{68}Ga]Ga-PSMA-617 was incorporated into a ME formulation. Additionally *in vitro* cytotoxicity studies revealed that a [^{68}Ga]Ga-PSMA-617 loaded ME was non-toxic to both PSMA-positive PC3 and PSMA-negative HEK 293 cell lines at 0.0625 mg/ml or lower, therefore allowing its evaluation as a delivery system for [^{68}Ga]Ga-PSMA-617 diagnostic studies. The [^{68}Ga]Ga-PSMA-617 loaded ME followed the typical enterohepatic metabolism of [^{68}Ga]Ga-PSMA-617, with rapid excretion from the blood pool with some biliary clearance into the (small and large) intestines which was elevated above the reported values for [^{68}Ga]Ga-PSMA-617 alone. This also indicates that there was also no *in vivo* toxicity observed and no concerns raised by the biodistribution data. This paves the way for further studies in tumour bearing animals to prove that the ME sufficiently enough alters the biodistribution of [^{68}Ga]Ga-PSMA-617 so that it offers the slower release of radiopharmaceuticals from the circulation but not retained by the kidneys for long periods of time when excreted thereby improving their overall tumour uptake and reducing the renal radiation burden.

Acknowledgements

The authors would like to thank and acknowledge the Nuclear Technologies in Medicine and the Biosciences Initiative (NTeMBI), a national technology platform developed and managed by the South African Nuclear Energy Corporation (Necsa) and funded by the Department of Science and Technology (DST). The authors would like to thank you to the Department of Nuclear Medicine at the University of Pretoria and the Council for Scientific and Industrial Research (CSIR) for resources provided. The authors thank Delene van Wyk for the image analysis and Janie Duvenhage for assistance with the biodistribution determination. The authors would also like to thank Biljana Marjanovic-Painter for the HPLC analysis, as well as Kobus Venter and Cor Bester from the North West University for assistance with the animal studies. A special thank you to the Carl and Emily Fuchs Foundation for assisting in funding this project.

References

1. Zhu H, Xie Q, Li N, Tian H, Liu F, Yang Z. Radio-synthesis and mass spectrometry analysis of ^{68}Ga-DKFZ- PSMA-617 for non-invasive prostate cancer PET imaging. J Radioanal Nucl Chem. Springer Netherlands 20^{16}; 309(2): 575–81.
2. Benešová M, Schäfer M, Bauder-Wüst U, Afshar-Oromieh A, Kratochwil C, Mier W, *et al*. Preclinical Evaluation of a Tailor-Made DOTA-Conjugated PSMA Inhibitor with Optimized Linker Moiety for Imaging and Endoradiotherapy of Prostate Cancer. J Nucl Med 2015; 56(6): 914–920.
3. Prostate cancer statistics. World Cancer Research Fund International 2017 November 24. Available from: http://www.wcrf.org/int/cancer-facts-figures/data-specific-cancers/prostate-cancer-statistics.
4. Xu J, Yu J, Xu X, Wang L, Liu Y, Li L, *et al*. Evaluation of PSMA-Targeted Glycol Chitosan Micelles for Prostate Cancer Therapy. J Nanomat 2014; 2014. 462356
5. Afshar-Oromieh A, Avtzi E, Giesel FL, Holland-Letz T, Linhart HG, Eder M, *et al*. The diagnostic value of PET/CT imaging with the ^{68}Ga-labelled PSMA ligand HBED-CC in the diagnosis of recurrent prostate cancer. Eur J Nucl Med Mol Imaging 2014; 42(2): 197–209. 2.
6. Afshar-Oromieh A, Hetzheim H, Kratochwil C, Benesova M, Eder M, Neels OC, *et al*. The novel theranostic PSMA-ligand PSMA-617 in the diagnosis of prostate cancer by PET/CT: biodistribution in humans, radiation dosimetry and first evaluation of tumor lesions. J Nucl Med 2015; jnumed.115.161299-. Available from: http://jnm.snmjournals.org/content/early/2015/08/19/jnumed.115.161299papetoc
7. Eder M, Neels O, Müller M, Bauder-Wüst U, Remde Y, Schäfer M, *et al.* Novel preclinical and radiopharmaceutical aspects of [^{68}Ga]Ga-PSMA-HBED-CC: A new PET tracer for imaging of prostate cancer. Pharmaceuticals 2014; 7: 779–96.
8. Herrmann K, Bluemel C, Weineisen M, Schottelius M, Wester H-J, Czernin J, *et al*. Biodistribution and radiation dosimetry for a novel probe targeting prostate specific membrane antigen for Imaging and Therapy (^{68}Ga-PSMA I&T). J Nucl Med 2015; 1–24. Available from: http://jnm.snmjournals.org/cgi/doi/10.2967/jnumed.115.156133
9. Nedrow JR, Latoche JD, Day KE, Modi J, Ganguly T, Zeng D *et al*. Targeting PSMA with a Cu-64 labeled phosporamidate inhibitor for PET/CT imaging of variant PSMA-expressing xenografts in mouse models of prostate cancer. Mol Imaging Biol 2015
10. Weineisen M, Simecek J, Schottelius M, Schwaiger M, Wester H-J. Synthesis and

preclinical evaluation of DOTAGA-conjugated PSMA ligands for functional imaging and endoradiotherapy of prostate cancer. EJNMMI Res 2014; 4(1): 1–15. Available from: http://www.ejnmmires.com/content/4/1/63

11. Weineisen M, Schottelius M, Simecek J, Baum RP, Yildiz A, Beykan S, *et al.* ^{68}Ga- and ^{177}Lu-Labeled PSMA I&T: Optimization of a PSMA-Targeted Theranostic Concept and First Proof-of-Concept Human Studies. J Nucl Med 2015; 56(8): 1169–76. Available from: http://www.ncbi.nlm.nih.gov/pubmed/26089548
12. Wong P, Li L, Chea J, Delgado MK, Crow D, Poku E, *et al*. PET imaging of ^{64}Cu-DOTA-scFv-anti-PSMA lipid nanoparticles (LNPs): Enhanced tumor targeting over anti-PSMA scFv or untargeted LNPs. Nucl Med Biol 2017; 47: 62–8. Available from: http://dx.doi.org/10.1016/j.nucmedbio.2017.01.004
13. Melariri P, Kalombo L, Nkuna P, Dube A, Ogutu B *et al*. Oral lipid-based nanoformulation of tafenoquine enhanced bioavailability and blood stage antimalarial efficacy and led to a reduction in human red blood cell loss in mice. Int J Nanomed 2015; 10: 1493–1503.
14. Muzaffar F, Singh UK, Chauhan L. Review on microemulsion as futuristic drug delivery. Int J Pharm Pharm Sci 2013; 5(3): 39–53.
15. Moghimipour E, Salimi A, Eftekhari S. Design and characterization of microemulsion systems for naproxen. Adv Pharm Bull 2013; 3(1): 63–71.
16. Emmett L, Willowson K, Violet J, Shin J, Blanksby A and Lee J.. Lutetium-177 PSMA radionuclide therapy for men with prostate cancer : a review of the current literature and discussion of practical aspects of therapy. J Med Rad Sci 2017; 64: 52-60
17. Breeman WAP, de Jong M, de Blois E, Bernard BF, Konijnenberg M and Krenning EP. Radiolabelling DOTA-peptides with ^{68}Ga. Eur J Nucl Med Mol Imaging 2005; 32(4): 478–485
18. Umbricht CA, Bene M, Schmid RM, Türler A, Schibli R, Meulen NP Van Der, *et al*. Sc-PSMA-617 for radiotheragnostics in tandem with ^{177}Lu-PSMA-617- preclinical investigations in comparison with ^{68}Ga-PSMA-11 and ^{68}Ga-PSMA-617. EJNMMI 2017; 7(9): 1-10.
19. Ebenhan T, Vorster M, Marjanovic-Painter B, Wagener J, Suthiram J, Modiselle M, *et al*. Development of a Single Vial Kit Solution for Radiolabeling of ^{68}Ga-DKFZ-PSMA-11 and Its Performance in Prostate Cancer Patients. Molecules 2015; 20(8): 14860–78.
20. Mokaleng BB, Ebenhan T, Ramesh S, Govender T, Kruger HG, Parboosing R, *et al*. Assessment of a Depsipeptide-Derived Compound as a Potential PET / CT Infection

Imaging Agent. BioMed Res Int 2015; 2015, 284354.

21. Parhi R, Suresh P. Preparation and Characterization of Solid Lipid Nanoparticles-A Review. Curr Drug Discov Technol 2012; 9: 2–16.
22. Baroli B, Lopez-quintela MA, Begona M, Fadda AM. Microemulsions for topical delivery of 8-methoxsalen. J Contr Rel 2000; 69: 209–18.
23. Li Y, Maux S, Xiao H and McClements. Emulsion based delivery systems for tributyrin, a potential colon cancer preventative agent. J Agric Food Chem 2009; 57(19): 9243-9249.
24. Chitambar CR. Medical Applications and Toxicities of Gallium Compounds. Int J Environ Res Public Health 2010; 7: 2337–2361.
25. Song Y, Ho E. Zinc and prostate cancer. NIH Public Access. 2009; 12(6): 640–645.
26. Wong P, Abubakar S. Comparative transcriptional study of the effects of high intracellular zinc on prostate carcinoma cells. Oncol Reports 2010; 23: 1501–16.
27. Yao V, Berkman CE, Choi JK, Keefe DSO, Bacich DJ. Expression of Prostate-Specific Membrane Antigen (PSMA), Increases Cell Folate Uptake and Proliferation and Suggests a Novel Role for PSMA in the Uptake of the Non-Polyglutamated Folate , Folic Acid. Wiley Interscience 2009; 1-12.
28. Selvaraj V, Bodapati S, Murray E, Rice KM, Winston N *et al*. Cytotoxicity and genotoxicity caused by yttrium oxide nanoparticles in HEK293 cells. Int J Nanomed 2014; 9: 1379–1391.

Chapter 4: Synthesis and *in vivo* evaluation of PSMA-targeted ^{68}Ga-PSMA-617 and microemulsion for prostate cancer PET/CT imaging

Vusani Mandiwana[1, 2], Lonji Kalombo[1], Philip Labuschagne[1], Rose Hayeshi[2], Thomas Ebenhan[3, 4], Jan Rijn Zeevaart[2, 5]

1 Centre for Polymers and Composites, Council for Scientific and Industrial Research, Pretoria, 0001, South Africa
2 DST/NWU, Preclinical Drug Development Platform, North West University, Potchefstroom, South Africa
3 Department of Nuclear Medicine, University of Pretoria, Pretoria, South Africa
4 Preclinical Imaging Facility, NuMeRI, Pelindaba, South Africa Radiochemistry, South African
5 South African Nuclear Energy Corporation (Necsa), Pelindaba, Pretoria, 0001, South Africa

* Vusani Mandiwana
Centre of Polymers and Composites, Council for Scientific and Industrial Research, P.O. Box 395, Pretoria, 0001, South Africa E-mail: +27 12 841 2985, VMandiwana@csir.co.za

Abstract

Microemulsions (MEs) are designed to potentially improve the therapeutic properties of the encapsulated drug and enhance its bioavailability. The prostate-specific membrane antigen (PSMA) targeting and therapeutic agent i.e. prostate-specific membrane antigen-617 (PSMA-617), which accumulates in prostate tumours, allows for [^{68}Ga]Ga^{3+}-radiolabelling and PET imaging of PSMA-expression *in vivo*. The encapsulation of radiolabelled PSMA-617 in a ME delivery system was hypothesized to enhance its pharmacokinetic properties. This study investigated the synthesis of [^{68}Ga]Ga-PSMA-617 and [^{68}Ga]Ga-PSMA-617 contained within a ME, and its microPET/CT imaging and biodistribution in PC3 xenograft nude male BALB/c mice. [^{68}Ga]Ga-PSMA-617 was synthesized in a combined solid phase and solution chemistry approach. ME was prepared by combining a non-ionic surfactant and long-chain carbon fatty acid ester with an aqueous phase. [^{68}Ga]Ga-PSMA-617 and [^{68}Ga]Ga-PSMA-617-ME, which was synthesized by homogenisation under high temperature, were administered intravenously in PC3-tuomur bearing nude BALB/c mice followed by microPET/CT imaging and *ex vivo* biodistribution. The pharmacokinetics of [^{68}Ga]Ga-PSMA-617 contained in the ME were similar to those of [^{68}Ga]Ga-PSMA-617. The kidneys had an average [^{68}Ga]Ga-PSMA-617-ME radioactivity accumulation of 6.85 %ID/g. The [^{68}Ga]Ga-PSMA-617-ME showed the highest uptake in the plasma (3.70 %ID/g), lungs (3.02 %ID/g) and small intestines (2.64 %ID/g) respectively following the kidney's accumulation. The highest trace amount of [^{68}Ga]Ga-PSMA-617 contained in the ME was reported in the left kidney (6.86 %ID/g) and the lowest in the brain (0.14 %ID/g). Encapsulation of [^{68}Ga]Ga-PSMA-617 in the ME resulted in lower tumour uptake (2.08 %ID/g vs 15.51 %ID/g) for free [^{68}Ga]Ga-PSMA-617).

Both the [^{68}Ga]Ga-PSMA-617 and [^{68}Ga]Ga-PSMA-617-ME followed a typically similar enterohepatic and excretion profile of [^{68}Ga]Ga-PSMA-617, with limited tumour uptake. There was relatively high kidney uptake reported for both test compounds employed under microPET/CT imaging and biodistribution study.

Keywords

Biodistribution, ^{68}Ga, In vivo imaging , Microemulsion, PET/CT, Prostate cancer, PSMA-617

4.1 Introduction

Prostate cancer is the most common cancer in men and one of the leading causes of morbidity globally and in South Africa (Vorster *et al.*, 2015; Zhu *et al.*, 2016). The incidence and mortality of prostate cancer is much higher in African black men than it is in white men (Sathekge *et al.*, 2018). Early detection of prostate cancer is vital for the successful management of the disease. Targeting molecules such as aptamers, folate and peptides have been conjugated with delivery systems to transport anti-tumour drugs or genes for diagnosis and treatment of prostate cancer (Xu *et al.*, 2014).

Prostate specific membrane antigen (PSMA) is a transmembrane glycoprotein that is over-expressed in most prostate cancer disease and is mapped to chromosome 11q14 (Sathekge *et al.*, 2018). PSMA expression increases in metastatic and hormone refractory prostate cancer, which makes it an ideal target for positron emission tomography/computed tomography (PET/CT) imaging and therapy (Sathekge *et al.*, 2018). The application of a PSMA-targeted ligand which is radiolabelled with a therapeutic radioisotope, offers a promising approach for PSMA-targeted diagnosis and/or radiotherapy. There are ongoing studies to evaluate the influence of [^{68}Ga]Ga-PSMA PET/CT on the management of prostate cancer (Afaq *et al.*, 2018; Sathekge *et al.*, 2018). PSMA is a transmembrane protein which is anchored in the cell membrane of prostate epithelial cells. Its presence is correlated to androgen independence, the presence of metastasis and progression of prostate cancer (Rahbar *et al.*, 2018).

Microemulsions (MEs) are used in various fields with increased interest and use in the pharmaceutics field in recent years. This could be due to their cost effective methods of easy preparation. MEs are used as drug delivery systems which can be administered inter alia, topically, orally, parenterally and through nasal routes (Nirmala and Nagarajan, 2016). MEs are designed to potentially improve the therapeutic properties of the encapsulated drug and enhance its bioavailability (Mehta *et al.*, 2016). MEs are colloidal delivery systems made out of a homogenous dispersion of oil, water and surfactants and/or co-surfactants (Mehta *et al.*, 2016). MEs are thermodynamically stable, nano-sized formulations which form spontaneously with an average droplet diameter of 10 to 140 nm and are transparent in appearance (Bhattacharya *et al.*, 2016; Muzaffar *et al.*, 2013). They can be classified as water-in-oil (w/o), oil-in-water (o/w) and bi-continuous phase MEs (Moghimipour *et al.*, 2013). MEs protect unstable drugs against environmental conditions, improve solubility of a poorly soluble drug

resulting in enhanced bioavailability of the encapsulated drug and prolong the shelf-life (Mehta *et al.,* 2016).

Dose and duration of administration of radiopharmaceuticals is limited due to systemic toxicity and the lack of sufficient selectivity to tumour (Xu *et al.,* 2014). Therefore there is a need to design and develop delivery systems that selectively target radiopharmaceuticals into the tumour cells. Delivery systems such as micelles (Xu *et al.,* 2014), liposomes (Wong *et al.,* 2017), lipid-based emulsions (Melariri *et al.,* 2015) and polymeric nanoparticles have demonstrated improved therapeutic index with minimal side effects (Xu *et al.,* 2014). The use of MEs could improve the efficacy of a drug, thus allowing the total dose to be reduced and therefore minimise toxic side effects of the encapsulated compound (Bhattacharya *et al.,* 2016; Muzaffar *et al.,* 2013). The encapsulation of radiopharmaceuticals into MEs offers potential prospects in the approach of diagnosing and/or treating patients with the potential to induce a controlled release of the radiotherapeutics via a slow release mechanism, therefore improving their overall target capabilities and reducing radiation burden to vulnerable organs such as the kidneys or salivary glands.

In this study, [^{68}Ga]Ga-PSMA-617 was encapsulated in a ME as a potential diagnostic tool designed to change the pharmacokinetics of the encapsulated [^{68}Ga]Ga-PSMA-617 with the aim of prolonging its systemic circulation. A subsequent reduction of excretion thereof through the kidneys with the subsequent high radiation burden is expected. The ME was designed to incorporate the radiopharmaceutical compounds so that non-specific delivery could be reduced by prolonging its systemic circulation time, therefore improving delivery to tumour. In the case of the [^{68}Ga]Ga-PSMA-617 encapsulated in the ME, the prolonged circulation time aimed to deliver a greater percentage of the compound to the target by slow release from the ME into the bloodstream and subsequent uptake into tissue creating a greater concentration gradient.

We discuss the synthesis of [^{68}Ga]Ga-PSMA-617 and ME delivery system containing [^{68}Ga]Ga-PSMA-617 ([^{68}Ga]Ga-PSMA-617-ME,) the comparison between [^{68}Ga]Ga-PSMA-617 and [^{68}Ga]Ga-PSMA-617-ME as well as [^{68}Ga]Ga-PSMA-617 and [^{68}Ga]Ga-PSMA-617-ME microPET/CT imaging and biodistribution in PC3 xenograft nude male BALB/c mice.

4.2 Materials and Methods

4.2.1 Materials

The following reagents were purchased from Sigma Aldrich (St Louis, MO, USA): sodium oleate, Tween 80, polyvinyl alcohol (PVA) (97-98% hydrolysed and Mw: 13-23kDa), lauric acid, polyethylene glycol (PEG) 4000 and d-α-tocopherol (Vitamin E). All chemicals, reagents and solvents for the radiosynthesis (i.e. ultrapure, metal-free water) and analysis of the compounds were of analytical grade and were purchased from Sigma Aldrich (St Louis, MO, USA). HPLC-grade ethanol was purchased from Radchem Products Inc. (Orlando Park, Il, USA). PSMA-617 ($C_{49}H_{71}N_9O_{16}$; MW=1042.1 g/mol) was purchased from Advanced Biochemical Compounds (Radeberg, Germany). The chemical structure of PSMA-617 ($C_{49}H_{71}N_9O_{16}$) including a $[^{68}Ga]Ga^{3+}$-complex with DOTA is shown in Figure 4.1.

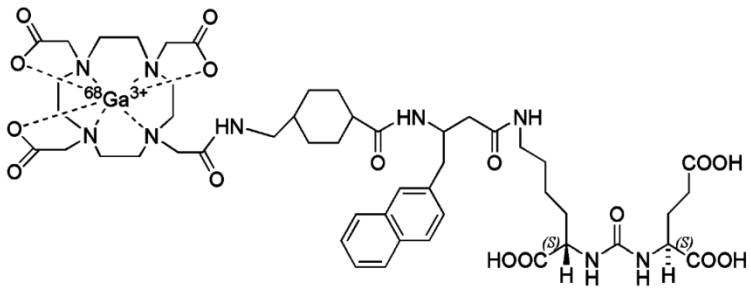

Figure 4.1: A schematic representation of radiolabelled $[^{68}Ga]Ga^{3+}$-PSMA-617

4.2.1.1 Formulation of microemulsion

A water-in-oil-in-water (w/o/w) ME loaded with PSMA-617 was formulated by mixing an aqueous solution with a small amount of an oil phase. An aqueous solution of sodium oleate 0.1% w/v combined with PVA 2% w/v was prepared in a volume ratio of 1:1 and mixed by stirring at room temperature. A lauric acid-PEG 4000 complex, which was obtained via a particles from gas saturated solution (PGSS) supercritical fluid process, was dissolved in ethanol while stirring at 75°C for 2 min. Tween 80, d-α-tocopherol and PSMA-617 were added drop-wise to the lauric acid-PEG 4000 wherein stirring was maintained at 75°C for a further 2 min. The resulting organic solution containing the PSMA-617 was subsequently mixed with the PVA/sodium oleate aqueous solution at room temperature by transferring the contents to

the PVA/sodium oleate dropwise while maintaining stirring for 10 min. The resulting emulsion thereby formed spontaneously producing a translucent ME whilst cooling.

4.2.1.2 Characterisation of microemulsion

Size distribution indicated as the polydispersity index (PDI) and droplet size were measured by dynamic laser scattering (DLS) using a Malvern Zetasizer Nano ZS (Malvern Instruments, Worcestershire, United Kingdom). Each sample was measured in triplicate. The intensity-weighted mean value was measured as the average of three independent measurements. The Zeta potential was determined using a Malvern Zetasizer Nano ZS (Malvern Instruments, Worcestershire, United Kingdom) at pH 6.8 at 25 °C. The instrument calculates the ME net-surface charge by determining the electrophoretic mobility using the Laser Doppler Velocimetry. Each sample was measured in triplicate to determine the Zeta potential values. The pH and conductivity values of each ME were measured at ambient temperature using a pH and conductivity meter (PC 8, Accsen, Lasec, South Africa) at 25 °C by inserting the probe into the ME sample. Characterisation of [^{68}Ga]Ga-PSMA-617 encapsulated into ME was performed after full decay of the radioactivity to below clearance levels. Evaluation of physical stability included visualisation of clarity and phase separation, including the particle size and Zeta potential which were determined by DLS.

4.2.2 ^{68}Ge/^{68}Ga generator elution

The radioactive [^{68}Ga]Ga^{3+} was obtained from a SnO_2-based generator that was loaded with 740 MBq Germamium-68 (iThemba LABS, Somerset West, South Africa). The [^{68}Ga]Ga^{3+} activity was eluted manually using the eluate-fractionation method as previously described (Breeman *et al.,* 2005), and measured in a Capintec dose calibrator (CRC15, Capintec Inc, Pittsburgh, PA, USA). All radioactive measurements were corrected for decay to the time of injection. [^{68}Ga]Ga^{3+} (half-life 68 min, maximum energy of positrons [β^+]: 1.9 MeV (88%)) was obtained as [^{68}Ga]$GaCl_3$ in 2 ml of 0.6 M HCl.

4.2.2.1 ^{68}Ga-radiolabelling of PSMA-617

[^{68}Ga]Ga^{3+}-radiolabelling of PSMA-617 was adopted from a previously described method (Umbricht *et al.,* 2017) making minor adaptations to manage the more acidic [^{68}Ga]Ga^{3+} eluate.

A 2.5 M sodium acetate solution was mixed with 2 ml of [^{68}Ga]Ga^{3+} eluate to adjust the pH to values ranging from 3.5- 4.5. These reaction mixtures were incubated at >95°C for 10-15 min. A 100 mg light Sep-Pak C18 cartridge (Waters, Ireland) was used to purify the mixture of uncomplexed [^{68}Ga]Ga^{3+} and traces of ^{68}Ge which were rinsed off with saline solution. The resulting [^{68}Ga]Ga-PSMA-617 product was extracted from the cartridge with a 50% ethanol saline solution (v/v) and aseptically filtered using a 0.22 µm low protein-binding membrane filter. The radiochemical identity and purity of the product, namely the percentage radiochemical yield (%RCY) and percentage labelling efficiency (%LE; decay-corrected) were determined.

4.2.2.2 High performance liquid chromatography

The quality control of [^{68}Ga]Ga-PSMA-617 was determined using high performance liquid chromatography (HPLC) and instant-thin layer chromatography (ITLC) (Mokaleng *et al.*, 2015) according to previously published methods (Ebenhan *et al.*, 2015). A reverse-phase HPLC column (Zorbax StableBond C18, 0.46 × 2 cm × 5 µm; Agilent Technologies, CA, USA) performing gradient elution (5-95% A-B over 15 min) at a flow rate of 1 mL/min, was employed (Solvent A = 0.1 % aqueous trifluoroacetic acid (TFA); solvent B= 0.1 % TFA in acetonitrile). The HPLC apparatus (Agilent 1200 series HPLC instrument, Agilent Technologies Inc., Wilmington DE, USA) combined radio-detection (GinaStar, Raytest, Straubenhardt, Germany) (counts per second) with a diode array detector following UV absorbance at 214, 220 and 240 nm. A radio-ITLC method employing a silica-gel based solid phase and 0.1 M sodium citrate as mobile phase (free [^{68}Ga]Ga^{3+} [R*f*=0.85] and [^{68}Ga]Ga-PSMA-617 [R*f*=0.2]) supported the HPLC analysis for the determination of %LE.

4.2.3 Encapsulation of [^{68}Ga]Ga-PSMA-617 into microemulsion

Similar to the production of the ME which is described above, Tween 80, d-α-tocopherol and the radiolabelled [^{68}Ga]Ga-PSMA-617 were added dropwise respectively to a lauric acid/PEG 4000 and ethanol solution and stirred continuously at 75°C for 2 minutes. The resulting organic solution containing the [^{68}Ga]Ga-PSMA-617 was transferred dropwise, to a PVA/sodium oleate (1:1) aqueous solution at room temperature and stirred for 10 min. The resulting emulsion was then quenched at ambient temperature, thereby spontaneously producing a radioactive translucent ME. For *in vivo* administration of MEs a physiological pH was desired,

hence; the pH was adjusted with the addition of ~20 µl 2.5 M sodium acetate successfully increasing it to pH in the range of 7-8.

4.2.4 Tumour mouse model

All *in vivo* experiments were approved by the North-West University Animal Care, Health and Safety Research Ethics Committee (NWU-AnimCareREC); ethics number: NWU-00333-15-A5). All mice were bred and obtained under specific pathogen free conditions at the DST/NWU PCDDP Vivarium, North West University (Potchefstroom, South Africa), at the age of 5-6 weeks. Animals were housed in enriched individually ventilated cages (IVC) Rack Isolator System (equipped with input and exhaust fan filter units that provide high efficiency particular air (HEPA) filtered inlet and outlet air) within the DST/NWU PCDDP Vivarium. The housing conditions in the facility were maintained at room temperature of 22 ± 1ºC, relative humidity of 55 ± 10 %, a light/dark cycle of 12 hours and ventilation of 20 air changes per hour under positive pressure. Animals were provided water ad libitum and fed standard rodent maintenance chow, and housed on bedding derived from dust free and non-toxic exfoliated corncob chips in order to absorb urine, excessive moisture and potentially hazardous ammonia vapours.

Human prostate cancer cells (PC3, ATCC-CRL-1435, kindly provided by the Department of Biosciences, Council for Scientific and Industrial Research, South Africa) were grown in Roswell Park Memorial Institute-1640 (RPMI-1640) media (Gibco, Life Technologies, NY, USA) containing L-glutamine and supplemented with 10% foetal bovine serum. The cell line was cultured at 37°C with 5% CO_2 (g) atmosphere. Cells were allowed to adhere to T-75 tissue flasks without antibiotics till they were 80-90% confluent. The adhered cells were detached from the flask into a cell suspension using trypsin, then centrifuged and the supernatant resuspended in PBS. Male nude BALB/c mice (30-40g) were subcutaneously inoculated with passage number 4 (P4) of PSMA-positive PC3 cells (1 x 10^6 cells in 100 µl PBS without $Ca^{2+/}Mg^{2+}$) on the right flank 2 weeks before the performance of the *in vivo* experiments. The tumour volumes were determined by measuring the largest length and the largest perpendicular width of the tumour using calipers and using the formula ½(length x width^2) to calculate the volume. Tumour sizes ranged from 14.55 – 36.29 mm^3 at start of the microPET/CT imaging study.

4.2.4.1 MicroPET/CT imaging study

MicroPET/CT imaging was performed utilizing small animal imaging camera (NanoScan PET/CT, Mediso Medical Systems, Hungary). Animals were immobilized on the scanner bed (orientation: prone, nose first) using a 1.5-2.5% isoflurane/ anaesthetic air mixture for the duration of the scans and were monitored for body temperature and breathing rate. CT X-ray images were acquired for anatomical reference and to allow for scatter and attenuation correction during PET data reconstruction, using the following parameters: 50 KeV, 200 ms, 1:5 binning and a matrix size of 125 x 125 x 125 µm. [^{68}Ga]Ga-PSMA-617-ME (0.38- 5.20 MBq, 100 µl) and [^{68}Ga]Ga-PSMA-617 (0.37-5.60 MBq, 100 µl) were intravenously injected per animal. For each tracer animals underwent dynamic PET/CT imaging for a duration of 1-40 min followed by a static image acquisitions at 120 min post injection. PET data reconstruction was done from list-mode: reconstruction algorithm 3D OSEM Terra Tomo (6 iterations), energy window 400–600 keV, coincidence mode 1–5, corrections for random events, detector normalization, decay and dead time and voxel size 0.6 mm. Mediso Inter View Fusion software (version 2.02.055.2010) was used for data visualization, yielding co-registered PET/CT images in axial, coronal and sagittal orientation. Maximum intensity projection (MIP) images were assessed qualitatively and time activity curves were drawn from dynamic PET data for organs of significant uptake compared to background activity. Therefore three dimensional regions of interest (ROI) were drawn manually including organ or representative tissue and total organ counts as well as tracer concentration were calculated. Image-guided tracer biodistribution data was expressed as standard uptake values (SUV mean) over time and percentage of injected dose per gram (%ID/g).

4.2.4.2 *Ex vivo* biodistribution study

Mice were euthanized by way of cervical dislocation immediately after completion of the last microPET image acquisition. Selected tissue/organs (blood, heart, lungs, liver, spleen, kidneys, intestines, stomach, urine, tissue, bone and brain) were harvested, weighed and measured in an automated γ-counter (Hidex Gamma Counter AMG, Turku, Finland). The results were decay-corrected and expressed as percent injected dose per gram of tissue or organ (% ID/g).

4.2.5 Statistical analysis

All experiments were performed in triplicates or more. Quantitative data was expressed as mean ± standard deviation of mean. Statistical analysis was carried out on the experimental data using the SAS statistical software (version 9.4). A one-sided Mann-Whitney U-test was also used to compare the two groups in terms of organ data. Where applicable, values were statistically validated using Student's *t* tests. *P* values <0.05 were considered statistically significant.

4.3 Results and Discussion

4.3.1 Size and Zeta potential

The chemical and physical properties of the blank ME and [^{68}Ga]Ga-PSMA-617-ME formulations were analysed, namely the droplet size, Zeta potential, pH and conductivity. These parameters have an impact on the stability and release kinetics of the encapsulated radiopharmaceutical. Table 1 summarises the data of blank ME and [^{68}Ga]Ga-PSMA-617-ME formulations (*n*=3). Various parameters, namely the masses, volumes, concentrations and types of excipients were optimised to obtain an average ME particle size ranging between 21.00 and 59.00 nm, with an average polydispersity index ≤0.3. This is referred to in chapter 3 of this thesis. Both ME formulations had a Zeta potential ranging between -18.00 mV and -28.00 mV. The bigger the Zeta potential of the suspension, the more likely it is to be stable because the charged particles repel each other and therefore overcome the natural tendency to aggregate and wherein it is accepted that Zeta potentials more than +/- 30.00 mV are sufficient for good electrostatic stabilization (Parhi and Suresh, 2012). The [^{68}Ga]Ga-PSMA-617 formulations were radioactive and therefore were not tested for size and Zeta potential prior to the *in vivo* study. The ambient room temperature did not affect the physical stability of the formulations, more specifically, it did not influence phase separation or clarity during the study.

Table 4.1: Physicochemical characteristics of ME (blank) and [^{68}Ga]Ga-PSMA-617-ME formulations

	F	Size (nm)	PDI	ZP (mV)	pH	Conductivity (µS/cm)
ME(blank) (Not buffered)	1	25.13 ± 0.02	0.35 ± 0.01	-26.25 ± 0.53	6.50	13.01
	2	22.25 ± 0.31	0.34 ± 0.00	-22.10 ± 3.55	6.89	12.20
	3	25.79 ± 0.13	0.32 ± 0.00	-27.22 ± 0.16	6.90	13.19
^{68}Ga-PSMA-ME (Decayed)	4	30.48 ± 5.06	0.34 ± 0.06	-19.25 ± 0.53	7.50	14.21
	5	58.43 ± 5.25	0.25 ± 0.01	-26.34 ± 0.29	7.00	15.01
	6	52.87 ± 0.38	0.44 ± 0.00	-27.96 ± 0.47	7.40	14.87

F= formulation; PDI=poly dispersity index; ZP=Zeta potential

The resulting pH of the blank ME and [^{68}Ga]Ga-PSMA-617-ME formulations after adjusting to a neutral pH was > 6.89. The pH values obtained from all the formulated MEs were all a pH ≤ 6 before buffering and approaching a neutral pH. For *in vivo* administration of MEs a physiological pH is desired, hence the pH was adjusted with 2.5 M sodium acetate to pH 7.5. The conductivity of the formulations increased slightly after the incorporation of [^{68}Ga]Ga-PSMA-617. Conductance of MEs increases as droplets tend to fuse as a result of the percolation effect, thereby allowing enhanced transportation of ions (Breeman *et al.*, 2005). Galium-68 was fully decayed before these analysis.

4.3.2. Generator elution and ^{68}Ga-radiolabelling of PSMA-617

Generator based eluate fractionation of the radioactivity yielded 138-357 MBq (88-92% [^{68}Ga]Ga^{3+}-activity) in 2 ml, sufficient for straightforward radiolabelling (>99% radionuclide purity). The optimal radiolabelling yield of [^{68}Ga]Ga-PSMA-617 was achieved as a function of pH (3.5-4.5) and temperature (10 -15 min at >95°C). Further optimisations have shown that as low as 20 µg PSMA-617 was sufficient to produce a high [^{68}Ga]Ga-PSMA-617 yield (%LE = 98 ± 2% at pH 3.5 using 9.20- 45.80 MBq/ml eluate; (*n*=5)). The % RCY of [^{68}Ga]Ga-PSMA-617 was ≥97 % (*n*=3) based on ITLC analysis. The radioactivity amount per synthesis yielded for [^{68}Ga]Ga-PSMA-617 ranged from 11 to 50 MBq/ml.

4.3.2.1 High performance liquid chromatography

ME-free samples were analysed immediately after [^{68}Ga]Ga-PSMA-617 radiolabelling. The retention time of [^{68}Ga]Ga-PSMA-617 was 6.44 min. This was after purification of the labelled product. The radiochemical purity of the final product was 100% and the labelling yield was 98%, shown in Figure 4.2. There was no free [^{68}Ga]Ga^{3+} detected in either of the HPLC chromatograms, therefore confirming the radiosynthesis of [^{68}Ga]Ga-PSMA-617. This confirmed that the [^{68}Ga]Ga-PSMA-617 was still intact after the radiolabelling procedure.

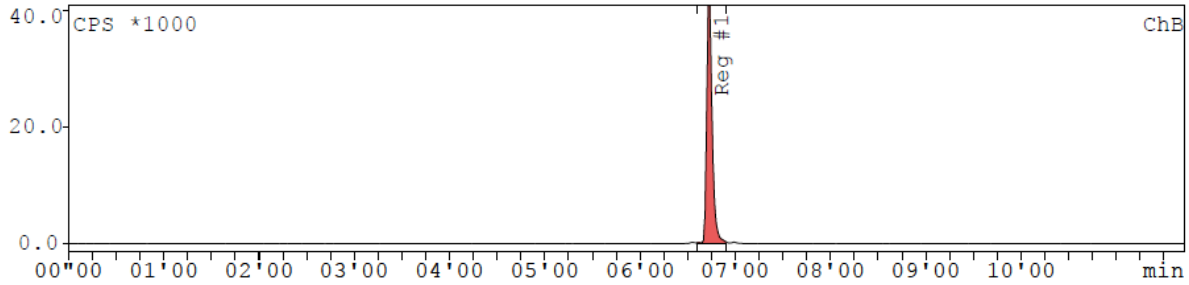

Figure 4.2: Radio-HPLC chromatogram of radiolabelled [^{68}Ga]Ga-PSMA-617, Reg #1 is displaying radioactivity retained at 6.8 min which met the retention time for PSMA-617.

4.3.2.2 Physicochemical characteristics of [^{68}Ga]Ga-PSMA-617-ME for *in vivo* administration

The encapsulation of radio-synthesised [^{68}Ga]Ga-PSMA-617 into MEs was achieved as described above. A decayed [^{68}Ga]Ga-PSMA-617-ME that otherwise would have been used for IV administration int mice were in the size range of 30.48 ± 5.06 nm to 58.43 ± 5.25 nm, a size distribution (polydispersity index) of 0.25 ± 0.01 to 0.44 ± 0.00 and a Zeta potential of -19.25 ± 0.53 mV to -27.96 ± 0.47 mV, respectively. This latter data was obtained from the analysis of fully decayed [^{68}Ga]Ga-PSMA-617-ME using a Malvern Zetasizer Nano ZS.

4.3.3 MicroPET/CT imaging

The biodistribution pathway of [^{68}Ga]Ga-PSMA-617 (0.5-5 nmol) encapsulated into MEs, was investigated by injecting the [^{68}Ga]Ga-PSMA-617-ME into the tail vein of PC3 tumour bearing BALB/c mice. The injected activity across all the mice was in the range of 0.37-5.60 MBq.

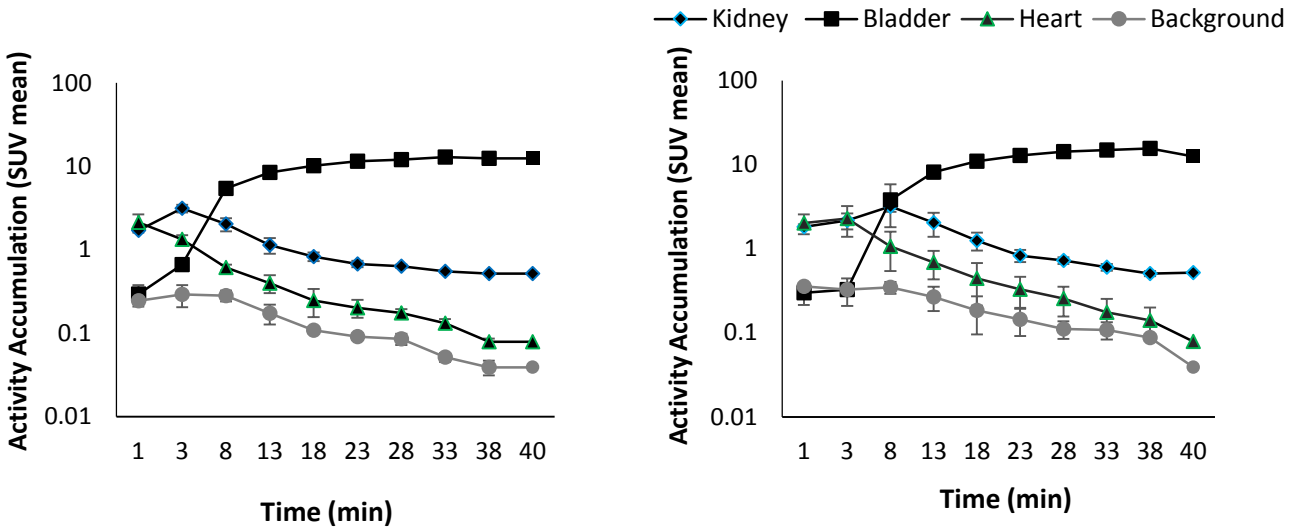

Figure 4.3: Time-activity curves of the heart, kidney and bladder up to 40 min after intravenous injection of [^{68}Ga]Ga-PSMA-617-ME (left) and [^{68}Ga]Ga-PSMA-617 (right). Results are expressed as mean ± SD (*n*=4)

Time activity curves, which were obtained using dynamic microPET/CT image analysis, demonstrated rapid clearance from the kidneys, followed by rapid recovery of radioactivity in the bladder. The highest radioactivity uptake was observed in the kidneys which peaked to 3.14 SUV at 3 min post IV injection of [^{68}Ga]Ga-PSMA-617-ME and decreased to 1.14 SUV after 13 min. The radioactivity subsequently accumulated in the bladder, peaking to a maximum of 12.46 SUV after 38 min (Figure 4.3). The rapid excretion of [^{68}Ga]Ga-PSMA-617 radioactivity is clearly demonstrated by the maximum intensity projection in Figure 4.4. Fast uptake and retention of [^{68}Ga]Ga-PSMA-617-ME over 40 min was observed, whereas the radioactivity was rapidly excreted out of non-target organs. [^{68}Ga]Ga-PSMA-617 followed a similar time activity curve pattern with the highest peak seen in the bladder at 15.57 SUV after 38 min. Small radiolabelled PSMA ligands are excreted primarily via the urinary system and collected in the bladder. Small amounts are excreted via the hepatobiliary system (Fendler *et al.*, 2017). Uptake of [^{68}Ga]Ga-PSMA ligands in the urinary system is partially due to the path of excretion of the agent and specific uptake from the expression of PSMA in mouse proximal renal tubules (Wong *et al.*, 2017). The high kidney uptake and rapid renal excretion of [^{68}Ga]Ga-PSMA depicted in Figure 4.3 shows an expected clearance behaviour for small radiopharmaceuticals (Benešová *et al.*, 2015).

Tumour radioactivity uptake was not evident in the time activity curves adapted from microPET/CT data or maximum intensity projections (MIP) but was however detectable in the *ex vivo* biodistribution data described below.

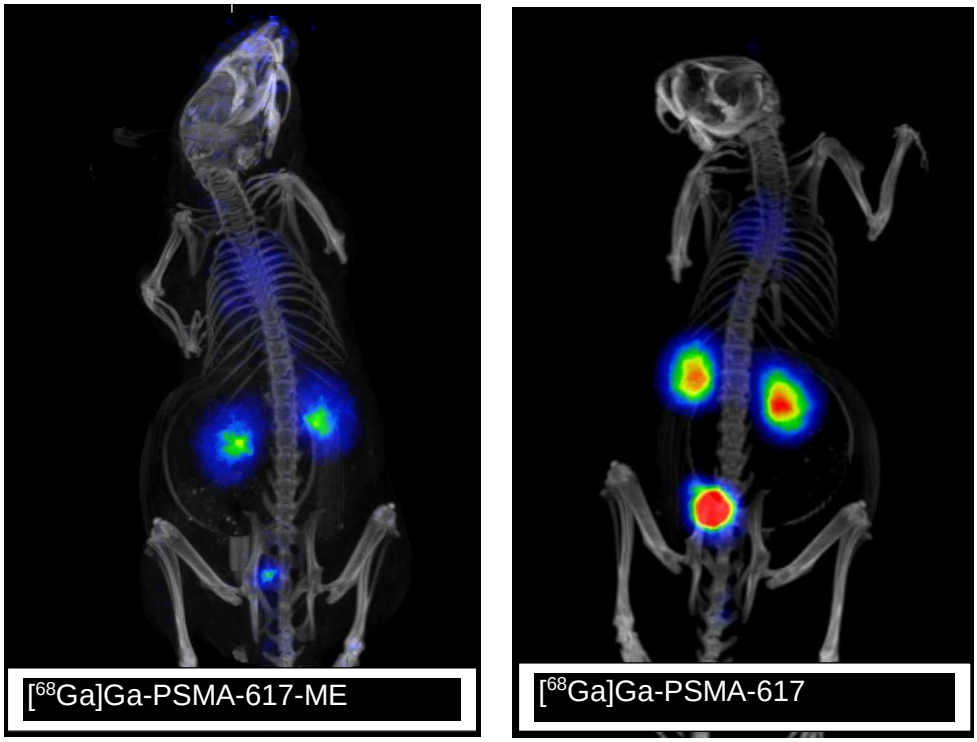

Figure 4.4: MicroPET/CT images as maximum intensity projections (MIPs) of PC3 tumour bearing BALB/c nude mice 40 min after tail vein IV injection of [^{68}Ga]Ga-PSMA-617-ME (left) and [^{68}Ga]Ga-PSMA-617 control (right)

Figure 4.4 shows microPET/CT images of [^{68}Ga]Ga-PSMA-617-ME (left) and [^{68}Ga]Ga-PSMA-617 control (right) 40 min post injection. Qualitative image analysis yielded the following results: rapid uptake of radioactivity was observed in the kidneys soon after injection of both the test compounds. Similar distribution profiles have been observed in mice injected with ^{68}Ga-DOTA labelled peptides as reported in Umbricht *et al*., 2017. There was also visible heart uptake of radioactivity detected after injection of both tracers. The biodistribution of encapsulated [^{68}Ga]Ga-PSMA-617 appeared to be different as compared to blank [^{68}Ga]Ga-PSMA-617. The biodistribution and clearance profile of the [^{68}Ga]Ga-PSMA-617-ME appeared to be slower over time than that of [^{68}Ga]Ga-PSMA-617, this is not visible in the 1-40 min pharmacokinetics but may possibly be at a later time (120 min image scan). However, both compounds showed an expected clearance profile for small-sized polar radiopharmaceuticals, with predominant renal clearance (Umbricht *et al.*, 2017). Despite the

fact that the mice were injected with [^{68}Ga]Ga-PSMA-617-ME three times less activity than those injected with [^{68}Ga]Ga-PSMA-617 the heart shows the same intensity. The amount of activity in the blood pool may be higher for ME as can also be seen from the activity still visible in a blood rich organs. Mice injected with [^{68}Ga]Ga-PSMA-617-ME appeared to show lower retention of radioactivity in the kidneys as compared to those injected with [^{68}Ga]Ga-PSMA-617. This may not necessarily have been the case, taking into account that lower radioactivity may have been injected and also the possibility that the ME may delay biodistribution of [^{68}Ga]Ga-PSMA-617. Tumour uptake is not visible in the microPET/CT images as would be expected, possibly because it was too early in time to detect tumour uptake.

4.3.4 *Ex vivo* biodistribution

Ex vivo biodistribution was done by way of image-guided organ quantification of radioactivity. The evaluation of [^{68}Ga]Ga-PSMA-617-ME and [^{68}Ga]Ga-PSMA-617 in mice revealed organ and tumour accumulation of the compounds shortly after IV injection and rapid excretion of the radioactivity through the kidneys over the 2 hour observation period. The biodistribution of [^{68}Ga]Ga-PSMA-617-ME was different to that of [^{68}Ga]Ga-PSMA-617, with most notably the higher uptake of [^{68}Ga]Ga-PSMA-617-ME in kidneys where there was a statistical difference ($P < 0.05$). There was a statistical difference ($P < 0.05$) between the two formulations which indicated that the lung, femur, tissue, heart, liver and spleen all had statistically significant higher uptake of [^{68}Ga]Ga-PSMA-617-ME than [^{68}Ga]Ga-PSMA-617.

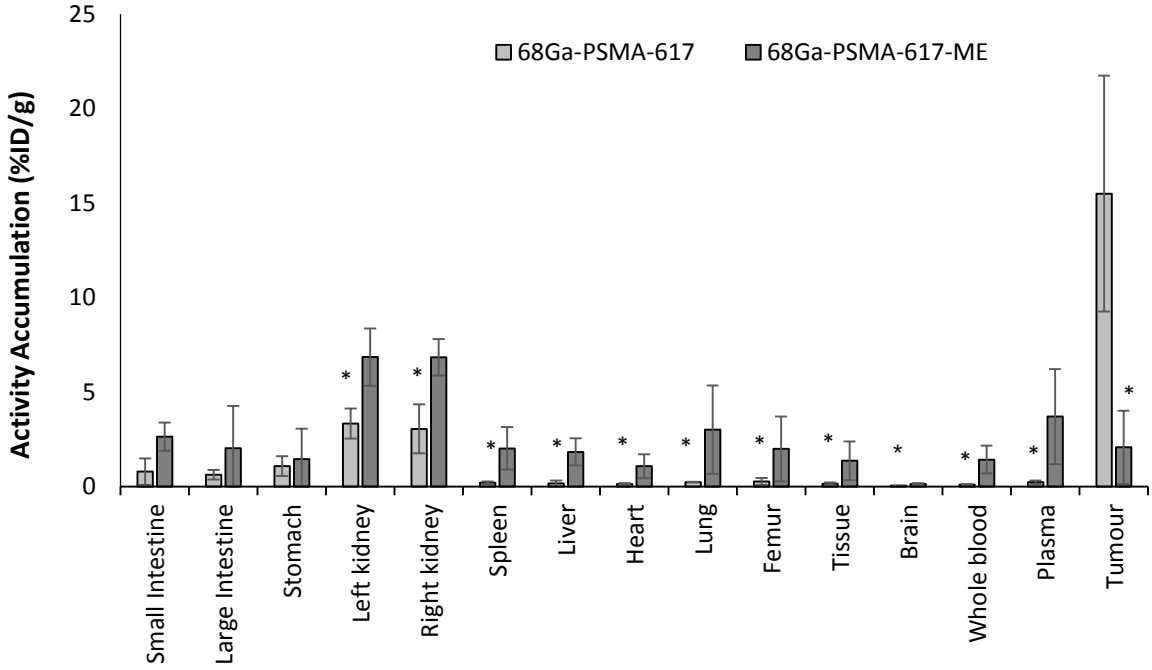

Figure 4.5: Organ biodistribution (%ID/g) of [^{68}Ga]Ga-PSMA-617 and [^{68}Ga]Ga-PSMA-617-ME 60 min after intravenous injection derived from *ex vivo* data. Results are expressed as mean ±SD (*n*=4). *P < 0.05

Statistically significant differences were found between the groups on the kidneys, spleen, liver, heart, lung, tissue, blood, plasma and femur ($p < 0.05$) whereas measurements for the other organ groups were not statistically significant ($p > 0.05$).

Figure 4.5 compares the organ biodistribution between [^{68}Ga]Ga-PSMA-617-ME and [^{68}Ga]Ga-PSMA-617 where the encapsulation of [^{68}Ga]Ga-PSMA-617 in the ME resulted in lower organ uptake and accumulation of radioactivity in most of the respective organs. Biodistribution analysis of both [^{68}Ga]Ga-PSMA-617 and [^{68}Ga]Ga-PSMA-617-ME after IV administration, showed accumulation of radioactivity mainly in the excretory organs, viz. the kidneys (Figure 4.5). The kidneys had an average [^{68}Ga]Ga-PSMA-617 radioactivity accumulation of 3.20 %ID/g. The free [^{68}Ga]Ga-PSMA-617 showed high uptake in the tumour (15.51 %ID/g), kidneys (3.20 %ID/g), and stomach (1.08 %ID/g) respectively (Benesova *et al.*, 2015). It has been previously reported that the highest [^{68}Ga]Ga-PSMA-617 uptake is observed in the kidneys, followed by the tumour, liver, spleen and stomach (Weineisen *et al.*, 2015; Umbricht *et al.*, 2017). Prolonged circulation and protection of [^{68}Ga]Ga-PSMA-617 by the ME should ideally reduce uptake and clearance of [^{68}Ga]Ga-PSMA-617 from the kidneys. Additionally PSMA is also expressed at reduced amounts in healthy cells such as the small intestines, colon, proximal renal tubules, kidneys, liver, spleen and salivary glands (Fendler *et*

al., 2017). This means that radiation dose is delivered to these organs when [^{68}Ga]Ga-PSMA-617 is used for radionuclide targeting. This has an effect on the side effect profile and safe dose that can be delivered without causing damage to non-target tissue (Emmett *et al.*, 2017). However, the prostate cancer would be expected to show a high tumour-to-background ratio compared to the surrounding tissue (Fendler *et al*., 2017).

The encapsulation of [^{68}Ga]Ga-PSMA-617 in a ME may have influenced and/or resulted in statistically significant ($P < 0.05$) lower tumour uptake (2.08 %ID/g) as compared to [^{68}Ga]Ga-PSMA-617 uptake (15.51 %ID/g). This could imply that the ME was delaying or shielding the release of PSMA. The biodistribution data showed that the [^{68}Ga]Ga-PSMA-617-ME had a 7-fold lower uptake in tumour compared to [^{68}Ga]Ga-PSMA-617. The [^{68}Ga]Ga-PSMA-617 showed significantly high ($P < 0.05$) uptake in tumour. There may have been significant variation ($P < 0.05$) in the mice tumour growths, which possibly may have influenced the ability of tumours to take up [^{68}Ga]Ga-PSMA-617, therefore this could also be the reason for the large standard deviation.

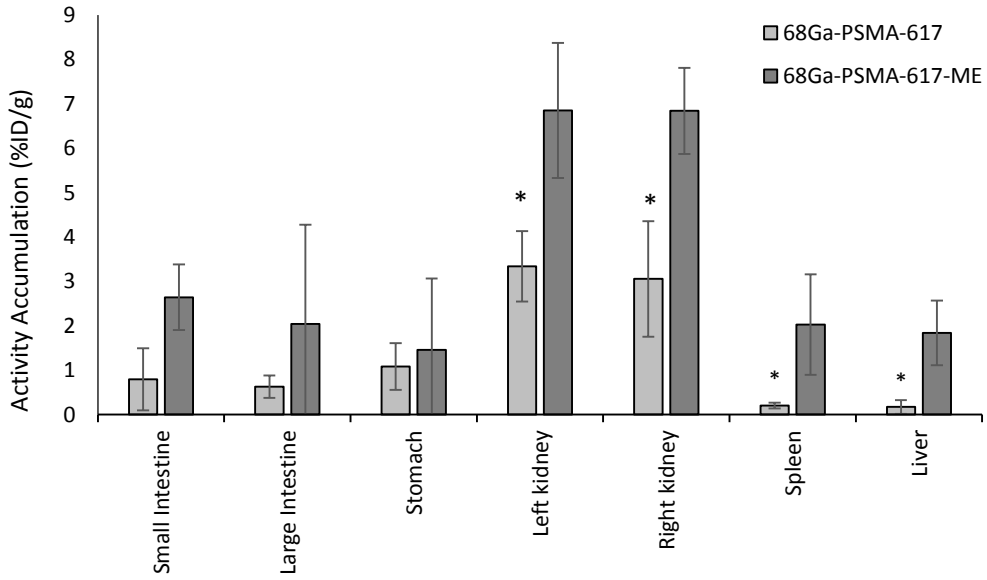

Figure 4.6: Close-up representation of Figure 4.5 organ biodistribution (%ID/g) of [^{68}Ga]Ga-PSMA-617 and [^{68}Ga]Ga-PSMA-617-ME. Results are expressed as mean ±SD (*n*=4). *P < 0.05

The cumulative kidney uptake of [^{68}Ga]Ga-PSMA-617-ME was 2-fold higher than that recorded with [^{68}Ga]Ga-PSMA-617 (averaged 6.85 %ID/g versus 3.20 %ID/g respectively).

The *ex vivo* biodistribution data for the small intestines, large intestines and stomach were not statistically significant ($p > 0.05$) (Figure 4.6).

The highest trace amount of [^{68}Ga]Ga-PSMA-617-ME was reported in the left kidney (6.86 %ID/g) and the lowest in the brain (0.14 %ID/g). Similarly [^{68}Ga]Ga-PSMA-617 had the lowest activity uptake in the brain (0.05 %ID/g). Similar trends in uptake of [^{68}Ga]Ga-PSMA-617 were reported by Weineisen *et al*., 2015. Low brain uptake is typical of [^{68}Ga]Ga-PSMA-617 (Weineisen *et al*., 2015). In this case it is best that the ME did not influence brain uptake since it is a non-target organ.

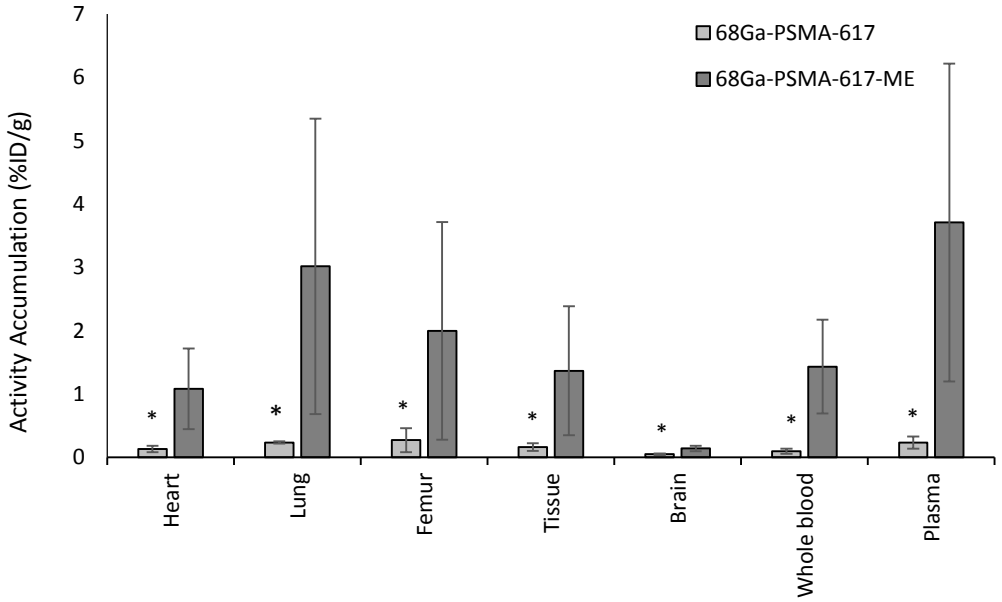

Figure 4.7: Close-up representation of Figure 5 organ biodistribution (%ID/g) of [^{68}Ga]Ga-PSMA-617 and [^{68}Ga]Ga-PSMA-617-ME. Results are expressed as mean ±SD (*n*=4). *P <0.05

The [^{68}Ga]Ga-PSMA-617 which was encapsulated in a ME had much higher blood uptake than the [^{68}Ga]Ga-PSMA-617 alone, representing a (15-fold) higher uptake than the[^{68}Ga]Ga-PSMA-617, shown in Figure 4.7. When [^{68}Ga]Ga-PSMA-617 is incorporated in polymeric nanoparticles (i.e microemulsion, micelles etc), it exhibits delayed blood clearance. MEs are designed to incorporate glycol based amphiphiles to increase blood circulation time *in vivo* and passive accumulation in tumour through the enhanced permeability and retention (EPR) effect (Xu *et al*., 2014). The biodistribution values of the heart, lungs, whole blood and plasma, shown in Figure 4.7 may be an indication of delayed uptake of [^{68}Ga]Ga-PSMA-617-ME to tumour.

4.4 Conclusion

The [^{68}Ga]Ga-PSMA-617 and its formulation into ME were successfully synthesised at a relatively high radiochemical yield featuring a required pH for IV administration under clinical settings as well as good stability of the formulation resulting in an acceptable IV dose. The evaluations of physical stability included visualisation of clarity and phase separation as well as droplet size and surface charge of the formulation which remained constant even after the incorporation of [^{68}Ga]Ga-PSMA-617 radiopharmaceutical and following its decay.

Both the [^{68}Ga]Ga-PSMA-617 and [^{68}Ga]Ga-PSMA-617-ME followed the typical enterohepatic metabolism of [^{68}Ga]Ga-PSMA-617, with rapid excretion from the blood pool and minimal biliary clearance into the small and large intestines. The ME did not alter the biodistribution pattern of [^{68}Ga]Ga-PSMA-617 and maintained distribution to the kidneys. Similarly, encapsulation in the ME may have resulted in delayed uptake into tumours. The ME was an effective and safe delivery system for intravenous administration of [^{68}Ga]Ga-PSMA-617. The radioactivity under *ex* vivo biodistribution data was still sufficient for the detection of tumour for prostate cancer diagnostic purposes but may have required longer scan times to be visualised under microPET/CT possibly due to slow or delayed accumulation of [^{68}Ga]Ga-PSMA-617 into tumours.

Acknowledgements

The authors would like to thank and acknowledge the Nuclear Technologies in Medicine and the Biosciences Initiative (NTeMBI), a national technology platform developed and managed by the South African Nuclear Energy Corporation (Necsa) and funded by the Department of Science and Technology (DST). The authors would like to thank the Department of Nuclear Medicine at the University of Pretoria and the Council for Scientific and Industrial Research (CSIR) for resources provided. The authors thank Delene van Wyk for the image analysis and Janie Duvenhage for assistance with the biodistribution determination. The authors would also like to thank Cor Bester from the North West University for assistance with the animal studies, Biljana Marjanovic-Painter for the HPLC analysis, Ambrose Okem for assistance with inoculation and establishment of the PC3 mouse model, Yolandy Lemmer for assistance with PC3 tumour cell line growth, Department of Biosciences (CSIR) for supplying PC3 tumour cell line. Thank you to the following statisticians Renee Koen (CSIR), Serlom Agbemavor and Rodney Owusu-Darko (University of Pretoria) for assisting with the statistical analysis. A special thank you to the Carl and Emily Fuchs Foundation for assisting in funding this project.

References

Afaq A, Alahmed S, Chen S, Lengana T, Haroon A, Payne H *et al.* 2018. Impact of ^{68}Ga-prostate-specific membrane antigen PET/CT on Prostate Cancer Management. *Journal of Nuclear Medicine* 59: 89–93

Bhattacharya R and Mukhopadhyay S. 2016. Review on microemulsion- as a potential novel drug delivery system. *World Journal of Pharmacy and Pharmaceutical Sciences* 5(6): 700–729

Benešová M, Schäfer M, Bauder-Wüst U, Afshar-Oromieh A, Kratochwil C, Mier W, *et al*. 2015. Preclinical Evaluation of a Tailor-Made DOTA-Conjugated PSMA Inhibitor with Optimized Linker Moiety for Imaging and Endoradiotherapy of Prostate Cancer. *Journal of Nuclear Med*icine 56(6): 914–920

Breeman WAP, de Jong M, de Blois E, Bernard BF, Konijnenberg M and Krenning EP. 2005. Radiolabelling DOTA-peptides with ^{68}Ga. *European Journal of Nuclear Medicine and Molecular Imaging* 32(4): 478–485

Emmett L, Willowson K, Violet J, Shin J, Blanksby A and Lee J. 2017. Lutetium-177 PSMA radionuclide therapy for men with prostate cancer : a review of the current literature and discussion of practical aspects of therapy. *Journal of Medical Radiation Science* 64: 52-60

Fendler WP, Eiber M, Beheshti M, Bomanji FC *et al*. 2017. ^{68}Ga-PSMA PET/CT: Joint EANM and SNMMI procedure guideline for prostate cancer imaging: version 1.0. *European Journal of Nuclear Medicine and Molecular Imaging* DOI 10.1007/s00259-017-3670-z

Kgatle MM, Kalla AA, Islam MM, Sathekge M and Moorad R. 2016. Prostate Cancer : Epigenetic Alterations , Risk Factors , and Therapy. *Prostate Cancer* 2016: 5653862

Mehta DP, Rathod HJ and Shah DP. 2016. Microemulsions: A potential novel drug delivery system. *International Journal of Pharma and Drug Development* 1(1): 37-47

Melariri P, Kalombo L, Nkuna P, Dube A, Ogutu B *et al*. 2015. Oral lipid-based nanoformulation of tafenoquine enhanced bioavailability and blood stage antimalarial efficacy and led to a reduction in human red blood cell loss in mice. *International Journal of Nanomedicine* 10: 1493–1503

Moghimipour E, Salimi A and Eftekhari S. 2013. Design and characterization of microemulsion systems for naproxen. *Advanced Pharmaceutical Bulletin* 3(1): 63–71

Mokaleng BB, Ebenhan T, Ramesh S, Govender T, Kruger HG, Parboosing R *et al*. 2015. Assessment of a Depsipeptide-Derived Compound as a Potential PET / CT Infection Imaging Agent. *BioMed Research International* 2015: 284354

Muzaffar F, Singh UK and Chauhan L. 2013. Review on microemulsion as futuristic drug delivery. *International Journal of Pharmaceutical Sciences* 5(3): 39–53

Nirmala and Nagarajan. 2016. Microemulsions as Potent Drug Delivery Systems. *Nanomedicine & Nanotechnology* 7(3): 7439

Parhi R, Suresh P. 2012. Preparation and Characterization of Solid Lipid Nanoparticles-A Review. *Current Drug Discovery Technology* 9: 2–16.

Rahbar K, Afshar-Oromieh A, Jadvar H and Ahmadzadehfar H. 2018. PSMA theranostics: Current status and future directions. *Molecular imaging* 17: 1-9

Sathekge M, Lengana T, Maes A, Vorster M, Zeevaart JR, Lawal I *et al.* 2018. ^{68}Ga-PSMA-11 PET / CT in primary staging of prostate carcinoma : preliminary results on differences between black and white South-Africans. *European Journal of Nuclear Medicine and Molecular Imaging* 45: 226–234

Umbricht CA, Bene M, Schmid RM, Türler A, Schibli R, Meulen NP Van Der *et al*. 2017. Sc-PSMA-617 for radiotheragnostics in tandem with ^{177}Lu-PSMA-617- preclinical investigations in comparison with ^{68}Ga-PSMA-11 and ^{68}Ga-PSMA-617. *EJNMMI* 7(9): 1-10

Vorster M, Modiselle M, Ebenhan T, Wagener C, Sello T, Zeevaart JR *et al*. 2015. Fluorine-18-Fluoroethylcholine PET/CT in the detection of prostate cancer: A South African experience. *Hellenic Journal of Nuclear Medicine* 18(1): 53–59

Weineisen M, Schottelius M, Simecek J, Baum RP, Yildiz A, Beykan S *et al.* 2015. ^{68}Ga- and ^{177}Lu-Labeled PSMA I&T: Optimization of a PSMA-Targeted Theranostic Concept and First Proof-of-Concept Human Studies. *Journal of Nuclear Medicine* 56(8): 1169–76

Wade CA and Kyprianou N. 2018. Profiling prostate cancer therapeutic resistance. *International Journal of Molecular Sciences* 19(904): 1-19

Wong P, Li L, Chea J, Delgado MK, Crow D, Poku E *et al*. 2017. PET imaging of ^{64}Cu-DOTA-scFv-anti-PSMA lipid nanoparticles (LNPs): Enhanced tumor targeting over anti-PSMA scFv or untargeted LNPs. *Nuclear Medicine and Biology* 47: 62–8

Xu J, Yu J, Xu X, Wang L, Liu Y, Li L *et al*. 2014. Evaluation of PSMA-Targeted Glycol Chitosan Micelles for Prostate Cancer Therapy. *Journal of Nanomaterial* 2014: 462356

Zhu H, Xie Q, Li N, Tian H, Liu F and Yang Z. 2016. Radio-synthesis and mass spectrometry analysis of ^{68}Ga-DKFZ- PSMA-617 for non-invasive prostate cancer PET imaging. *Journal of Radioanalitical and Nuclear Chemistry* 309(2): 575–81

Chapter 5*: In vivo* evaluation of acute intravenous toxicity of a microemulsion

Vusani Mandiwana[1, 2], Lonji Kalombo[1], Philip Labuschagne[1], Rose Hayeshi[2], Thomas Ebenhan[3, 4], Jan Rijn Zeevaart[2, 5]

1 Centre for Polymers and Composites, Council for Scientific and Industrial Research, Pretoria, 0001, South Africa

2 DST/NWU, Preclinical Drug Development Platform, North West University, Potchefstroom, South Africa

3 Department of Nuclear Medicine, University of Pretoria, Pretoria, South Africa

4 Preclinical Imaging Facility, NuMeRI, Pelindaba, South Africa Radiochemistry, South African

5 Nuclear Energy Corporation, Pelindaba, Pretoria, 0001, South Africa

Abstract

Microemulsions (MEs) are reported to improve the efficacy of a drug, minimise side effects and toxicity of the encapsulated compound. MEs are hypothesized to aid in making the encapsulated compound, which has been incorporated within the ME, safe *in vivo* due to reduced side effects and toxicity to the kidneys and other non-target organs. The rationale of this study was to provide a clear toxicity profile of intravenously administered MEs and ME containing [^{68}Ga]Ga-PSMA-11. ME and [^{68}Ga]Ga-PSMA-11-ME which were synthesized by homogenisation under high temperature were administered intravenously in healthy male BALB/c mice. Mice were observed for 14 days, which involved observation of clinical signs, mortality, body weights, and gross necropsy findings. Animals were euthanized after 14 days and respective organs and blood samples were isolated. Blood test results included assessment of ALT, AST, total protein, urea, creatinine and serum lipid levels. There were no abnormal changes observed in the body weight, coat condition, respiration, mobility and behaviour of any of the mice during the study. None of the mice died during the 14 day study. None of the treatment groups showed any treatment related toxicity of either ME and [^{68}Ga]Ga-PSMA-11-ME treatment compounds.

Keywords

[^{68}Ga]Ga-PSMA-11-ME, In vivo, Microemulsion, Toxicity

5.1 Introduction

There is a medical need to develop drug delivery systems that selectively transport anti-tumour drugs or radiopharmaceuticals into tumour cells with the intention of enhancing the efficacy of existing drugs. Delivery systems, which have demonstrated improved therapeutic index with minimal side effects, include micelles (Xu *et al.*, 2014), liposomes (Wong *et al.*, 2017), lipid-based emulsions (Melariri *et al.*, 2015) and polymeric nanoparticles (Xu *et al.*, 2014). The use of delivery systems such as microemulsions (MEs) can improve the efficacy of a drug, allowing the total dose to be reduced and therefore minimise side effects and toxicity of the encapsulated compound (Muzaffar *et al*., 2013). Preparation of a ME typically involves dissolving an appropriate amount of a drug in either an oil or aqueous phase and surfactant and mixing the solubilized mixture with co-surfactant to form the ME at specific temperatures (Ma *et al.*, 2013). The ME that will be discussed below was adapted from Melariri *et al*, 2015, which aimed to enhance the solubility of an anti-malaria drug and envisaged that a ME could lead to a reduction in toxicity (Melariri *et al*., 2015). The ME was reported to enhance the oral bioavailability of tafenoquine, which could be ascribed to enhanced solubility through formulation as a ME. The maximum plasma concentration (C_{max}) of the encapsulated drug was also increased when the drug was incorporated into the ME. Furthermore, the doses of the drug could be increased without corresponding toxicity in mice (Melariri *et al.*, 2015). An intravenous (IV) ME would typically contain lipids/oils, medium-chain triglycerides, polyethylene glycol (PEG) and water (Aboumanei *et al*., 2018; Hippalgaonkar *et al.*, 2010; Ma *et al.*, 2013). The small droplet size of the ME enables the delivery system to escape uptake and phagocytosis by the reticuloendothelial system and increase the circulation time of the encapsulated drug. The ME discussed in herein is similar in protocol to the one discussed by Melariri *et al.*, 2015 and Ma *et al*, 2013 for IV administration.

A ME is a colloidal system made up of various components including water, oil and an amphiphile, which is optically isotropic and a dispersion of homogenous oil and water (Muzaffar *et al.*, 2013). MEs are translucent and form spontaneously with an average droplet diameter of 10 to 140 nm (Muzaffar *et al.*, 2013). MEs can be classified as water-in-oil (w/o), oil-in-water (o/w) and bi-continuous phase MEs (Moghimipour *et al.*, 2013). They are thermodynamically stable and nanostructured (Moghimipour*et al.*, 2013). MEs offer numerous advantages over other dosage systems as drug delivery systems. The following are

some of the advantages of MEs; they are thermodynamically stable and therefore need minimal energy to formulate, allow controlled drug release and targeting and improve the efficacy of the drug, therefore allowing the total dose to be reduced and thus reducing side effects of the drug (Bhattacharya *et al*., 2016;; Lopes, 2014; Mehta *et al.*, 2016;):

Furthermore, MEs offer the ability to slowly release drugs from their core averting a burst release observed with conventional formulations (Bhattacharya *et al.*, 2016). The rationale behind encapsulation of radiopharmaceuticals into MEs is that it offers potential prospects in the approach of diagnosing and/or treating patients with slow-release radiotherapeutics, improving their overall uptake and reducing radiation burden to vulnerable organs such as the kidneys or salivary glands. It is hypothesized that encapsulation of radiopharmaceuticals into a ME would reduce the dose of radiation exposure and ultimately lower expenses in diagnosis and radiotherapy. It is also hypothesized that the ME would aid in better delivery mechanisms through addition of polyethylene glycol therefore having increased systemic circulation time.

We have been investigating the ME as a delivery system for [^{68}Ga]Ga-PSMA-11, a prostate cancer targeting compound. The rationale of this study was to provide a clearer toxicity profile of IV administered MEs and ME delivery system containing [^{68}Ga]Ga-PSMA-11 henceforth referred to as [^{68}Ga]Ga-PSMA-11-ME. Radiopharmaceutical agent, namely [^{68}Ga]Ga-PSMA-11 which was incorporated in a ME delivery system to evaluate the IV toxicity in mice was a critical step in the investigation of this ME application. This could also impact other uses of this ME formulation developed in future. This approach to encapsulate radiopharmaceutical prostate cancer targeting compounds into a ME delivery system could lead to optimised delivery systems, which serve to prevent toxicity and kidney accumulation of the radiopharmaceutical compound. The ME delivery system was hypothesized to aid in making the diagnostic compound, which had been incorporated within the ME, safe *in vivo* due to reduced side effects and toxicity to the kidneys and other non-target organs. These delivery systems should ideally distribute the incorporated radioactive [^{68}Ga]Ga-PSMA-11 to the prostate cancer through passive targeting via the enhanced permeability and retention (EPR) effect reducing toxic uptake or accumulation in the kidneys.

This study aimed to contribute to knowledge on the toxicity of the ME delivery system with specific reference to IV administration. This was a critical investigation since IV applications (i.e. propofol, Intralipid®) of this technology are currently progressing to more clinical

applications. In the acute toxicity study that was conducted, the effects of a single dose ME, were evaluated. Acute toxicity testing attempts to derive maximum information from a minimum number of study animals where the following can be determined; the clinical signs attributable to high doses (i.e. high dose volume or high concentration/ activity of the radioactive agent) of the test substance, time of onset and remission of those signs, possible determination of a minimum lethal dose and of effects leading to death or recovery (Gad, 2014).

The aim of this study was to synthesize radiolabelled [^{68}Ga]Ga-PSMA-11, entrap it in a ME and to obtain more information on the toxicity profile of a ME formulation in conjunction with clinically approved [^{68}Ga]Ga-PSMA-11. Characterised MEs were administered IV to healthy male BALB/c mice.

5.2 Materials and Methods

5.2.1 Materials

Sodium oleate, Tween 80, polyvinyl alcohol (PVA) (97-98% hydrolysed and Mw: 13-23kDa), lauric acid, polyethylene glycol (PEG) 4000 and d-α-tocopherol were purchased from Sigma Aldrich (St Louis, MO, USA). All these excipients are FDA approved and safe for both oral and IV administration (Katiyar *et al.*, 2013; Melariri *et al.*, 2015). Ethanol was purchased from Radchem Products Inc. (Orlando Park, Il, USA). PSMA-11 was supplied by NTP (Necsa, Pelindaba, South Africa).

5.2.1.1 Formulation of microemulsion

A ME was formulated by mixing an aqueous solution of non-ionic surfactant with an organic phase. Sodium oleate 0.1% w/v and PVA 2% w/v were prepared by stirring at room temperature in volume ratio of 1:1. Lauric acid-PEG 4000, was dissolved in ethanol while stirring at 75°C for 2 min. Tween 80, d-α-tocopherol and saline were added drop-wise to the organic phase while maintaining stirring at the same heating temperature for a further 2 min. The resulting organic solution was mixed into the PVA/sodium oleate aqueous solution at room temperature while maintaining stirring for 10 min. The resulting emulsion was thereby formed spontaneously producing a translucent ME formulation (Melariri *et al*., 2015).

5.2.1.2 Radiolabelling of [^{68}Ga]Ga-PSMA-11

[^{68}Ga]Ga^{3+} was obtained from a SnO_2-based generator that was loaded with 298.9 MBq Germamium-68 (iThemba LABS, Somerset West, South Africa). The [^{68}Ga]Ga^{3+} activity was manually eluted by way of an eluate-fractionation method as previously described by Breeman *et al.*, 2005, measured in a dose calibrator (CRC15, Capintec Inc, Pittsburgh, PA, USA). [^{68}Ga]Ga^{3+} was obtained as [^{68}Ga]$GaCl_3$ in 2 ml of 0.6 M HCl.

The [^{68}Ga]Ga^{3+}-radiolabelling of PSMA-11 was adopted from a previously described method (Umbricht *et al.*, 2017) making minor adaptations to manage the more acidic [^{68}Ga]Ga^{3+} eluate. A 2.5 M sodium acetate solution was mixed with 2 ml of [^{68}Ga]Ga^{3+} eluate to adjust the pH to values ranging from 3.5- 4.5. The [^{68}Ga]Ga^{3+} and PSMA-11 reaction mixture was incubated at 95°C for 15 min. A Sep-Pak C18 (100 mg light) cartridge (Waters, Ireland) was used to purify the mixture from un-labelled [^{68}Ga]Ga^{3+} and traces of ^{68}Ge which were rinsed off using saline solution. The resulting [^{68}Ga]Ga-PSMA-11 product was extracted from the cartridge with a 50% ethanol saline solution (v:v) and aseptically filtered using a 0.22 µm low protein-binding membrane filter.

5.2.1.3 Formulation of [^{68}Ga]Ga-PSMA-11-ME

Similar to the formulation of the ME described above in 5.2.1.1., Tween 80, d-α-tocopherol and the radiolabelled [^{68}Ga]Ga-PSMA-11 were added dropwise respectively to a lauric acid-PEG 4000 solution and maintained stirring at a 75°C for 2 minutes. The resulting organic solution containing the [^{68}Ga]Ga-PSMA-11 was transferred dropwise, to a PVA/sodium oleate (1:1) aqueous solution at room temperature and maintained stirring for 10 min. The resulting emulsion was adjusted to a neutral pH with a few drops of 2.5 M sodium acetate and quenched at ambient temperature, thereby spontaneously producing a radioactive translucent ME.

5.2.2 Characterisation of microemulsion

Droplet size and the polydispersity index (PDI) were measured by dynamic laser scattering or photon correlation spectroscopy using a Malvern Zetasizer Nano ZS (Malvern Instruments, Worcestershire, United Kingdom). Each sample was measured in triplicate. The intensity-weighted mean value was measured as the average of three independent measurements. The

Zeta potential was determined using a Malvern Zetasizer Nano ZS (Malvern Instruments, Worcestershire, United Kingdom) at pH 6.8, 25 °C. The instrument calculates the ME net-surface charge by determining the electrophoretic mobility using the Laser Doppler Velocimetry. Each sample was measured in triplicate to determine the Zeta potential. The pH values of the MEs were determined at ambient temperature using a pH meter (PC 8, Accsen, Lasec, South Africa) at 25 °C by inserting the probe into the ME. The ME formulations were evaluated for physical stability by observing clarity and phase separation of the formulations over more than 8 weeks at ambient room temperature.

5.2.3 *In vivo* toxicity assays

This *in vivo* toxicity study was approved by the North-West University Animal Care, Health and Safety Research Ethics Committee (NWU-AnimCareREC); ethics number: NWU-00183-18-A5). Male BALB/c mice (15- 25 g) were bred at the DST/NWU PCDDP Vivarium, North West University (Potchefstroom, South Africa).. This facility is an OECD Good Laboratory Practice (GLP) compliant facility for toxicity studies accredited by the South African National Accreditation System (SANAS). Mice were housed in group cages based on breeding batch and behaviour, and were monitored once during the first 30 minutes, twice during the first 24 hours and daily thereafter. The temperature in the housing facility was maintained at 21 ± 2°C and a relative humidity of 55 ± 10% for the duration of the study. The BALB/c mice were 6 weeks old at the time of enrolment into the study and assigned to two treatment groups (n= 5 per group). The animals were selected randomly for each treatment test formulation. Weighing and consumption of food was monitored daily, including animal health observations for the duration of the study. The assessment, health check and monitoring involved observation of changes in physical condition (skin coat, eyes, mucous membranes), excretion (presence of abnormal urinary symptoms and diarrhoea), behavioural changes and respiratory abnormalities.

The study design was adapted from the OECD 420 acute oral toxicity. Groups of animals were divided into two test groups and administered with a fixed dose of 150 µl of ME or [^{68}Ga]Ga-PSMA-11-ME. The control group was allocated only one test animal due to unforeseen circumstances, which was a limitation because this cohort would result in data that is not statistically significant.

A Limit test was done starting with a dose of 150 µl (*n*=1) followed by dosing a further four animals. The starting dose was 150 µl, which was the maximum dose that could be injected into a mouse IV (Vanhove *et al*., 2015). This dose in volume was the upper limit of the IV dose that could result into the required tolerable radiation during our previous biodistribution study (not presented here). The test compound was administered to one test animal via the IV route with 24 hours between each test animal. The ME and [^{68}Ga]Ga-PSMA-11-ME test compounds were prepared eleven weeks prior and ready to use. A health check was done on each animal prior to administration of the test compound and recorded. The study animals were weighed and their weights recorded. Injection containing 150 µl of ME or [^{68}Ga]Ga-PSMA-11-ME was administered once to one mouse via the IV tail vein. This injected dose, route of administration and administered substance were then recorded. The animals were monitored over 24 hours. Once the first animal which received the upper limit dose had survived, the second animal subsequently received the same dose. Once the total of the subsequent four animals had been dosed and no deaths or distress due to toxicity had occurred after 14 days, the Limit test was then terminated. Euthanasia of all the mice was performed on the respective 14th day via cervical dislocation.

5.2.4 Haematology and clinical biochemistry

Blood samples were collected in SST II Advance tubes for haematological and clinical chemistry analysis directly after euthanasia. Clinical biochemistry of blood samples which were analysed measured the amount of sodium, potassium, urea and creatinine as an indicator of kidney function. Total protein, albumin, bilirubin, phosphatase, alanine transaminase (ALT), aspartate transaminase (AST) and Amylase were measured as indicators of liver function. A lipid profile (total cholesterol, high density lipoproteins (HDL), low density lipoproteins (LDL) and triglycerides) was also analysed. This data provided additional information regarding toxicity and subsequently contributed more information. The clinical biochemistry and haematology were done on all the test animals.

For histopathology, the organs of each animal were isolated during the gross necropsy in a manner that ensured integrity of the organs and subsequently weighed individually. The isolated organs included the heart, lungs, liver, spleen, kidneys, brain, stomach, small intestines and large intestines which were stored in 10% formalin. Additionally, histopathology involved

slicing, fixing and staining of organ tissue on glass slides and analysing tissue under a microscope to investigate normal and abnormal tissue structures.

5.3 Results and discussion

5.3.1 Characterisation of microemulsion

Both the ME formulations; one containing [^{68}Ga]Ga-PSMA-11 depicted as [^{68}Ga]Ga-PSMA-11-ME and one without [^{68}Ga]Ga-PSMA-11 depicted as blank ME were analysed for droplet size, distribution (polydispersity index (PDI)) and surface charge (Zeta potential) as shown in Table 5.1. Both the ME and [^{68}Ga]Ga-PSMA-11-ME contained similar components which differed only in the inclusion of [^{68}Ga]Ga-PSMA-11 in the latter.

The average droplet size of the blank ME was 72.23 nm ± 0.18, whereas the size for the [^{68}Ga]Ga-PSMA-11-ME was 27.61 nm ± 1.11. The average size of the blank ME was significantly higher than that of the [^{68}Ga]Ga-PSMA-11-ME, which indicated that the addition of saline increased the droplet particle size whereas the addition of [^{68}Ga]Ga-PSMA-11 maintained a narrow droplet size. The average particle size of a ME without saline ranged between 20 and 40 nm with a distribution between 0.1 and 0.30 prior to addition of saline. The PDI of the ME and [^{68}Ga]Ga-PSMA-11-ME were 0.26 ± 0.005 and 0.53 ± 0.006 respectively. The PDI for the [^{68}Ga]Ga-PSMA-11-ME was higher than that of the blank ME, which may have been a result of the addition of [^{68}Ga]Ga-PSMA-11 leading to the formation of a system with multiple particle size. Under neutral conditions (pH ~7), both the MEs had a negative charge. The ME had a Zeta potential of -2.87 mV ± 0.53 whereas the [^{68}Ga]Ga-PSMA-11-ME had a Zeta potential of -2.31 mV ± 1.49. High Zeta potential is an indicator of the stability of the formulation and aids in predicting particle aggregation and/or phase precipitation (Subongkot and Ngawhirunpat, 2017). The results reported in this study showed low Zeta potential values, which may indicate that low negative charge might not be a good indicator of ME stability. Similarly, Subongkot and Ngawhirunpat reported stable ME formulations at low negative charge Zeta potentials. Measurement of Zeta potential serves as a predictor of storage stability of a colloidal system. Particle aggregation is less likely to occur in charged particles with high Zeta potential due to electric repulsion (Parhi *et al.,* 2012). This is true for kinetically stable emulsions (i.e. nanoemulsions), whereas in case of thermodynamically stable emulsions (i.e. microemulsions), only a measurable change in one of the variables (concentration, temperature or pressure) could lead to a change in the physical characteristics of the ME. There

was no phase separation and ME formulations remained translucent after storage for over 10 weeks at room temperature.

Table 5.1: Specifications of the ME formulations employed in the toxicity study

Test formulation:	ME
Size:	72.23 nm ± 0.18
PDI:	0.26 ± 0.005
Zeta potential:	-2.87 mV ± 0.53
pH:	6.89
Appearance:	Golden-translucent liquid

Composition of formulation (v/v)
1. Lauric acid-PEG 4000 (0.17 %)
2. Ethanol (8.28 %)
3. Polyvinyl alcohol (41.39 %)
4. Sodium oleate (41.39 %)
5. d-α-tocopherol (0.17 %)
6. Tween 80 (0.33 %)
7. Saline (8.28 %)

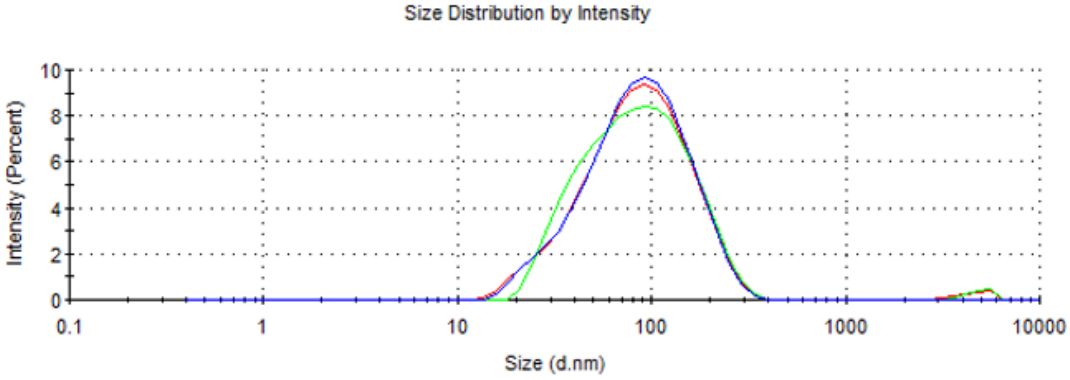

Test formulation:	[^{68}Ga]Ga-PSMA-11-ME
Size:	27.61 nm ± 1.11 nm
PDI:	0.53 ± 0.006
Zeta potential:	-2.31 ± 1.49 mV
pH:	7.00
Appearance:	Golden-translucent liquid

Composition of formulation (v/v)
1. Lauric acid-PEG 4000 (0.17 %)
2. Ethanol (8.28 %)
3. Polyvinyl alcohol (41.39 %)
4. Sodium oleate (41.39 %)
5. d-α-tocopherol (0.17 %)
6. Tween 80 (0.33 %)
7. [^{68}Ga]Ga-PSMA-11(8.28 %)

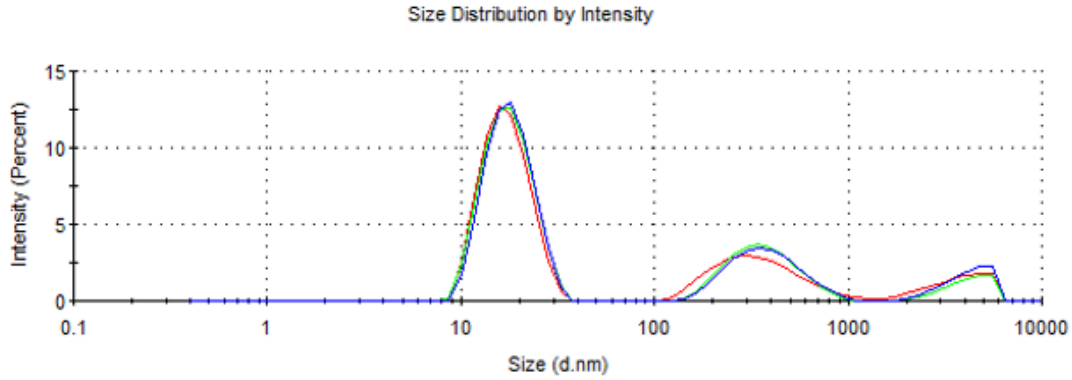

Each value represents the mean ± standard deviation (n=3)

5.3.2 *In vivo* toxicity assay

5.3.2.1 Food consumption

During the 14 day acute toxicity study, none of the BALB/c mice which were intravenously injected with either the ME or [^{68}Ga]Ga-PSMA-11-ME died or exhibited any adverse events or abnormalities. There were no abnormal changes in the food consumption recorded during the scheduled examination study period. The food consumption of mice was constant throughout the study, with an average food consumption rate of 3.74 g ± 0.32 per mouse per day. There were respectively no abnormal changes observed in the body weight, coat condition, respiration, mobility and behaviour of any of the mice during the study.

5.3.2.2 Effect of treatment on body weight

The initial and final body weights of the BALB/c mice in the different test groups are presented in Figure 5.2. Four out of five mice from the ME treatment group and two out of five mice out of the [^{68}Ga]Ga-PSMA-11-ME treatment group experienced statistically significant weight loss ($P < 0.05$) with an average weight loss of 2.31% ± 0.32 and 1.37% ± 0.43 respectively. Only one mouse which received a blank ME treatment completed the study with a final weight lower than that of the initial weight at treatment dosing, with a resulting weight loss of 1.36%. The study animals gradually gained weight after 48 hours as would be expected if the treatment is not toxic. It is difficult to say whether the weight loss was influenced by the treatment compounds per se considering the weights of each mouse which was enrolled into the treatment groups. The ME treatment group was assigned mice with a starting mean weight of 18.05 g ± 2.55, the lowest and highest starting weights being 15.93 g and 22.90 g respectively. The [^{68}Ga]Ga-PSMA-11-ME treatment group had a starting mean weight of 19.86 g ± 1.21, with the lowest and highest weights being 18.53 g and 21.84 g.

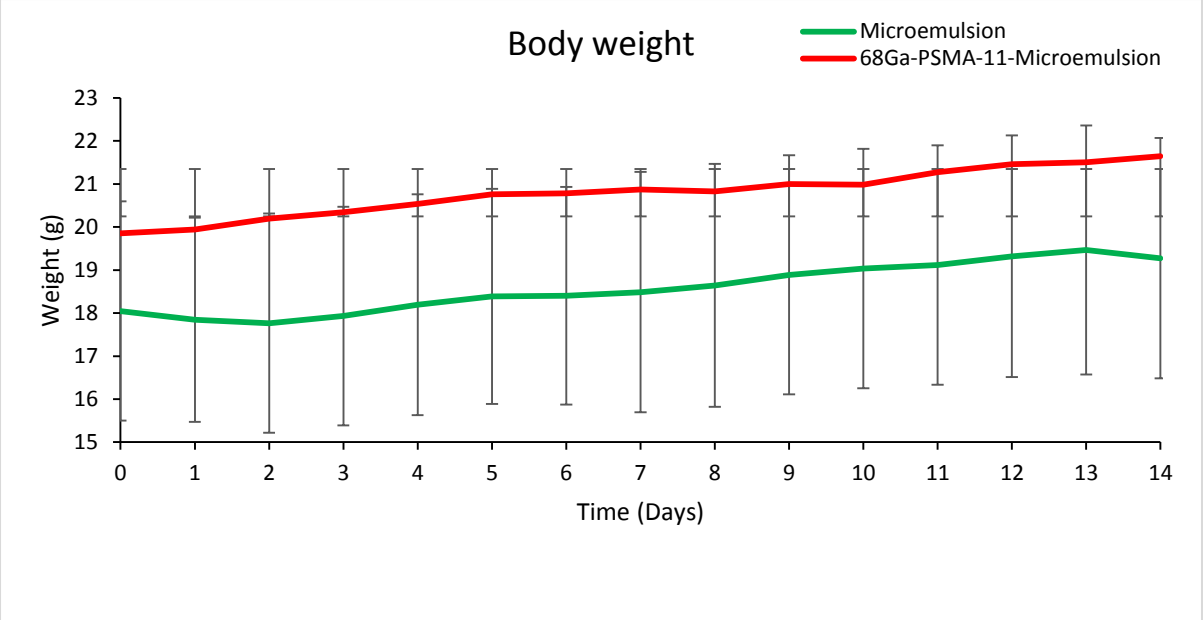

Figure 5.2: The body weight distribution of BALB/c mice measured over a 14 day period after IV administration of test groups. Each point represents the mean value of mice in the group. Results are expressed as mean ± standard deviation

A linear regression model using the SAS statistical software (version 9.4) was fitted to determine whether the treatment compound (ME or [^{68}Ga]Ga-PSMA-11-ME) had a statistically significant effect on the body weight. The model indicated that the effect of [^{68}Ga]Ga-PSMA-11-ME was statistically different ($P < 0.0001$) to the ME treatment group in the rate of growth and therefore it could be concluded that the two groups had statistically significant differences in body weight profiles over time based on the information for n=5 animals per treatment group and considering the different starting weights. The analysis compared the slopes of the regression lines fitted to the data for each group, since both groups showed a linear profile in the body weight over time. The two graphs below in Figure 5.3 showed data for the individual animals within the two groups. Note that even though an individual animal may not show a linear pattern of growth over time, the average growth of the groups seemed to be relatively linear, and therefore comparison of linear trends seemed to be appropriate.

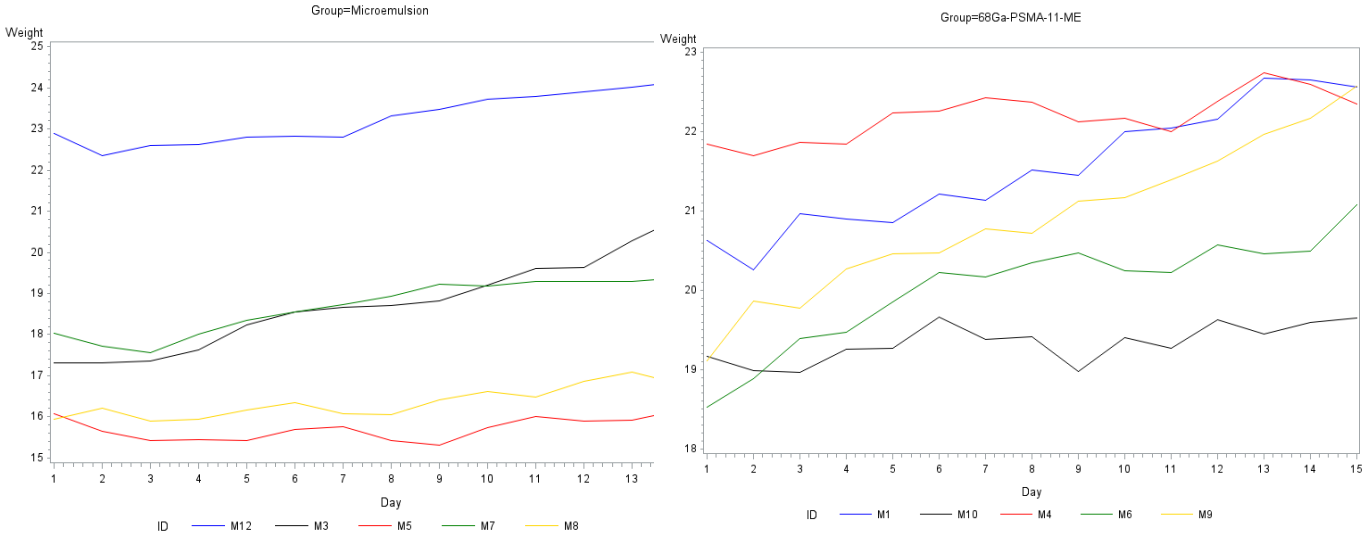

Figure 5.3: The body weight growth pattern of BALB/c mice measured over a 14 day period after IV administration of ME (left) and [^{68}Ga]Ga-PSMA-11-ME

The drop in body weight distribution between day 13 and 14 in the mice treated with the ME formulation was the result of two outlier mice which did not maintain a constant body weight distribution or expected pattern of weight gain over the 14 day period of the study. The Q-test was used to determine the outliers. The organ weights were determined after euthanasia of the animals enrolled in the study and represented in Table 5.2.

Table 5.2: Organ weights (g) (mean ± SD) of BALB/c mice

	ME (n=5)	***[^{68}Ga]Ga-PSMA-11-ME (n=5)***
Heart	0.13 ± 0.03	0.14 ± 0.01
Lungs	0.17 ± 0.03	0.18 ± 0.02
Liver	0.92 ± 0.22	1.01 ± 0.10
Spleen	0.05 ± 0.01	0.05 ± 0.01
Stomach and SI	1.28 ± 0.29	1.21 ± 0.16
Large intestine	0.22 ± 0.04	0.27 ± 0.08
Kidneys	0.30 ± 0.05	0.33 ± 0.03
Brain	0.35 ± 0.03	0.35 ± 0.05

SD: Standard deviation

Each value before "±" is a mean value of five replicates (n= 5) expressed to the nearest two decimal places and values after the "±" represents standard deviations expressed to the nearest two decimal places. A one-way ANOVA statistical analysis using the Statgraphics Centurion

XVI software indicated that the treatment compounds had no significant ($P > 0.05$) effect on the body weight of the participants in this study. This is because in all cases, the p-values were found to be more than 0.05. In this case, no significant ($P > 0.05$) interaction was found between the treatment compounds and the body organs analysed.

5.3.3 Haematology and clinical biochemistry

Blood biochemical profiles represent the physiological conditions of the animal and can serve as a diagnostic tool for disease or abnormalities.

Blood test results for typical liver function involved assessment of ALT and AST levels. A decrease in ALT levels is associated with healthy liver function whereas an in increase implies the destruction of hepatocytes and subsequent liver damage (Fernades *et al.,* 2018). Normal ALT levels in mice range from 25 to 60 IU/L. There was an increase in ALT levels in animals which received the [^{68}Ga]Ga-PSMA-11-ME treatment, although they were still within a healthy liver function range. Healthy AST levels in mice range from 50- 100 U/L. We recorded AST levels above 100 U/L. In literature, elevated AST levels in mice is reported to be common (Fernandes *et al.,* 2018). An increase in both ALT and AST levels could indicate liver injury or malfunction. Based on the gross necropsy observation and the histopathology report, this was not the case; mice livers did not exhibit any abnormalities or injury. Despite the difference between the treatment compounds, the results suggested no liver damage and the monitored study animals remained healthy throughout the experimental period.

Kidney function is represented by urea and creatinine levels in the blood. Urea was in the normal range (3.90- 10.67 mmol/L) in both mice groups receiving the treatment compounds and slightly higher in the control animal. An increase in urea would be associated with kidney malfunction, however this conclusion cannot be made when referring to an individual animal (n=1). Creatinine was lower in the test groups which could be an indication of clearance of creatinine by the kidneys and indication of clinical health in mice (Tabrizi *et al.,* 2012). The results in Table 5.3 are represented as mean ± standard deviation. Data presented in Table 5.3 is not statistically significant ($P > 0.05$) due to insufficient blood sample for clinical biochemistry analysis of some of the study animals, therefore leading to results that are not representative of n= 5 animals per treatment group. A control group of n= 1 is not statistically significant because one animal would not be representative of a cohort of five animals.

Table 5.3: Summary of clinical biochemistry results

Serum proteins	***Normal range ****	***Microemulsion***	***^{68}Ga-PSMA-11-ME***	***Control (n=1)***
Total protein (g/L)	3.50- 70	49	47.67 ± 1.25	49
Albumin (g/L)	20.50- 30	31	27	27
Bilirubin (umol/L)	0- 1	-	2 ± 0.00	-
Phosphatase (IU/L)	-	359	210.67 ± 60.05	157
Hepatic function				
ALT (IU/L)	10- 35	26.50 ± 1.50	38 ± 4.90	34
AST (IU/L)	54- 298	-	135	110
Pancreatic function				
Amylase (IU/L)	1496- 3200	1494	-	-
Kidney function				
Urea (mmol/L)	3.90- 10.67	8.35 ± 0.95	10.85 ± 1.15	13.20
Creatinine (umol/L)	40- 70	19	30.67 ± 9.81	50
Electrolytes				
Na+ (mmol/L)	140- 160	149 ± 2.00	138 ± 7.35	145
K+ (mmol/L)	4.50- 7.50	7.40	6.40	-
Serum lipids				
Total cholesterol (mmol/L)	4.72- 7.21	-	1.95 ± 0.05	2.70
HDL (mmol/L)	-	1.60 ± 0.10	1.63 ± 0.05	2.10
LDL (mmol/L)	-	-	0.30	-
Triglycerides (mmol/L)	5.55- 9.99	1.04	1.23 ± 0.28	1.68

(-): Insufficient blood sample * Tabrizi *et al.*, 2012; Fernandes *et al.*, 2018

A one-sided Mann-Whitney U-test (also called the Wilcoxon two-sample test) using the SAS statistical software (version 9.4) was used to compare the two treatment groups (Microemulsion (M) vs [^{68}Ga]Ga-PSMA-11-ME (G)). This test is more appropriate to use than the Student's t-test to test for statistically significant differences because of the small sample sizes. A t-test requires the underlying data to be from a normal distribution, but this assumption may not hold on a very small sample such as the ones in this study ($n \leq 5$). Results from the test were as seen below in Table 5.4.

Table 5.4: Statistical interpretation of clinical biochemistry results

Measure	Usable data points	p-value from test	Interpretation
Albumin	M: N=1 G: N=1	No test possible	
ALT	M: N=2 G: N=3	0.0745	Not statistically significant
Amylase	M: N=0 G: N=1	No test possible	
AST	M: N=1 G: N=3	0.5000	Not statistically significant
Bilirubin	M: N=0 G: N=2	No test possible	
Calcium	M: N=2 G: N=3	0.0745	Not statistically significant
Creatinine	M: N=1 G: N=3	0.3187	Not statistically significant
HDL	M: N=0 G: N=2	No test possible	
K+	M: N=1 G: N=1	No test possible	
LDL	M: N=0 G: N=1	No test possible	
Na+	M: N=2 G: N=3	0.1181	Not statistically significant
Phosphatase	M: N=1 G: N=3	0.8944	Not statistically significant
Total cholesterol	M: N=0 G: N=2	No test possible	
Total protein	M: N=1 G: N=3	0.4714	Not statistically significant
Triglycerides	M: N=1 G: N=3	0.5000	Not statistically significant
Urea	M: N=2 G: N=2	0.1226	Not statistically significant

The statistical test could not find any statistically significant differences in any of the measurements. However, note that the results of the test should be taken as indicative only, since the number of usable animal samples was low, and for some of the animals the measure could not be recorded, so that n- values were very low and often zero for the ME treatment group. Very low sample sizes could mean that patterns of differences could not be detected by the statistical test, but that it would be detectable in a larger sample size.

The histopathology reported negative for any treatment related toxicity and showed no abnormalities or malfunction of the organs. The microscopic evaluation of selected organs showed no diagnostically significant changes in any of the heart, lungs, liver, kidneys, spleen,

brain, stomach, small intestines, large intestines and pancreas sections which were evaluated. Refer to annexure test reports.

5.4 Conclusion

The *in vivo* assay indicated no adverse toxic effects of both the ME and ME containing [^{68}Ga]Ga-PSMA-11 during the 14 day period of the study after IV administration. None of the mice employed in the study died during the 14 day period. There were no treatment related clinical signs or lesions observed. The maximum tested dose for both ME and [^{68}Ga]Ga-PSMA-11-ME was 150 µl, administered via IV tail vein in male BALB/c mice.

Acknowledgements

The authors would like to thank and acknowledge the Nuclear Technologies in Medicine and the Biosciences Initiative (NTeMBI) and the South African Nuclear Energy Corporation (Necsa) for funding this study. The authors would like to thank the Council for Scientific and Industrial Research (CSIR) for the resources provided, Ms Lerato Thindisa and Mr Jacob Mabena for assisting with the animal study and Renee Koen (CSIR) for assisting with the statistical analysis. A special thank you to the Laboratory animal technicians involved in this study, Mr Kobus Venter and Mrs Antoinette Fick from the DST/NWU PCDDP Vivarium, North West University. Thank you to the following statisticians Renee Koen (CSIR), Serlom Agbemavor and Rodney Owusu-Darko (University of Pretoria) for assisting with the statistical analysis.

References

Aboumanei MA, Abdelbary AA, Ibrahim IT, Tadros MI and El-Kolaly MT. 2018. Design and development of microemulsion systems of a new antineoplaston A10 analog for enhanced intravenous antitumor activity: In vitro characterization, molecular docking, ^{125}I-radiolabeling and *in vivo* biodistribution studies. *International Journal of Pharmaceutics* 545: 240-253

Bhattacharya R, Mukhopadhyay S and Kothiyal P. 2016. Review on microemulsion- As a potential novel drug delivery system. *World Journal of Pharmacy and Pharmaceutical Sciences* 5(6): 700-729

Fernandes DP, Pimentel MML, Dos Santos FA, Praxedes EA *et al*. 2018. Hematological and biochemical profile of BALB/c nude and C57BL/6 SCID female mice after ovarian xenograft. *Annals of the Brazilian Academy of Sciences*, 90(4): 3941-3948

Hippalgaonkar K, Majumdar S and Kansara V. 2010. Injectable lipid emulsions-Advancements, opportunities and challenges. *American Association of Pharmaceutical Sciences* 11(4): 1526- 1540

Ma S, Chen F, Ye X, Dong Y, Xue Y, Zhang W *et al*. 2013. Intravenous microemulsion of docetaxel containing an anti-tumor synergistic ingredient (Brucea javanica oil): formulation and pharmacokinetics. *Int J Nanomed*, 8: 4045-4052

Melariri P, Kalombo L, Nkuna P, Dube A, Ogutu B *et al*. 2015. Oral lipid-based nanoformulation of tafenoquine enhanced bioavailability and blood stage antimalarial efficacy and led to a reduction in human red blood cell loss in mice. *Int J Nanomed*, 10: 1493–1503

Moghimipour E, Salimi A and Eftekhari S. 2013. Design and characterization of microemulsion systems for naproxen. *Adv Pharm Bull*, 3(1): 63–71

Muzaffar F, Singh UK and Chauhan L. 2013. Review on microemulsion as futuristic drug

delivery. *Int J Pharm Pharm Sci*, 5(3): 39–53

Parhi R and Suresh P. 2012. Preparation and characterization of solid lipid nanoparticles- A review. *Current Drug Discovery Technologies* 9(1): 2-16

Stallard N, Whitehead A and Ridgway P. 2002. Statistical evaluation of the revised fixed-dose procedure. *Human & Experimental Toxicology*, 21: 183-186

Subongkot T and Ngawhirunpat T. 2017. Development of a novel microemulsion for oral absorption enhancement of all-trans retinoic acid. *International Journal of Nanomedicine*, 12: 5585-5599

Tabrizi BA, Kararoudi MN and Mahmoudian B. 2012. Evaluation of serumal levels of AST, ALT, total bilirubin, glucose, urea and creatinin in mice after administration of Tc-99m MIBI. *International Journal of Animal and Veterinary Advances*, 4(1); 68-70

OECD. 2001. Guidelines for the Testing of Chemicals. OECD 420. Acute Oral Toxicity – Fixed Dose Procedure. Organisation for Economic Cooperation and Development, Paris.

Vanhove C, Bankstahl JP, Kramer SD, Visser E, Belcari N and Vandenberghe S. 2015. Accurate molecular imaging of small animals taking into account animal models, handling, anaesthesia, quality control and imaging system performance. *EJNMMI Physic*,. 2:31

Wong P, Li L, Chea J, Delgado MK, Crow D, Poku E, *et al*. 2017. PET imaging of ^{64}Cu-DOTA-scFv-anti-PSMA lipid nanoparticles (LNPs): Enhanced tumor targeting over anti-PSMA scFv or untargeted LNPs. *Nucl Med Biol*, 47: 62–8

Xu J, Yu J, Xu X, Wang L, Liu Y, Li L, *et al*. 2014. Development, characterization and evaluation of PSMA-Targeted Glycol Chitosan Micelles for Prostate Cancer Therapy. *J Nanomat*, 2014. 462356

Chapter 6: Conclusion, limitations and future perspectives

6.1 Conclusion

The physical and chemical characteristics of the optimised microemulsion (ME) formulation validated the safety and toxicity aspects of the ME for both *in vitro* and *in vivo* experiments. The physical stability of the formulations remained constant even with the incorporation of [^{68}Ga]Ga-PSMA-617 and [^{68}Ga]Ga-PSMA-11 radiopharmaceuticals. [^{68}Ga]Ga-PSMA-617 and [^{68}Ga]Ga-PSMA-11 were successfully synthesised at high radiochemical yields under determined conditions. The radiopharmaceutical [^{68}Ga]Ga-PSMA-617 was successfully incorporated into a ME formulation. Additionally *in vitro* cytotoxicity assays revealed that the ME loaded with [^{68}Ga]Ga-PSMA-617 was non-toxic to both PSMA-positive PC3 and PSMA-negative HEK 293 cell lines at 0.0625 mg/ml or lower, therefore rendering its evaluation as a delivery system for [^{68}Ga]Ga-PSMA-617 diagnostic studies possible.

Both the [^{68}Ga]Ga-PSMA-617 and [^{68}Ga]Ga-PSMA-617-ME followed an expected clearance profile for small-sized polar radiopharmaceuticals, with predominant renal clearance. The ME did alter the biodistribution pattern of [^{68}Ga]Ga-PSMA-617 but maintained distribution to the kidneys, albeit at statistically significant higher levels. Similarly, encapsulation in the ME may have resulted in delayed uptake into tumours as can be seen from the higher blood pool values. The encapsulation of [^{68}Ga]Ga-PSMA-617 in a ME may have influenced the outcome of a statistically significant ($P < 0.05$) lower tumour uptake as compared to [^{68}Ga]Ga-PSMA-617 uptake which could imply that the delivery system delays the transportation or release of the encapsulated PSMA. The biodistribution data showed that the [^{68}Ga]Ga-PSMA-617-ME had a 7-fold lower uptake in tumour compared to [^{68}Ga]Ga-PSMA-617. The ME is known as an effective and safe delivery system for intravenous administration and also of [^{68}Ga]Ga-PSMA-617. The effect of the ME in delaying its distribution and postulated higher tumour uptake over time can better be visualised at later time points and in animal models using a tumour cell line more specific for PSMA such as LNCaP. However, it needs to be kept in mind that xenograft tumour models in an *in vivo* microenvironment will not necessary express similar outcomes as those expressed in human prostate cancer disease. This hints as a challenge in precision diagnosis because xenograft tumour disease does not necessarily translate to wildtype disease and may present false-negative results due to tumour cell lines' inability to fully express

disease. Therefore, clinical trials in humans may prove to be more worthwhile, considering the toxicity and ethics of the test compounds. The *in vivo* toxicity assays indicated no adverse toxic effects of both the ME and ME containing [^{68}Ga]Ga-PSMA-11 after intravenous tail vein administration. There was no treatment related toxicity. There was a successful 100 % survival rate of all the test subjects which were enrolled in the study.

6.2 Limitations

The manufacturing and supply of PSMA-617 ($C_{49}H_{71}N_9O_{16}$; MW=1042.1 g/mol) by Advanced Biochemical Compounds (Radeberg, Germany) was discontinued by the company which resulted in the choice of an alternative peptide, PSMA-11 to be used in subsequent experiments which were done, more specifically the ME toxicity study (Chapter 5).
The stability of peptides is dependent on its sequence and storage conditions. Lyophilized PSMA-617 and PSMA-11 were stable for several months when stored at -20°C, away from light, but however lost integrity and stability after 6 months under these conditions.

The half-life of ^{68}Ga is a limitation in microPET/CT imaging where radioactivity decays quite rapidly especially if the injected dose was of low radioactivity. This becomes an even bigger challenge in cases where 2 hour (or longer) image acquisitions are required but the starting ^{68}Ga radioactivity was too low and the half-life being relatively short. Inadequate radioactivity doses result in low quality microPET image acquisition that would be better suited for *ex vivo* biodistribution data.

The choice of nude BALB/c mice as an animal model for the study proved to be very challenging due to the sensitivity and low stress tolerance of mice as compared to another animal model such as rats (Ellenbroek and Youn, 2016). However, the choice of mice was well justified in the inception of the study (Festing and Altman, 2002).

The ME is known as an effective and safe delivery system for intravenous administration and also of [^{68}Ga]Ga-PSMA-617. The effect of the ME in delaying its distribution and postulated higher tumour uptake over time can better be visualised at later time points and in animal models using a tumour cell line more specific for PSMA such as LNCaP.

Another limitation was the use of only one control mouse in the *in vivo* evaluation of acute intravenous toxicity of a microemulsion study. A control group was not planned for in the study design and therefore mice were not available to use at time of the study. This error was realised during the study that a control group was needed to compare against the treatment groups.

6.3 Future perspectives

The ultimate goal in an extension of this study would be to incorporate the theranostic aspect and compare it to the diagnostic dosimetry. The [^{68}Ga]Ga-PSMA-617 encapsulated in a ME could be synthesized as a potential diagnostic match for therapeutic [^{177}Lu]Lu-PSMA-617, also encapsulated in a ME delivery system. This would first need to be screened at low diagnostic levels of ^{177}Lu in an appropriate tumour model (LNCaP) to prove the higher uptake of the ME formulation in tumours over a time period beyond 2 hours. Further optimisation of this ME would be highly recommended to further investigate whether the [^{68}Ga]Ga-PSMA-617-ME can significantly evade high kidney accumulation and possibly follows a different pathway as compared to the reported typical enterohepatic metabolic pathway of [^{68}Ga]Ga-PSMA-617.

References:

Ellenbroek B and Youn J. 2016. Rodent models in neuroscience research: is it a rat race? *Disease Models and Mechanisms* 9(10): 1079-1087

Festing MFW and Altman DG. 2002. Guidelines for the design and statistical analysis of experiments using laboratory animals. *ILAR Journal* 43(4): 244-258

ANNEXURES

PathCare Veterinary Laboratories
Neels Bothma Str, N1 City
Tel : +27 21 596 3400
Vet Facility No: FR16/14260
Prac.No. : 5200539

PathCare
Drs Dietrich, Voigt, Mia
Vennote • Partners

FINAL REPORT - Lab Ref : 617195386

Report To
NORTH WEST UNIVERSITY VIVARIUM
ATT: COR BESTER
11 HOFFMAN STREET
2531 POTCHEFSTROOM

Patient Name
MOUSE1 M1 OTHER

Identity Number : NOT AVAILABLE
Species : Sex : OTHER:M
Other Number : NONE
Employee/Clock No : NOT AVAILABLE

Specimen : 0314:BA03975U
Collection Date : 2019-03-14 Not Supplied
Received Date : 2019-03-14 13:50
Report Date : 2019-03-25 10:02

Comment
BREED: NS
AGE:DOB 09/01/2019
Please note that the collection date or time was not provided and could not be verified by PathCare.

Tests Requested :
POTASSIUM-S*,SODIUM-S,UREA-S,CREATININE-S,CHOLESTEROL,TRIGLYCERIDE,CHOL HDL CHOL:HDL RATIO,LDL CHOL (MEAS),COMBINED REL. RISK,TOTAL PROTEIN-S,ALT (SGPT) ALBUMIN-S (VET),BILI TOTAL-S,ALK. PHOSP.-S,AST (SGOT),AMYLASE,CALCIUM VET

Specimen Types : Blood

----- BIOCHEMISTRY -----

Test	Result	Flag	Reference
SAMPLE APPEARANCE			
> LIPAEMIC	ABSENT		
> ICTERIC	ABSENT		
> HAEMOLYSIS	4+		
ELECTROLYTES			
> S-SODIUM	129		mmol/L
> S-POTASSIUM	Test not done		mmol/L
	: Haemolysis present - Potassium falsely elevated - Repeat : on a fresh free flowing specimen.		
> S-UREA	9.7		mmol/L
> S-CREATININE	19		umol/L
SERUM/PLASMA ANALYSIS			
> S-CALCIUM (total)	2.40		mmol/L
> SPECIMEN TAKEN	NOT SPECIFIED		
> LIPAEMIA	ABSENT		
> S-CHOLESTEROL	Test not done		mmol/L
> S-LDL CHOLESTEROL (meas)	Test not done		< 3.0 mmol/L
> S-TRIGLYCERIDE	1.34		mmol/L
> S-HDL CHOLESTEROL	1.6		> 1.0 mmol/L
> S-TOTAL PROTEIN	49		g/L

** Report Continues on Page : 2 **

PathCare
Drs Dietrich, Voigt, Mia
Vennote • Partners

	Lab Ref		Page : 2
NORTH WEST UNIVERSITY VIVARIUM	617195386		MOUSE1 M1 OTHER
Specimen	**Collection Date**	**Received Date**	**Report Date**
0314:BA03975U	2019-03-14 UNK	2019-03-14 13:50	2019-03-25 10:02

----- BIOCHEMISTRY -----

Test	Result	Flag	Reference
SERUM/PLASMA ANALYSIS cont...			
> S-ALBUMIN (VET)	27		g/L
> S-TOTAL BILIRUBIN	Test not done		umol/L
> S-ALK. PHOSPHATASE	130		IU/L
> S-ALT	32		IU/L
> S-AST	Test not done		IU/L
> S-AMYLASE	Test not done		IU/L

Signed Out by Dr Sophette Gers on 2019-03-15 09:34:00
For consultation, contact a Veterinary Pathologist - +27 83 285 1919
*H=High, L=Low, *H=Critically High, *L=Critically Low*
In rare cases, analytical interference may cause erroneous results.
Please inform pathologist if results and clinical picture do not concur.
END OF REPORT : Total Number of Pages : 2

PathCare Drs Dietrich, Voigt, Mia Vennote • Partners

PathCare Veterinary Laboratories
Neels Bothma Str, N1 City
Tel : +27 21 596 3400
Vet Facility No: FR16/14260
Prac.No. : 5200539

FINAL REPORT - Lab Ref : 617195102

Report To
NORTH WEST UNIVERSITY VIVARIUM
ATT: COR BESTER
11 HOFFMAN STREET
2531 POTCHEFSTROOM

Specimen : 0311:BA04563U
Collection Date : 2019-03-11 13:40
Received Date : 2019-03-11 14:56
Report Date : 2019-03-25 10:02

Patient Name
MOUSE M3 OTHER

Identity Number : NOT AVAILABLE
Species : Sex : OTHER:M
Other Number : NONE
Employee/Clock No : NOT AVAILABLE

Comment
AGE: NS
BREED: NS
MOUSE DOB 19/01/2019
Tests Requested :
POTASSIUM-S*,SODIUM-S,UREA-S,CREATININE-S,CHOLESTEROL,TRIGLYCERIDE,CHOL HDL CHOL:HDL RATIO,LDL CHOL (MEAS),COMBINED REL. RISK,TOTAL PROTEIN-S,ALT (SGPT) BILI TOTAL-S,ALK. PHOSP.-S,AST (SGOT),AMYLASE,CALCIUM VET

Specimen Types : Blood

----- BIOCHEMISTRY -----

Test	Result	Flag	Reference
SAMPLE APPEARANCE			
> LIPAEMIC	ABSENT		
> ICTERIC	ABSENT		
> HAEMOLYSIS	2+		
ELECTROLYTES			
> S-SODIUM	147		mmol/L
> S-POTASSIUM	Test not done		mmol/L
	SAMPLE HAEMOLYSED		
> S-UREA	7.4		mmol/L
> S-CREATININE	19		umol/L
SERUM/PLASMA ANALYSIS			
> S-CALCIUM (total)	2.32		mmol/L
> SPECIMEN TAKEN	NOT SPECIFIED		
> LIPAEMIA	ABSENT		
> S-CHOLESTEROL	Test not done		mmol/L
	SAMPLE INSUFFICIENT		
> S-LDL CHOLESTEROL (meas)	Test not done		< 3.0 mmol/L
	SAMPLE INSUFFICIENT		
> S-TRIGLYCERIDE	1.04		mmol/L
> S-HDL CHOLESTEROL	1.6		> 1.0 mmol/L
> S-NON-HDL-CHOLESTEROL	Test not done		< 3.8 mmol/L
> CHOL:HDL RATIO	Test not done		< 4.0
> S-TOTAL PROTEIN	49		g/L
> S-TOTAL BILIRUBIN	Test not done		umol/L
	SAMPLE INSUFFICIENT		

** Report Continues on Page : 2 **

PathCare
Drs Dietrich, Voigt, Mia
Vennote • Partners

	Lab Ref		Page : 2
NORTH WEST UNIVERSITY VIVARIUM	617195102		MOUSE M3 OTHER
Specimen	**Collection Date**	**Received Date**	**Report Date**
0311:BA04563U	2019-03-11 13:40	2019-03-11 14:56	2019-03-25 10:02

----- BIOCHEMISTRY -----

Test	Result	Flag	Reference
SERUM/PLASMA ANALYSIS cont...			
> S-ALK. PHOSPHATASE	359		IU/L
> S-ALT	28		IU/L
> S-AST	Test not done		IU/L
	SAMPLE INSUFFICIENT		
> S-AMYLASE	Test not done		IU/L
	SAMPLE INSUFFICIENT		

Authorised on 2019-03-11 16:33:00
For consultation, contact a Veterinary Pathologist - +27 83 285 1919
*H=High, L=Low, *H=Critically High, *L=Critically Low*
In rare cases, analytical interference may cause erroneous results.
Please inform pathologist if results and clinical picture do not concur.
END OF REPORT : Total Number of Pages : 2

PathCare Drs Dietrich, Voigt, Mia Vennote • Partners

PathCare Veterinary Laboratories
Neels Bothma Str, N1 City
Tel : +27 21 596 3400
Vet Facility No: FR16/14260
Prac.No. : 5200539

FINAL REPORT - Lab Ref : 617195101

Report To
NORTH WEST UNIVERSITY VIVARIUM
ATT: COR BESTER
11 HOFFMAN STREET
2531 POTCHEFSTROOM

Specimen : 0311:BA04586U
Collection Date : 2019-03-11 13:56
Received Date : 2019-03-11 14:58
Report Date : 2019-03-25 10:02

Patient Name
MOUSE M4 OTHER

Identity Number : NOT AVAILABLE
Species : Sex : OTHER:M
Other Number : NONE
Employee/Clock No : NOT AVAILABLE

Comment
BREED: NS
AGE: NS DOB 19/01/2019
Tests Requested :
POTASSIUM-S*,SODIUM-S,UREA-S,CREATININE-S,CHOLESTEROL,TRIGLYCERIDE,CHOL HDL CHOL:HDL RATIO,LDL CHOL (MEAS),COMBINED REL. RISK,TOTAL PROTEIN-S,ALT (SGPT) BILI TOTAL-S,ALK. PHOSP.-S,AST (SGOT),AMYLASE,CALCIUM VET

Specimen Types : Blood

----- BIOCHEMISTRY -----

Test	Result	Flag	Reference
SAMPLE APPEARANCE			
> LIPAEMIC	ABSENT		
> ICTERIC	ABSENT		
> HAEMOLYSIS	2+		
ELECTROLYTES			
> S-SODIUM	138		mmol/L
> S-POTASSIUM	Test not done		mmol/L
	SPECIMEN HAEMOLYSED		
> S-UREA	Test not done		mmol/L
	INSUFFICIENT SAMPLE		
> S-CREATININE	433		umol/L
SERUM/PLASMA ANALYSIS			
> S-CALCIUM (total)	2.98		mmol/L
> SPECIMEN TAKEN	NOT SPECIFIED		
> LIPAEMIA	ABSENT		
> S-CHOLESTEROL	1.9		mmol/L
> S-LDL CHOLESTEROL (meas)	Test not done		< 3.0 mmol/L
	SAMPLE INSUFFICIENT		
> S-TRIGLYCERIDE	0.84		mmol/L
> S-HDL CHOLESTEROL	1.7		> 1.0 mmol/L
> S-NON-HDL-CHOLESTEROL	0.20		< 3.8 mmol/L
> CHOL:HDL RATIO	1.1		< 4.0
	TC:HDL >4: Moderate risk; TC:HDL >5: High CVD risk		
	For more accurate CVD risk, ApoB & ApoA1 is recommended		
> S-TOTAL PROTEIN	46		g/L

** Report Continues on Page : 2 **

PathCare
Drs Dietrich, Voigt, Mia
Vennote • Partners

	Lab Ref		Page : 2
NORTH WEST UNIVERSITY VIVARIUM	617195101		MOUSE M4 OTHER
Specimen	**Collection Date**	**Received Date**	**Report Date**
0311:BA04586U	2019-03-11 13:56	2019-03-11 14:58	2019-03-25 10:02

----- BIOCHEMISTRY -----

Test	Result	Flag	Reference
SERUM/PLASMA ANALYSIS cont...			
> S-TOTAL BILIRUBIN	2		umol/L
> S-ALK. PHOSPHATASE	274		IU/L
> S-ALT	38		IU/L
> S-AST	131		IU/L
> S-AMYLASE	1494		IU/L

Authorised on 2019-03-11 16:31:00

For consultation, contact a Veterinary Pathologist - +27 83 285 1919

*H=High, L=Low, *H=Critically High, *L=Critically Low*

In rare cases, analytical interference may cause erroneous results.
Please inform pathologist if results and clinical picture do not concur.

END OF REPORT : Total Number of Pages : 2

PathCare Drs Dietrich, Voigt, Mia Vennote • Partners

PathCare Veterinary Laboratories
Neels Bothma Str, N1 City
Tel : +27 21 596 3400
Vet Facility No: FR16/14260
Prac.No. : 5200539

FINAL REPORT - Lab Ref : 617195162

Report To
NORTH WEST UNIVERSITY VIVARIUM
ATT: COR BESTER
11 HOFFMAN STREET
2531 POTCHEFSTROOM

Specimen : 0312:BA04707U
Collection Date : 2019-03-12 13:14
Received Date : 2019-03-12 14:11
Report Date : 2019-03-25 10:02

Patient Name
MOUSE 5 M5 MANDIWANA OTHER

Identity Number : NOT AVAILABLE
Species : Sex : OTHER:M
Other Number : NONE
Employee/Clock No : NOT AVAILABLE

Comment
BREED : NOT SUPPLIED AGE : NOT SUPPLIED

Tests Requested :
POTASSIUM-S*,SODIUM-S,UREA-S,CREATININE-S,CHOLESTEROL,TRIGLYCERIDE,CHOL HDL
LDL CHOL (MEAS),TOTAL PROTEIN-S,ALBUMIN-S (VET),BILI TOTAL-S,ALK. PHOSP.-S
ALT (SGPT),AST (SGOT),AMYLASE,CALCIUM VET

Specimen Types : Blood

----- BIOCHEMISTRY -----

Test	Result	Flag	Reference
SAMPLE APPEARANCE			
> LIPAEMIC	1+		
> ICTERIC	ABSENT		
> HAEMOLYSIS	3+		
ELECTROLYTES			
> S-SODIUM	151		mmol/L
> S-POTASSIUM	7.4		mmol/L
Haemolysis may falsely increase potassium levels.			
> S-UREA	9.3		mmol/L
SERUM/PLASMA ANALYSIS			
> S-CALCIUM (total)	2.38		mmol/L
> SPECIMEN TAKEN	NOT SPECIFIED		
> LIPAEMIA	1+		
> S-ALBUMIN (VET)	31		g/L
> S-ALT	25		IU/L

Signed Out by Dr Sophette Gers on 2019-03-13 08:41:00
For consultation, contact a Veterinary Pathologist - +27 83 285 1919
*H=High, L=Low, *H=Critically High, *L=Critically Low*
In rare cases, analytical interference may cause erroneous results.
Please inform pathologist if results and clinical picture do not concur.
END OF REPORT : Total Number of Pages : 1

PathCare
Drs Dietrich, Voigt, Mia
Vennote • Partners

PathCare Veterinary Laboratories
Neels Bothma Str, N1 City
Tel : +27 21 596 3400
Vet Facility No: FR16/14260
Prac.No. : 5200539

FINAL REPORT - Lab Ref : 617195818

Report To
NORTH WEST UNIVERSITY VIVARIUM
ATT: COR BESTER
11 HOFFMAN STREET
2531 POTCHEFSTROOM

Patient Name
MOUSE 6 MANDIWANA OTHER

Identity Number : NOT AVAILABLE
Species : Sex : OTHER:M
Other Number : NONE
Employee/Clock No : NOT AVAILABLE

Specimen : 0318:BA01827U
Collection Date : 2019-03-18 08:30
Received Date : 2019-03-18 09:22
Report Date : 2019-03-25 10:02

Comment
BREED: NOT SUPPLIED
AGE : 2 MONTHS 9 DAYS
Tests Requested :
POTASSIUM-S*,SODIUM-S,UREA-S,CREATININE-S,CHOLESTEROL,TRIGLYCERIDE,CHOL HDL
CHOL:HDL RATIO,LDL CHOL (MEAS),THERAPEUTIC GOALS,COMBINED REL. RISK
TOTAL PROTEIN-S,ALBUMIN-S (VET),BILI TOTAL-S,ALK. PHOSP.-S,ALT (SGPT)
AST (SGOT),CALCIUM VET

Specimen Types : Blood

----- BIOCHEMISTRY -----

Test	Result	Flag	Reference
SAMPLE APPEARANCE			
> LIPAEMIC	ABSENT		
> ICTERIC	ABSENT		
> HAEMOLYSIS	1+		
ELECTROLYTES			
> S-SODIUM	147		mmol/L
> S-POTASSIUM	6.4		mmol/L
Haemolysis may falsely increase potassium levels.			
> S-UREA	12.0		mmol/L
> S-CREATININE	30		umol/L
SERUM/PLASMA ANALYSIS			
> S-CALCIUM (total)	2.53		mmol/L
> SPECIMEN TAKEN	NOT SPECIFIED		
> LIPAEMIA	ABSENT		
> S-CHOLESTEROL	2.0		mmol/L
> S-LDL CHOLESTEROL (meas)	< 0.3	*L	< 3.0 mmol/L
> S-TRIGLYCERIDE	1.51		mmol/L
> S-HDL CHOLESTEROL	1.6		> 1.0 mmol/L
> S-NON-HDL-CHOLESTEROL	0.40		< 3.8 mmol/L
> CHOL:HDL RATIO	1.3		< 4.0
TC:HDL >4: Moderate risk; TC:HDL >5: High CVD risk			
For more accurate CVD risk, ApoB & ApoA1 is recommended			
> S-TOTAL PROTEIN	48		g/L
> S-ALBUMIN (VET)	Test not done		g/L

** Report Continues on Page : 2 **

PathCare
Drs Dietrich, Voigt, Mia
Vennote • Partners

	Lab Ref		Page : 2
NORTH WEST UNIVERSITY VIVARIUM	617195818		MOUSE 6 MANDIWANA OTHER
Specimen	**Collection Date**	**Received Date**	**Report Date**
0318:BA01827U	2019-03-18 08:30	2019-03-18 09:22	2019-03-25 10:02

----- BIOCHEMISTRY -----

Test	Result	Flag	Reference
SERUM/PLASMA ANALYSIS cont...			
> S-TOTAL BILIRUBIN	2		umol/L
> S-ALK. PHOSPHATASE	228		IU/L
> S-ALT	44		IU/L
> S-AST	139		IU/L

> THERAPEUTIC GOALS (mmol/L):

High risk patients:Tot Chol <4.5, LDL-C <2.5, Non-HDL-C <3.3
Very high risk pts:Tot Chol <4.0, LDL-C <1.8, Non-HDL-C <2.6
Ref: SA Dyslipid. Guideline Consensus Statement - SAMJ 2012

Signed Out by Dr Sophette Gers on 2019-03-19 09:14:00
For consultation, contact a Veterinary Pathologist - +27 83 285 1919
*H=High, L=Low, *H=Critically High, *L=Critically Low*
In rare cases, analytical interference may cause erroneous results.
Please inform pathologist if results and clinical picture do not concur.
END OF REPORT : Total Number of Pages : 2

PathCare Veterinary Laboratories
Neels Bothma Str, N1 City
Tel : +27 21 596 3400
Vet Facility No: FR16/14260
Prac.No. : 5200539

PathCare
Drs Dietrich, Voigt, Mia
Vennote • Partners

Pathology Report - Lab Ref : 617195429

Report To
NORTH WEST UNIVERSITY VIVARIUM
ATT: COR BESTER
11 HOFFMAN STREET
2531 POTCHEFSTROOM

Specimen : 19:ZH830
Collection Date : 2019-03-13 13:02
Received Date : 2019-03-14 Not Suppl
Report Date : 2019-03-25 10:02

Patient Name
MOUSE 9 ORGANS MANDIWANA OTHER

Identity Number : NOT AVAILABLE
Species : Sex : OTHER:M
Other Number : NONE
Employee/Clock No : NOT AVAILABLE

Tests Requested :
HISTOPATHOLOGY

----- Histopathology -----

CLINICAL HISTORY:
This is a mouse (M9). No clinical history provided.

MACROSCOPY:
Heart, lung, liver, kidney, spleen, brain, stomach, small intestine, large intestine were presented in formalin for histopathology.

MICROSCOPY:
No diagnostically significant microscopic changes were noted in any of the heart, lung, liver, kidney, spleen, brain, stomach, small/large intestine, pancreas or thymus sections evaluated.

COMMENT:
Unfortunately no specific diagnosis is possible from the microscopic evaluation.

DIAGNOSIS:
NO SPECIFIC DIANGOSIS POSSIBLE FROM THE HISTOPATHOLOGY

ICD-10 : Z01.7

Signed Out by Dr Sophette Gers on 2019-03-18 09:25:00
For consultation, contact a Veterinary Pathologist - +27 83 285 1919
END OF REPORT : Total Number of Pages : 1

PathCare Drs Dietrich, Voigt, Mia Vennote • Partners

PathCare Veterinary Laboratories
Neels Bothma Str, N1 City
Tel : +27 21 596 3400
Vet Facility No: FR16/14260
Prac.No. : 5200539

FINAL REPORT - Lab Ref : 617195161

Report To
NORTH WEST UNIVERSITY VIVARIUM
ATT: COR BESTER
11 HOFFMAN STREET
2531 POTCHEFSTROOM

Patient Name
MOUSE M10 OTHER

Identity Number : NOT AVAILABLE
Species : Sex : OTHER:M
Other Number : NONE
Employee/Clock No : NOT AVAILABLE

Specimen : 0312:BA04711U
Collection Date : 2019-03-12 13:26
Received Date : 2019-03-12 14:13
Report Date : 2019-03-25 10:02

Comment
BREED: NS
AGE: NS DOB: 09/01/2019
Tests Requested :
POTASSIUM-S*,SODIUM-S,UREA-S,CREATININE-S,CHOLESTEROL,TRIGLYCERIDE,CHOL HDL
LDL CHOL (MEAS),TOTAL PROTEIN-S,ALBUMIN-S (VET),BILI TOTAL-S,ALK. PHOSP.-S
ALT (SGPT),AST (SGOT),AMYLASE,CALCIUM VET

Specimen Types : Blood

----- BIOCHEMISTRY -----

Test	Result	Flag	Reference
SAMPLE APPEARANCE			
> LIPAEMIC	Insufficient sample		
> ICTERIC	Insufficient sample		
> HAEMOLYSIS	Insufficient sample		
ELECTROLYTES			
> S-SODIUM	Insufficient sample		mmol/L
> S-POTASSIUM	Insufficient sample		mmol/L
> S-UREA	Insufficient sample		mmol/L
> S-CREATININE	Insufficient sample		umol/L
SERUM/PLASMA ANALYSIS			
> S-CALCIUM (total)	Insufficient sample		mmol/L
> SPECIMEN TAKEN	NOT SPECIFIED		
> LIPAEMIA	Insufficient sample		
> S-CHOLESTEROL	Insufficient sample		mmol/L
> S-LDL CHOLESTEROL (meas)	Insufficient sample		< 3.0 mmol/L
> S-TRIGLYCERIDE	Insufficient sample		mmol/L
> S-HDL CHOLESTEROL	Insufficient sample		> 1.0 mmol/L
> S-TOTAL PROTEIN	Insufficient sample		g/L
> S-ALBUMIN (VET)	Insufficient sample		g/L
> S-TOTAL BILIRUBIN	Insufficient sample		umol/L
> S-ALK. PHOSPHATASE	Insufficient sample		IU/L
> S-ALT	Insufficient sample		IU/L
> S-AST	Insufficient sample		IU/L
> S-AMYLASE	Insufficient sample		IU/L

Authorised on 2019-03-13 11:16:00
For consultation, contact a Veterinary Pathologist - +27 83 285 1919
*H=High, L=Low, *H=Critically High, *L=Critically Low*
In rare cases, analytical interference may cause erroneous results.
Please inform pathologist if results and clinical picture do not concur.

PathCare Drs Dietrich, Voigt, Mia Vennote • Partners

PathCare Veterinary Laboratories
Neels Bothma Str, N1 City
Tel : +27 21 596 3400
Vet Facility No: FR16/14260
Prac.No. : 5200539

FINAL REPORT - Lab Ref : 617195385

Report To
NORTH WEST UNIVERSITY VIVARIUM
ATT: COR BESTER
11 HOFFMAN STREET
2531 POTCHEFSTROOM

Patient Name
MAISE CONTROL MANDIWANA OTHER

Identity Number : NOT AVAILABLE
Species : Sex : OTHER:M
Other Number : NONE
Employee/Clock No : NOT AVAILABLE

Specimen : 0314:BA04195U
Collection Date : 2019-03-14 Not Supplied
Received Date : 2019-03-14 13:51
Report Date : 2019-03-25 10:02

Comment
AGE/DOB 09/01/2019
BREED M.CONTROL
Please note that the collection date or time was not provided and could not be verified by PathCare.

Tests Requested :
POTASSIUM-S*,SODIUM-S,UREA-S,CREATININE-S,CHOLESTEROL,TRIGLYCERIDE,CHOL HDL CHOL:HDL RATIO,LDL CHOL (MEAS),COMBINED REL. RISK,TOTAL PROTEIN-S,ALT (SGPT) ALBUMIN-S (VET),BILI TOTAL-S,ALK. PHOSP.-S,AST (SGOT),AMYLASE,CALCIUM VET

Specimen Types : Blood

----- BIOCHEMISTRY -----

Test	Result	Flag	Reference
SAMPLE APPEARANCE			
> LIPAEMIC	ABSENT		
> ICTERIC	ABSENT		
> HAEMOLYSIS	2+		
ELECTROLYTES			
> S-SODIUM	145		mmol/L
> S-POTASSIUM	Test not done		mmol/L
	: Haemolysis present - Potassium falsely elevated - Repeat :		
	: on a fresh free flowing specimen. :		
> S-UREA	13.2		mmol/L
> S-CREATININE	50		umol/L
SERUM/PLASMA ANALYSIS			
> S-CALCIUM (total)	2.48		mmol/L
> SPECIMEN TAKEN	NOT SPECIFIED		
> LIPAEMIA	ABSENT		
> S-CHOLESTEROL	2.7		mmol/L
> S-LDL CHOLESTEROL (meas)	Test not done		< 3.0 mmol/L
> S-TRIGLYCERIDE	1.68		mmol/L
> S-HDL CHOLESTEROL	2.1		> 1.0 mmol/L
> S-NON-HDL-CHOLESTEROL	0.60		< 3.8 mmol/L

** Report Continues on Page : 2 **

PathCare
Drs Dietrich, Voigt, Mia
Vennote • Partners

	Lab Ref		Page : 2
NORTH WEST UNIVERSITY VIVARIUM	617195385		MAISE CONTROL MANDIWANA OTHER
Specimen	**Collection Date**	**Received Date**	**Report Date**
0314:BA04195U	2019-03-14 UNK	2019-03-14 13:51	2019-03-25 10:02

----- BIOCHEMISTRY -----

Test	Result	Flag	Reference
SERUM/PLASMA ANALYSIS cont...			
> CHOL:HDL RATIO	1.3		< 4.0
	TC:HDL >4: Moderate risk; TC:HDL >5: High CVD risk		
	For more accurate CVD risk, ApoB & ApoA1 is recommended		
> S-TOTAL PROTEIN	49		g/L
> S-ALBUMIN (VET)	27		g/L
> S-TOTAL BILIRUBIN	Test not done		umol/L
> S-ALK. PHOSPHATASE	157		IU/L
> S-ALT	34		IU/L
> S-AST	110		IU/L
> S-AMYLASE	Test not done		IU/L

Signed Out by Dr Sophette Gers on 2019-03-15 09:34:00
For consultation, contact a Veterinary Pathologist - +27 83 285 1919
*H=High, L=Low, *H=Critically High, *L=Critically Low*
In rare cases, analytical interference may cause erroneous results.
Please inform pathologist if results and clinical picture do not concur.
END OF REPORT : Total Number of Pages : 2